GDSA Framework Development and Process Model Integration FY2022

Spent Fuel and Waste Disposition

Prepared for
U.S. Department of Energy
Spent Fuel and Waste Science and Technology

P.E. Mariner, B.J. Debusschere,
D.E. Fukuyama, J.A. Harvey,
T.C. LaForce, R.C. Leone, F.V. Perry,
L.P. Swiler, A.M. Taconi

Sandia National Laboratories

September 20, 2022
M2SF-22SN010304093
SAND2022-14304 R

DISCLAIMER

This information was prepared as an account of work sponsored by an agency of the U.S. Government. Neither the U.S. Government nor any agency thereof, nor any of their employees, makes any warranty, expressed or implied, or assumes any legal liability or responsibility for the accuracy, completeness, or usefulness, of any information, apparatus, product, or process disclosed, or represents that its use would not infringe privately owned rights. References herein to any specific commercial product, process, or service by trade name, trade mark, manufacturer, or otherwise, does not necessarily constitute or imply its endorsement, recommendation, or favoring by the U.S. Government or any agency thereof. The views and opinions of authors expressed herein do not necessarily state or reflect those of the U.S. Government or any agency thereof.

DISCLAIMER

This is a technical report that does not take into account contractual limitations or obligations under the Standard Contract for Disposal of Spent Nuclear Fuel and/or High-Level Radioactive Waste (Standard Contract) (10 CFR Part 961). For example, under the provisions of the Standard Contract, spent nuclear fuel in multi-assembly canisters is not an acceptable waste form, absent a mutually agreed to contract amendment.

To the extent discussions or recommendations in this report conflict with the provisions of the Standard Contract, the Standard Contract governs the obligations of the parties, and this report in no manner supersedes, overrides, or amends the Standard Contract.

This report reflects technical work which could support future decision making by DOE. No inferences should be drawn from this report regarding future actions by DOE, which are limited both by the terms of the Standard Contract and Congressional appropriations for the Department to fulfill its obligations under the Nuclear Waste Policy Act including licensing and construction of a spent nuclear fuel repository.

Sandia National Laboratories is a multi-mission laboratory managed and operated by National Technology & Engineering Solutions of Sandia, LLC., a wholly owned subsidiary of Honeywell International, Inc., for the U.S. Department of Energy's National Nuclear Security Administration under contract DE-NA0003525.

U.S. DEPARTMENT OF ENERGY

APPENDIX E

NFCSC DOCUMENT COVER SHEET[1]

Name/Title of Deliverable/Milestone/Revision No. GDSA Framework Development and Process Model Integration FY 2022 / M2SF-22SN010304093

Work Package Title and Number GDSA – Framework Development – SNL / SF-22SN01030409

Work Package WBS Number 1.08.01.03.04

Responsible Work Package Manager Paul Mariner
(Name/Signature)

Date Submitted

Quality Rigor Level for Deliverable/Milestone[2]	☐ QRL-1 ☐ Nuclear Data	☐ QRL-2	☒ QRL-3	☐ QRL-4 Lab QA Program[3]

This deliverable was prepared in accordance with Sandia National Laboratories
(Participant/National Laboratory Name)

QA program which meets the requirements of

☒ DOE Order 414.1 ☐ NQA-1 ☐ Other

This Deliverable was subjected to:

☒ Technical Review ☐ Peer Review

Technical Review (TR)
Review Documentation Provided

☐ Signed TR Report or,

☐ Signed TR Concurrence Sheet or,

☐ Signature of TR Reviewer(s) below

Peer Review (PR)
Review Documentation Provided

☐ Signed PR Report or,

☐ Signed PR Concurrence Sheet or,

☐ Signature of PR Reviewer(s) below

Name and Signature of Reviewers

David Sassani

NOTE 1: *Appendix E should be filled out and submitted with the deliverable. Or, if the PICS:NE system permits, completely enter all applicable information in the PICS:NE Deliverable Form. The requirement is to ensure that all applicable information is entered either in the PICS:NE system or by using the NFCSC Document Cover Sheet.*

- *In some cases there may be a milestone where an item is being fabricated, maintenance is being performed on a facility, or a document is being issued through a formal document control process where it specifically calls out a formal review of the document. In these cases, documentation (e.g., inspection report, maintenance request, work planning package documentation or the documented review of the issued document through the document control process) of the completion of the activity, along with the Document Cover Sheet, is sufficient to demonstrate achieving the milestone.*

NOTE 2: *If QRL 1, 2, or 3 is not assigned, then the QRL 4 box must be checked, and the work is understood to be performed using laboratory QA requirements. This includes any deliverable developed in conformance with the respective National Laboratory / Participant, DOE or NNSA-approved QA Program.*

NOTE 3: *If the lab has an NQA-1 program and the work to be conducted requires an NQA-1 program, then the QRL-1 box must be checked in the work Package and on the Appendix E cover sheet and the work must be performed in accordance with the Lab's NQA-1 program. The QRL-4 box should not be checked.*

ACKNOWLEDGEMENTS

This report documents fiscal year (FY) 2022 accomplishments in GDSA Framework development and process model integration. Many of the accomplishments are described in more detail in other GDSA reports. Highlights are included in the current report and cited.

Coauthors contributing written sections are gratefully acknowledged:

Section 4.2.2	Geologic Framework Model – Geology and Hydrology of Glacial Deposits to Support Biosphere Modeling in a Crystalline Rock Environment	Frank Perry
Section 4.2.3	Voronoi Meshing and Simulation	Tara LaForce
Section 4.2.4	Uncertainty and Sensitivity Analysis	Laura Swiler
Appendix B	Fuel Matrix Degradation Process Model Code Development in FORTRAN	Jacob Harvey, Anna Taconi
Appendix C	Surrogate Modeling of the Fuel Matrix Degradation (FMD) Process Model	Bert Debusschere
Appendix D	Groundwater Chemistry Modeling for the Crystalline Reference Case	David Fukuyama

In addition, the following people are acknowledged for past contributions included in edited form in this report: Geoff Freeze (Section 2), Glenn Hammond (Section 4.3.2), and Aubrey Eckert-Gallup (Section 4.2.1).

The authors thank David Sassani of Sandia National Laboratories (SNL) for his thoughtful technical review and thank the staff from U.S. Department of Energy Office of Nuclear Energy (DOE-NE), Prasad Nair (DOE NE-81) and Tim Gunter (DOE NE-81), for their discussions, oversight, and guidance on topics addressed in this report.

EXECUTIVE SUMMARY

The Spent Fuel and Waste Science and Technology (SFWST) Campaign of the U.S. Department of Energy (DOE) Office of Nuclear Energy (NE), Office of Spent Fuel & Waste Disposition (SFWD) is conducting research and development (R&D) on geologic disposal of spent nuclear fuel (SNF) and high-level nuclear waste (HLW). A high priority for SFWST disposal R&D is disposal system modeling (Sassani et al. 2021). The SFWST Geologic Disposal Safety Assessment (GDSA) work package is charged with developing a disposal system modeling and analysis capability for evaluating generic disposal system performance for nuclear waste in geologic media.

Purpose: This report describes fiscal year (FY) 2022 advances of the Geologic Disposal Safety Assessment (GDSA) performance assessment (PA) development groups of the SFWST Campaign. The common mission of these groups is to develop a geologic disposal system modeling capability for nuclear waste that can be used to assess probabilistically the performance of generic disposal options and generic sites. The modeling capability under development is called GDSA Framework (pa.sandia.gov). GDSA Framework is a coordinated set of codes and databases designed for probabilistically simulating the release and transport of disposed radionuclides from a repository to the biosphere for post-closure performance assessment. Primary components of GDSA Framework include PFLOTRAN to simulate the major features, events, and processes (FEPs) over time, Dakota to propagate uncertainty and analyze sensitivities, meshing codes to define the domain, and various other software for rendering properties, processing data, and visualizing results.

FY 2022 Accomplishments: The FY 2022 advances in GDSA Framework development include:

- *Software and hardware infrastructure*. Completed second year of operational use of specialized software for managing, prioritizing, and tracking PFLOTRAN development requests (Section 4.1.1.1); established 22 software requirements for RICHARDS (unsaturated) flow mode and related verification tests in the GDSA Quality Assurance (QA) test framework (Section 4.1.1.2)

- *PFLOTRAN performance improvements*. Added a custom characteristic curve capability to mitigate PFLOTRAN convergence problems (Section 4.1.2.1); added the Newton Trust Region Dogleg Cauchy solver to the PETSc solver library with two demonstrations showing advantages of the solver (Section 4.1.2.2); implemented full implicit coupling of salt effects on liquid phase properties, salt transport, and flow (Section 4.1.2.3); implemented a stairstep correction in the mapdfn.py code for use in fracture path upscaling to a nonconforming equivalent continuous porous media mesh (Section 4.1.2.4)

- *PFLOTRAN model capability development*. Sharpened strategies for prioritizing and implementing new model capabilities in PFLOTRAN (Section 4.1.3.1); completed a detailed implementation plan for a buffer erosion and waste package corrosion model for GDSA Framework (Section 4.1.3.2); completed 75% of a flexible, PFLOTRAN-compatible fuel matrix degradation (FMD) process model (Section 4.1.3.3; Appendix B); developed and tested a new second-generation FMD surrogate model approach (Section 4.1.3.3; Appendix C); improved the multi-continuum modeling of coupled fracture-matrix processes (Section 4.1.3.4); implemented a new material evolution process model (Section 4.1.3.5); implemented a new lookup table interpolation capability (Section 4.1.3.6); implemented salinity-dependent equations of state and an innovative reactive transport model for salt (Section 4.1.3.7); began developing a groundwater evolution model for the crystalline reference case (Section 4.1.3.8; Appendix D); completed a design document for a multifaceted biosphere model (Section 4.1.3.9)

- *Other GDSA Framework development*. Applied the recently developed GDSA Workflow graphical interface to the DECOVALEX crystalline repository reference case (Section 4.2.1); developed a Geologic Framework Model for the interface between crystalline rock and the biosphere (Section 4.2.2); created a new open-source version of the meshing code VoroCrust and used it in a shale repository demonstration (Section 4.2.3); developed and tested uncertainty and sensitivity analysis methods on applications involving discrete fracture networks and the new neural network FMD surrogate model (Section 4.2.4); developed and simulated new repository reference case models for Task F of the international DECOVALEX project (Section 4.2.5); improved generic reference case models for crystalline, salt, and unsaturated alluvium host rocks (Section 4.2.6); expanded documentation of GDSA calculations and GDSA Framework model capabilities (Section 4.2.7)

- *Outreach*. Engaged internationally via leadership in DECOVALEX and geologic repository clubs and participation in conferences, papers, and external reviews (Section 4.3.1); developed and shared new versions and applications of open-source and freely available software used in GDSA Framework (Section 4.2.3); held a virtual PFLOTRAN short course (Nole et al. 2022, Section 2.4.5); maintained an external GDSA Framework website (Section 4.3.3)

- *Integration and planning*. Mapped FY 2022 GDSA activities to SFWST disposal near-term GDSA thrusts and showed that each near-term GDSA thrust is being addressed (Section 3)

An important responsibility of the GDSA Framework development team is to integrate with disposal R&D activities across the SFWST Campaign to ensure that R&D activities support the development of GDSA Framework. In FY 2022, the team continued to participate with other scientists and engineers at LANL, LBNL, PNNL, ORNL, INL, ANL, DOE, and SNL in the development of fracture network models, Geologic Framework Models, FMD model integration, DECOVALEX-2023 Task F performance assessment, multi-continuum modeling, machine learning approaches, and advanced biosphere modeling.

The ability to simulate increasingly complex repository reference cases continues to affirm that GDSA Framework can be used to simulate important multi-physics couplings directly in a total system safety assessment demonstration. Reference-case-repository applications show that GDSA Framework can simulate complex coupled processes in a multi-kilometer domain while simultaneously simulating sub-meter-scale coupled behavior in the vicinity of each modeled waste package. Continued development will further enhance the preparedness of GDSA Framework for application in the future when transitioning to a program with potential sites.

Future Work: The SFWST Disposal Research R&D 5-Year Plan will continue to guide GDSA work in the development of:

- Advanced coupled process simulation capabilities,
- State-of-the-art uncertainty and sensitivity analysis,
- Traceable, user-friendly workflow for GDSA Framework,
- Repository systems analysis for various disposal concepts and selected host rocks, and
- Development of geologic models with interactive, web-based visualization.

This report fulfills the GDSA Framework Development Work Package Level 2 Milestone – *GDSA Framework Development and Process Model Integration*, M2SF-22SN010304093.

CONTENTS

FIGURES

Page

TABLES

Page

NOMENCLATURE

1D, 2D, 3D	one-, two-, and three-dimensional
ADE	advection-dispersion equation
ANL	Argonne National Laboratory
ANN	artificial neural network
CLT	corrosion layer thickness
DCDM	Dual Continuum Disconnected Matrix
DECOVALEX	Development of COupled models and their VALidation against Experiments
DFN	discrete fracture network
DOE	U.S. Department of Energy
DPC	dual-purpose canister
DR	disposal research
DRZ	disturbed rock zone
EBS	engineered barrier system
ECPM	equivalent continuous porous medium
Eq.	equation
FDR	fractional dissolution rate
FEP	feature, event, or process
FMD	Fuel Matrix Degradation
FY	fiscal year
g	gram
GB	gigabytes
GDSA	Geologic Disposal Safety Assessment
GFM	geological framework model
GPM	gallons per minute
GUI	graphical user interface
GWd	gigawatt day
HDF5	hierarchical data format, version 5
HLW	high-level nuclear waste
HPC	high-performance computing
IAEA	International Atomic Energy Agency
ID	identification number
INL	Idaho National Laboratory
IRF	instant release fraction
IWM	Integrated Waste Management
K	Kelvin
K_D	distribution coefficient
km	kilometer
kNNr	k Nearest-Neighbors regressor
LANL	Los Alamos National Laboratory
LBNL	Lawrence Berkeley National Laboratory
LGPL	lesser general public license
LHS	Latin hypercube sampling
m	meter

M	molar
MATLAB	programming language by MathWorks
MB	megabytes
ML	machine learning
mm	millimeter
mM	millimolar
mol	mole
MPa	megapascal
MS	Microsoft
MTHM	metric tons of heavy metal
MWd	megawatt day
NA	not applicable
NBS	natural barrier system
NE	Office of Nuclear Energy
NEA	Nuclear Energy Agency
NGW	Next-Generation Workflow
NM	New Mexico
NTRDC	Newton Trust Region Dogleg-Cauchy
OECD	Organization for Economic Co-operation and Development
OFCT	Office of Fuel Cycle Technology
OoR	out of reactor
ORNL	Oak Ridge National Laboratory
OWL	Online Waste Library
PA	performance assessment
PCE	Polynomial Chaos Expansion
PDE	partial differential equation
PETSc	Portable Extensible Toolkit for Scientific Computation
PFLOTRAN	massively parallel reactive flow and transport model for describing subsurface processes (pflotran.org)
pH	negative logarithm of hydrogen ion activity
PNNL	Pacific Northwest National Laboratory
PWR	pressurized water reactor
QA	quality assurance
QoI	quantity (or quantities) of interest
RAM	random access memory
R&D	research and development
s	seconds
S&T	Storage and Transportation
SA	sensitivity analysis
SDA	SFWD Document Archive
SFWD	Spent Fuel and Waste Disposition
SFWST	Spent Fuel and Waste Science and Technology
SKB	Swedish Nuclear Fuel and Waste Management Company
SNF	spent nuclear fuel
SNL	Sandia National Laboratories
THMC	thermal-hydrologic-mechanical-chemical
UA	uncertainty analysis

UFD	Used Fuel Disposition
UO_2	uranium dioxide
UQ	uncertainty quantification
U.S.	United States of America
W	watt
WF	waste form
WIPP	Waste Isolation Pilot Plant
WP	waste package
yr	year

1. INTRODUCTION

The Spent Fuel and Waste Science and Technology (SFWST) Campaign of the U.S. Department of Energy (DOE) Office of Nuclear Energy (NE), Office of Spent Fuel & Waste Disposition (SFWD) is conducting research and development (R&D) on geologic disposal of spent nuclear fuel (SNF) and high-level nuclear waste (HLW). A high priority for SFWST disposal R&D is disposal system modeling (Sassani et al. 2021).

The SFWST Geologic Disposal Safety Assessment (GDSA) Framework Development work package is charged with developing an open-source probabilistic modeling and analysis capability for evaluating/estimating generic disposal system post-closure performance for nuclear waste disposal concepts in a range of geologic media. The modeling capability under development is called GDSA Framework (pa.sandia.gov). GDSA Framework is a coordinated set of codes and databases designed for probabilistically simulating the release and transport of disposed radionuclides from a repository to the biosphere for post-closure performance assessment.

The primary components of GDSA Framework include PFLOTRAN to simulate the major features, events, and processes (FEPs) over time, Dakota to propagate uncertainty and analyze sensitivities, meshing codes to define the domain, and various other software for rendering properties, processing data, and visualizing results. PFLOTRAN is a multi-physics thermal-hydrologic-chemical reaction and mass transport code (pflotran.org), and Dakota (dakota.sandia.gov) is used to propagate uncertainty and variability using multiple realizations and to quantify the effects of model parameters on model outputs (see Section 2.2 for details of both). These codes are designed for massively-parallel processing in a high-performance computing (HPC) environment.

Developing GDSA Framework in an open-source environment promotes collaboration with regulators, stakeholders, and the scientific community, facilitates development of the software, and enhances communication in a regulatory environment. GDSA Framework is being developed currently for generic disposal concepts so it is poised to be applied efficiently in future programs to specific disposal concepts being evaluated for comparison to regulatory safety criteria.

GDSA Framework defines the state-of-the-art by evolving continuously with progress of the technology and science and provides a nimble tool for application in the full range of possible future systems for more specific evaluations once a program is reinstituted for performance assessment (PA) of any potential candidate sites within this century. Although the current focus is on incorporation of the most important technical processes for barrier capabilities/functions (e.g., radionuclide retention), advances in computing speed are expected to continue for ultimate application in any future program.

For the near term, objectives are focused on including essential FEPs in GDSA Framework and on developing a suite of probabilistic generic repository reference case applications. In addition, the products of the near-term objectives are useful for evaluating the effects of FEPs and input parameters on repository performance, which is useful for R&D planning.

For fiscal year (FY) 2022, six tasks were planned and addressed:

- Use the 5-year Disposal Research R&D Plan (Sassani et al. 2021) to help identify additional capabilities needed in the short term and long term to advance GDSA Framework (e.g., multiphase processes, temperature dependencies, chemical processes, engineered barrier system (EBS) degradation processes, computational efficiency, gridding capability).

- Integrate subsystem models developed under this and other SFWST work packages into GDSA Framework software and safety assessments (e.g., waste form (WF) degradation, waste package (WP) degradation, EBS chemistry, EBS flow and transport, discrete fracture networks, thermal-hydrologic-mechanical-chemical (THMC) processes, natural system flow and transport, geologic framework models).
- Develop and implement methods for computationally efficient multi-scale, multi-physics modeling (e.g., surrogate models, reduced-order models, physics-based machine learning, nested models, Voronoi cell refinement). This task aims to improve integration of complicated processes in probabilistic safety assessments.
- Document, test, and maintain model capabilities of GDSA Framework (e.g., conceptual and mathematical models, assumptions, ranges, limitations), expand regression testing as needed to demonstrate and assure continued quality, and work toward a GDSA Framework release package that enhances traceability, reproducibility, user-friendliness, and integration of components (e.g., dfnWorks, Online Waste Library).
- Demonstrate components of GDSA Framework at national and international forums and support an international DECOVALEX activity for a multi-year PA modeling comparison of reference repository systems. Plan to conduct an international workshop to promote accelerated use of PFLOTRAN and other components of GDSA Framework worldwide to expand the user base, which creates additional testing of GDSA Framework components and further development by outside contributors.
- Participate in technical training (e.g., classes/workshops in Python, simulation and analysis software, or computational and analysis methods), technical conferences, and international clubs and initiatives with direct benefit to GDSA.

Section 2 of this report describes the conceptual model framework and the PFLOTRAN-based computational framework for GDSA Framework. Section 3 examines how the FY 2022 activities of the GDSA Framework development team are linked to the 5-Year Plan near-term GDSA thrusts. Section 4 (and its supporting appendices) highlights the team's major advances and activities in FY 2022. Conclusions are summarized in Section 5.

This report fulfills the requirements of the GDSA Framework Development work package (SF-22SN01030409) Level 2 Milestone – GDSA Framework Development and Process Model Integration FY2022, M2SF- 22SN010304093. The work presented herein builds on previous reports, i.e., Freeze et al. (2013a); Sevougian et al. (2013); Sevougian et al. (2014); Mariner et al. (2015); Mariner et al. (2016); Mariner et al. (2017); Mariner et al. (2018); Mariner et al. (2019); Sevougian et al. (2019a); Sevougian et al. (2019b); Mariner et al. (2020a); Mariner et al. (2020b), and Mariner et al. (2021).

2. GDSA FRAMEWORK

A safety case for a deep geologic disposal facility is a comprehensive set of bases and analyses designed, in part, to assess regulatory compliance with respect to safety standards. More specifically, it is a widely accepted approach for documenting the bases for the understanding of the disposal system, describing the key justifications for its safety, and acknowledging the unresolved uncertainties and their safety significance (OECD 2004; IAEA 2006; Freeze et al. 2013b). A full safety case may only be constructed for a specific site with an integrated design, but aspects of a safety case may also be developed for generic systems being evaluated in the SFWST Campaign.

Building a generic safety case focuses on three primary components related most directly to post-closure safety assessments: 1) a safety strategy for the generic disposal concept, 2) technical bases for the natural and engineered barriers, and 3) a safety assessment of system performance.

- The safety strategy provides direction and boundaries for the safety case. It guides the safety case by identifying requirements for site location, repository design, and safety objectives.
- Technical bases are the laws of nature and the physical and chemical barriers that govern the system. They address each FEP that could potentially facilitate or inhibit the transport of radionuclides from the repository to the biosphere. Development of the technical bases involves site characterization (mainly as defined/constrained characteristics for generic sites), FEPs identification including waste inventory, barriers to radionuclide release and migration, radionuclide behavior, and using natural analogs, model validation, code verification, and uncertainty quantification.
- Safety assessment involves the analysis of technical bases to evaluate whether the objectives of the safety strategy are met. In safety assessment, each FEP screened in the technical bases is either included/incorporated into the probabilistic performance assessment (PA) model or is excluded and addressed in separate analyses or process model simulations. In the PA model, regulatory metrics (e.g., annual dose rate) are estimated with probabilistic calculations to compare to regulatory limits.

The goals and objectives of the GDSA Framework development team focus on safety assessment and, more specifically, on the development of the GDSA Framework modeling capability and the PA models of generic reference case applications simulated using GDSA Framework.

Performance assessment for underground geologic disposal of nuclear waste is an iterative process for evaluating a comprehensive set of FEPs to determine the safety relevant FEPs to include in a PA model. Probabilistic PA model simulations are performed to estimate the full range of behavior of the system including the pertinent variability and uncertainty in the system, and results are evaluated against system performance metrics (e.g., for evaluating key sensitivities needing further constraint or for assessing performance against regulatory requirements). Uncertainty and sensitivity analyses may also be performed to inform prioritization of additional research and/or model development within a program.

A PA model has a conceptual model framework and a computational framework. These frameworks are summarized in Sections 2.1 and 2.2, respectively. An overview of PA methodology and terminology is presented in Sevougian et al. (2014, Section 2.2), Meacham et al. (2011, Section 1) and elsewhere (Rechard 2002).

2.1 Conceptual Model Framework

A conceptual model framework for a PA model requires a coherent representation of pertinent FEPs. Figure 2-1 schematically illustrates the conceptual model framework for a repository system. To calculate a dose to a receptor in the biosphere, radionuclides released from the waste form must pass through the repository EBS and the surrounding natural barrier system (NBS).

A FEPs database like the one developed and described in Freeze et al. (2011) can be used to help identify a full set of potentially important FEPs for a specific conceptual repository model. Many of the FEPs in a FEPs database may be directly simulated in the PA model. In a comprehensive PA, excluded FEPs (i.e., FEPs not simulated in the PA model) must be addressed in separate analyses and arguments.

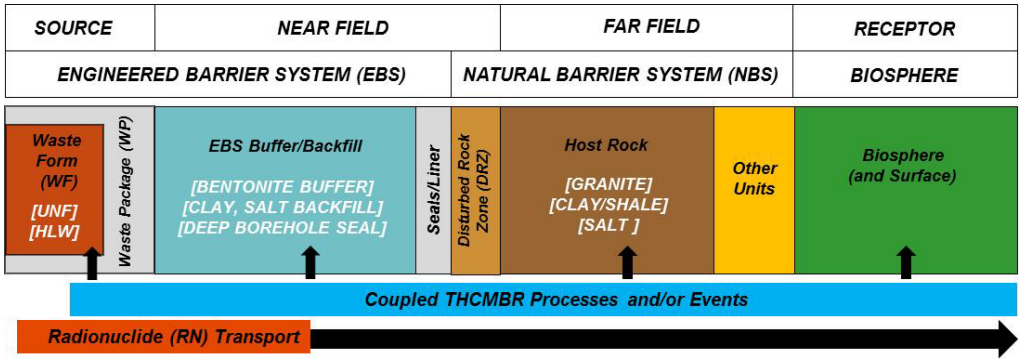

Figure 2-1 Schematic diagram of the conceptual model framework of a generic geologic disposal system PA model

2.2 Computational Framework

Performance assessment of a geologic repository is aided by directly modeling the important coupled processes in the system and executing multiple probabilistic realizations. The approach of propagating uncertainty in computational PA models is a continuation of the successful modeling approaches adopted for the Waste Isolation Pilot Plant (WIPP) PAs (Rechard 1995; Rechard 2002; Rechard and Tierney 2005) and for disposal of SNF and HLW in volcanic tuff (Rechard and Stockman 2014).

GDSA Framework is used to execute the computational PA model. GDSA Framework consists of the following components:

- Input parameter databases
- Software for sampling, sensitivity analysis, uncertainty quantification (UQ), workflow, and traceability (Dakota)
- Petascale multiphase flow and reactive transport code (PFLOTRAN), working in concert with coupled process model codes (e.g., Fuel Matrix Degradation (FMD) model)
- Computational support software and scripts for meshing, stochastic preprocessing, output processing, and visualization of results (e.g., CUBIT, VoroCrust, dfnWorks, Python, ParaView).

The two primary components of this computational framework are PFLOTRAN and Dakota. PFLOTRAN is a thermal-hydrologic-chemical multi-physics code used to simulate coupled multi-physics processes affecting waste isolation in a repository system and transport of released radionuclides to the biosphere over time. Simulated processes include heat flow, fluid flow, waste dissolution, radionuclide release, radionuclide decay and ingrowth, precipitation and dissolution of secondary phases, and

radionuclide transport. Dakota is an uncertainty sampling and propagation code. Dakota is used to propagate uncertainty in PFLOTRAN simulations and to analyze PFLOTRAN results to assess sensitivities of model processes and inputs. Dakota is also used to graphically run and document the entire workflow of probabilistic simulations. These two codes are described in more detail in Sections 2.2.1 and 2.2.2.

The flow of data and calculations through the components of GDSA Framework is illustrated in Figure 2-2. In a probabilistic simulation, Dakota's Next Gen Workflow manages the entire simulation from the generation of stochastic input for each PA realization to the execution of PFLOTRAN and production of custom output files via Python scripts. The sampled inputs are used by PFLOTRAN and its coupled process models to simulate source term release, EBS evolution, flow and transport through the EBS and NBS, and uptake in the biosphere. After the simulation, various software (e.g., Python, Matplotlib, ParaView) may be used to reduce and illustrate the output results of parameters and performance metrics. Dakota may also be used to evaluate the effects of parameter uncertainty on specific outputs.

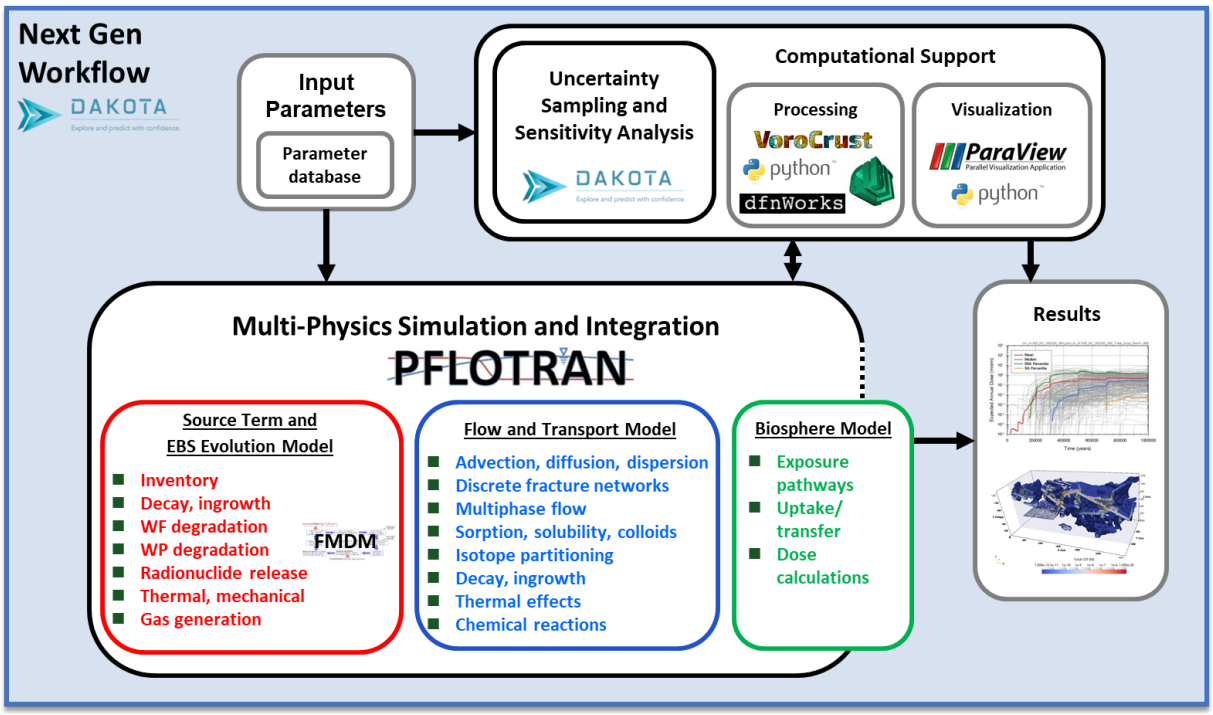

Figure 2-2 GDSA Framework structure

2.2.1 PFLOTRAN

PFLOTRAN (Hammond et al. 2011a; Lichtner and Hammond 2012) is an open source, reactive multi-phase flow and transport simulator designed to leverage massively-parallel HPC to simulate subsurface earth system processes. PFLOTRAN has been employed on petascale leadership-class DOE computing resources (e.g., Jaguar [at Oak Ridge National Laboratory (ORNL)] and Franklin/Hopper [at Lawrence Berkeley National Laboratory (LBNL)]) to simulate THC processes at the Nevada Test Site (Mills et al. 2007), multi-phase CO_2-H_2O for carbon sequestration (Lu and Lichtner 2007), CO_2 leakage within shallow aquifers (Navarre-Sitchler et al. 2013), and uranium fate and transport at the Hanford 300 Area (Hammond et al. 2007; Hammond et al. 2008; Hammond and Lichtner 2010; Hammond et al. 2011b; Chen et al. 2012; Chen et al. 2013). PFLOTRAN is also under development for use in PA at the Waste Isolation Pilot Plant (WIPP).

PFLOTRAN solves the non-linear partial differential equations describing non-isothermal multi-phase flow, reactive transport, and geomechanics in porous media. Parallelization is achieved through domain decomposition using the Portable Extensible Toolkit for Scientific Computation (PETSc) (Balay et al. 2013). PETSc provides a flexible interface to data structures and solvers that facilitate the use of parallel computing. PFLOTRAN is written in Fortran 2003/2008 and leverages state of the art Fortran programming (i.e. Fortran classes, pointers to procedures, etc.) to support its object-oriented design. The code provides "factories" within which the developer can integrate a custom set of process models and time integrators for simulating surface and subsurface multi-physics processes. PFLOTRAN employs a single, unified framework for simulating multi-physics processes on both structured and unstructured grid discretizations (i.e., there is no duplication of the code that calculates multi-physics process model functions in support of structured and unstructured discretizations). The code requires a small, select set of third-party libraries (e.g., MPI, PETSc, BLAS/LAPACK, HDF5, Metis/Parmetis). Both the unified structured/unstructured framework and the limited number of third-party libraries greatly facilitate usability for the end user.

2.2.2 Dakota

The Dakota software toolkit is open-source software developed and supported at Sandia National Laboratories (Adams et al. 2012; Adams et al. 2013). Dakota provides deterministic codes an extensible interface for propagating uncertainty into a set of realizations and for performing sensitivity analysis and optimization. GDSA Framework uses Dakota's sampling schemes, principally Latin Hypercube Sampling (LHS), to propagate input value uncertainty into probabilistic PFLOTRAN simulations. Dakota is also used in sensitivity analyses to analyze the effects of input value uncertainty on probabilistic GDSA Framework results. In addition, Dakota's Next Gen Workflow capability was recently incorporated to develop a graphical workflow interface to execute and manage probabilistic GDSA Framework applications.

3. GDSA FRAMEWORK DEVELOPMENT PLAN

This section identifies high priorities for GDSA Framework development (Sections 3.1 and 3.2) and how those priorities are being addressed (Section 3.3).

3.1 5-Year Plan

The priorities of SFWST disposal research are documented in *SFWST Disposal Research R&D 5-Year Plan – FY2021 Update* (Sassani et al. 2021). In the plan, activities for each disposal research R&D technical area are evaluated and categorized in terms of near-term (1-2 years) and longer-term (3-5 years) thrusts. The objective of the GDSA technical area is "to develop and continuously maintain a state-of-the-art software framework for probabilistic post-closure performance assessment analyses of facilities for deep geologic disposal of nuclear waste."

The near-term primary thrusts for the GDSA technical area are:

- Advanced coupled process simulation capabilities (G01),
- State-of-the-art uncertainty and sensitivity analysis (G02),
- Traceable, user-friendly workflow for GDSA Framework (G03),
- Repository systems analysis for various disposal concepts and selected host rocks (G04), and
- Development of geologic models with interactive, web-based visualization (G05).

The near-term GDSA thrusts are provided verbatim in Appendix A. Longer-term (3-5 years) thrusts include multi-fidelity modeling, in-package chemistry, gas flow in the EBS, cement seal evolution, new repository designs, and preparation for site applications. An additional GDSA focus area identified in Section 3 of the plan addresses in-drift coupled chemistry modeling and major chemical reactions with materials over appropriate temperature ranges.

3.2 2019 Roadmap Update for GDSA

Development of the 5-year plan was influenced by the 2019 Disposal Research R&D Roadmap Update (Sevougian et al. 2019a) and the 2012 Used Fuel Disposition (UFD) Campaign Roadmap (DOE 2012). The 2019 Roadmap Update highlighted progress, priorities, and remaining gaps in disposal research R&D activities.

Activities defined and tracked in the 2019 Roadmap Database are a collection of specific disposal research objectives focused on improving knowledge of FEPs and how they affect repository performance. They include:

- Collecting and measuring the properties of features (e.g., radionuclides, waste forms, waste packages, buffer, damaged rock zone, repository layout, host rock, etc.) and their associated uncertainties
- Identifying and modeling important processes (e.g., flow of heat and groundwater, waste package degradation, waste form degradation, radionuclide adsorption, buffer evolution, etc.) at small scale and/or in repository simulations
- Estimating the magnitudes, consequences, and probabilities of events that might affect repository performance (e.g., criticality, disruptive events)

- Developing tools and processes to propagate uncertainties in repository performance calculations and to enhance sensitivity analysis

A total of 17 activities were defined for GDSA PA in the 2019 Roadmap Update (Sevougian et al. 2019a). They are listed in Table 3-1. The linkages between the GDSA thrusts and the GDSA Roadmap activities are evaluated in Mariner et al. (2021, Section 5.3).

Table 3-1 GDSA PA activities in the Roadmap Database of the 2019 Disposal R&D Roadmap update

Activity	*Gap	Name
P-01		*CSNF repository argillite reference case*
P-02		*CSNF repository crystalline reference case*
P-03		*CSNF repository bedded salt reference case*
P-04		*CSNF repository unsaturated zone (alluvium) reference case*
P-05		*Disruptive events*
P-06		*(Pseudo) colloid-facilitated transport model*
P-07		*Intrinsic colloid model*
P-08	*	*Other missing FEPs (processes) in PA-GDSA*
P-09		*Surface processes and features*
P-10		*Uncertainty and sensitivity analysis*
P-11	*	*Pitzer model*
P-12		*WP degradation model framework*
P-13	*	*Full representation of chemical processes in PA*
P-14		*Generic capability development for PFLOTRAN*
P-15	*	*Species and element properties*
P-16	*	*Solid solution model*
P-17	*	*Multi-component gas transport*

3.3 Alignment of GDSA Framework Development Activities with Near-Term GDSA Thrusts and 2019 Roadmap

GDSA Framework development activities undertaken in FY 2022 are listed in Table 3-2. They are linked in Table 3-2 to near-term GDSA thrusts (Section 3.1) and 2019 Roadmap activities (Section 3.2). As indicated, each GDSA near-term thrust was addressed to some degree in FY 2022.

GDSA Framework development activities commonly involve careful integration between SNL GDSA work packages and other parties. The major parties involved in the FY 2022 GDSA Framework development activities are also identified in Table 3-2.

Table 3-2 FY 2022 GDSA Framework development activities mapped to GDSA Roadmap activities and 5-Year Plan near-term GDSA thrusts

FY 2022 GDSA Framework Development Activities	FY 2022 Participants	Roadmap Database PA Activity	Near-Term GDSA Thrusts
Agile/Jira system operation (Section 4.1.1.1)	SNL	-	G01, G03
Biosphere modeling (Section 4.1.3.9)	PNNL, SNL	P-08, P-09	G01, G04
Buffer evolution (Section 4.1.3.2)	SNL	P-01, P-02, P-14	G01
DECOVALEX-2023 Task F: Performance assessment (Section 4.2.5)	SNL, LBNL, LANL, International	P-02, P-03, P-05, P-12	G02, G04
dfnWorks development and integration (Sections 4.2.5.1, 4.2.6, and 4.2.7.1)	LANL, SNL	P-02, P-10, P-14	G01, G02
Fracture path upscaling (Section 4.1.2.4)	SNL, LANL	P-02	G01, G03
Fuel matrix degradation (Section 4.1.3.3, Appendix B, and Appendix C)	SNL, ANL, PNNL	P-13, P-14	G01
GDSA documentation (Section 4.2.7.1)	SNL	-	G01, G03
GDSA Workflow (Section 4.2.1)	SNL	-	G02, G03
Geologic Framework Model (Section 4.2.2)	SNL, LANL, INL	P-01, P-02, P-04, P-09	G03, G04, G05
Groundwater chemistry modeling (Section 4.1.3.7, Section 4.1.3.8, and Appendix D)	SNL	P-11, P-13	G01
Machine-learning surrogate models (Sections 4.1.3.3 and 4.2.4)	SNL, LBNL	P-14	G01
Material evolution (Section 4.1.3.5)	SNL	P-14	G01
Multi-continuum transport development (Section 4.1.3.4)	SNL, LANL	P-02, P-14	G01
Multifidelity uncertainty methods (Section 4.2.4.1)	SNL	P-10	G02
PFLOTRAN convergence (Section 4.1.2)	SNL	P-01, P-02, P-03, P-04, P-17	G01
Process/surrogate model coupling (Sections 4.1.3.1 and 4.1.3.6)	SNL	P-14	G01
QA toolbox and test suite development (Section 4.1.1.2)	SNL	-	G03
Repository reference case development (Section 4.2.6)	SNL	P-01, P-02, P-03, P-04, P-10	G02, G03, G04
Re-saturation modeling (Sections 4.1.2.1 and 4.1.3.7)	SNL	P-14	G01, G04
Uncertainty and sensitivity analysis (UQ/SA) (Section 4.2.4)	SNL, International	P-02, P-03, P-10	G02, G04
Voronoi meshing and simulation (Section 4.2.3)	SNL, LANL	P-01, P-02, P-03, P-04, P-09	G01, G04, G05
Waste package degradation (Section 4.1.3.2)	SNL	P-12, P-13	G01

4. GDSA FRAMEWORK DEVELOPMENT

GDSA Framework is maturing into a highly capable PA modeling tool for deep geologic disposal of nuclear waste. Since adoption of the PFLOTRAN-Dakota approach in 2013, many features and processes important to disposal PA have been added to the framework. In addition, generic reference cases have been developed for different host rocks and disposal concepts, and probabilistic and sensitivity analysis tools have been refined and demonstrated on a subset of those reference cases. Advances in the capabilities of the framework are aided by collaboration with other work packages of the SFWST Campaign (and the previous Used Fuel Disposition (UFD) Campaign) and by ongoing interaction with the international community. A historical summary of developments in GDSA Framework from 2010 to 2019 is provided in Mariner et al. (2019).

Guided by the SFWST Disposal Research R&D 5-Year Plan – FY2021 Update (Sassani et al. 2021), and more distantly by the Roadmap reevaluation exercise in FY 2019 (Sevougian et al. 2019a), the GDSA Framework development team continued to make advances in FY 2022. This section describes advances pertaining to general code development, meshing, uncertainty quantification, workflow, outreach, and international collaboration.

PFLOTRAN advances in FY 2022 are summarized in Section 4.1. Much of this development is described in detail in the recent PFLOTRAN development report (Nole et al. 2022). More general GDSA Framework advances are described in Section 4.2, many of which are also covered in more detail in other reports (e.g., LaForce et al. 2022; Swiler et al. 2022). Section 4.3 addresses international and outreach activities.

4.1 PFLOTRAN Development

The development of PFLOTRAN for GDSA Framework continued at a strong pace in FY 2022. Important advances were made in PFLOTRAN infrastructure (Section 4.1.1), code performance (Section 4.1.2), and process model development (Section 4.1.3).

4.1.1 Software and Hardware Infrastructure

4.1.1.1 Code Management System

To help manage code development activities, the PFLOTRAN development team uses the Atlassian Jira issue and project tracking software. Jira issues range from major upgrades and additions to small tasks and bug corrections. Every two weeks, the team assesses progress made, categorizes newly submitted issues, re-prioritizes issues as needed, and confirms assignments for the next two weeks.

Figure 4-1 shows a running tally of task statuses from May 2020 to June 2022. Details about the tracking software, how the team utilizes it, and specific issues addressed can be found in Section 2.1.1 of Nole et al. (2022).

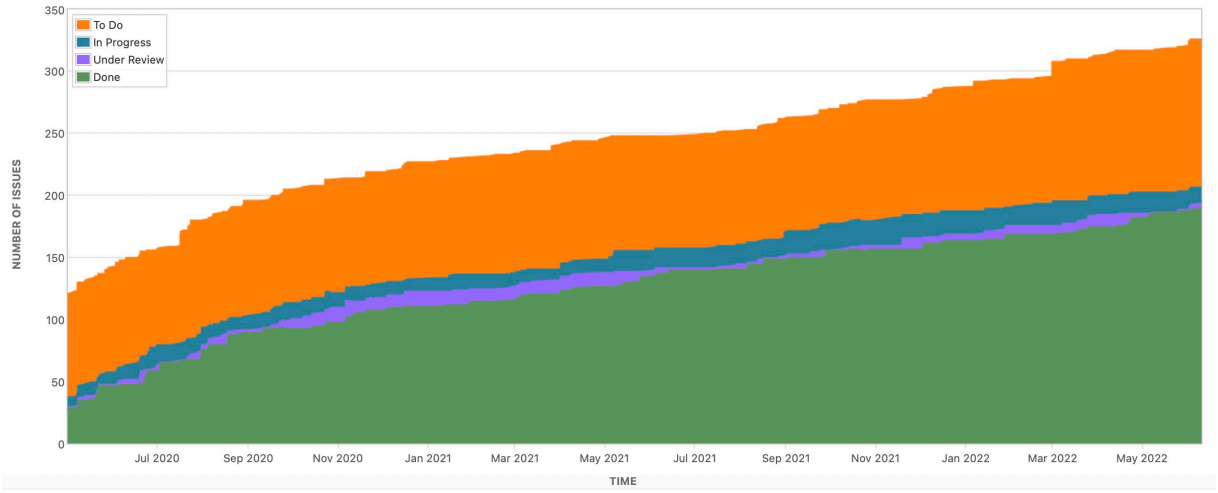

Figure 4-1 Number and status of sprint issues over time (Nole et al. 2022)

4.1.1.2 Quality Assurance

The PFLOTRAN development team continued in FY 2022 to expand and upgrade the Quality Assurance (QA) test framework. This year's work focused largely on the QA for RICHARDS mode of PFLOTRAN for simulating fluid flow. A total of 22 requirements for RICHARDS mode were defined to satisfy functionality needed for GDSA Framework. Tests were identified for each requirement, many of which came from the existing test suite. Several tests were added, including a test comparison against a different flow simulator, TOUGH3.

The full test suite for RICHARDS mode was automated to run the tests and calculate error metrics. Currently, all error metrics are within tolerances and therefore all requirements are met. If a future change causes a test to fail, the software will notify the user. Further details of this work are presented in Section 2.1.2 of Nole et al. (2022).

4.1.2 Code Performance Improvements

4.1.2.1 Characteristic Curve Enhancements

In FY 2021, characteristic curves for media saturation in PFLOTRAN were smoothed so that PFLOTRAN solvers could handle transition to dry conditions (Nole et al. 2021). In FY 2022, the ability to use an experimentally measured characteristic curve, or other point-by-point characteristic curve, was added. This capability was needed because models for characteristic curves in PFLOTRAN are not always sufficient to capture some of the features of experimentally derived curves. Care must be taken, however, because values between points for these new curves are determined by linear interpolation. Linear interpolation can cause discontinuous or non-smooth derivatives if the capillary pressure and relative permeability datasets are not of sufficiently high resolution in regions of high curvature. Work is ongoing to study whether the use of splines can address that issue. More detailed information on this work is provided in Nole et al. (2022).

4.1.2.2 Solvers

Rapid solver convergence is a continuing challenge for increasingly complicated PFLOTRAN simulations. Flow and transport calculations rely heavily on solvers and preconditioners. In the past two years, significant advances have been made for both.

In FY 2022, the Newton Trust Region Dogleg Cauchy solver (NTRDC) was added as an option to PFLOTRAN and PETSc. NTRDC is a new trust region-based nonlinear solver developed by Heeho Park (Nole et al. 2021). PETSc is the solver library upon which PFLOTRAN is built. The NTRDC solver code was officially released March 30, 2022 in PETSc version 3.17.0 (Nole et al. 2022).

The performance of the NTRDC solver was tested in FY 2022 on three unsaturated alluvium repository simulations with three different thermal loads due to emplacing three different waste package types: 12 PWR (pressurized water reactor), 24 PWR, or 37 PWR. Higher thermal loads cause increased frequency of phase changes between liquid and gas. The NTRDC solver performed well while the default Newton Raphson nonlinear solver failed for all waste package types. Details of this study and another study (on grid convergence) using the NTRDC solver are presented in Nole et al. (2022).

4.1.2.3 Full Coupling of Salt Effects, Salt Transport, and Flow

Three major advances were made this year in PFLOTRAN flow and transport modeling in saline groundwater systems. Two advances are described in the process model development section (Section 4.1.3) because they are process model developments: new salinity-dependent equations of state and expanded solute mass balance equations (Section 4.1.3.7). The advance qualifying as a code performance improvement (Section 4.1.2) is that these new equations are now fully coupled to the flow solution.

Coupling these equations to the flow solution is a major advance over sequential coupling. With sequential coupling, salinity effects on flow properties and solute mass balances are updated during the transport solution time step and then handed to the flow solution as inputs. Sequentially coupled simulations can converge on an erroneous solution if the timestep is not sufficiently low for a given fluid velocity and grid meshing. Fully implicit coupling of the transport and flow equations provides a solution that is unconditionally stable and is not subject to the aforementioned timestep limitations.

The fully implicit solute implementation was compared to the sequential implementation by running the classic Elder problem. In the Elder problem, saltwater intrudes into an underlying freshwater aquifer by density driven flow. The results of these simulations are shown in Figure 4-2. Those of the fully implicit simulation more closely resemble those of Voss and Souza (1987). A more detailed discussion of this study is provided in Section 2.2.9.1 of Nole et al. (2022).

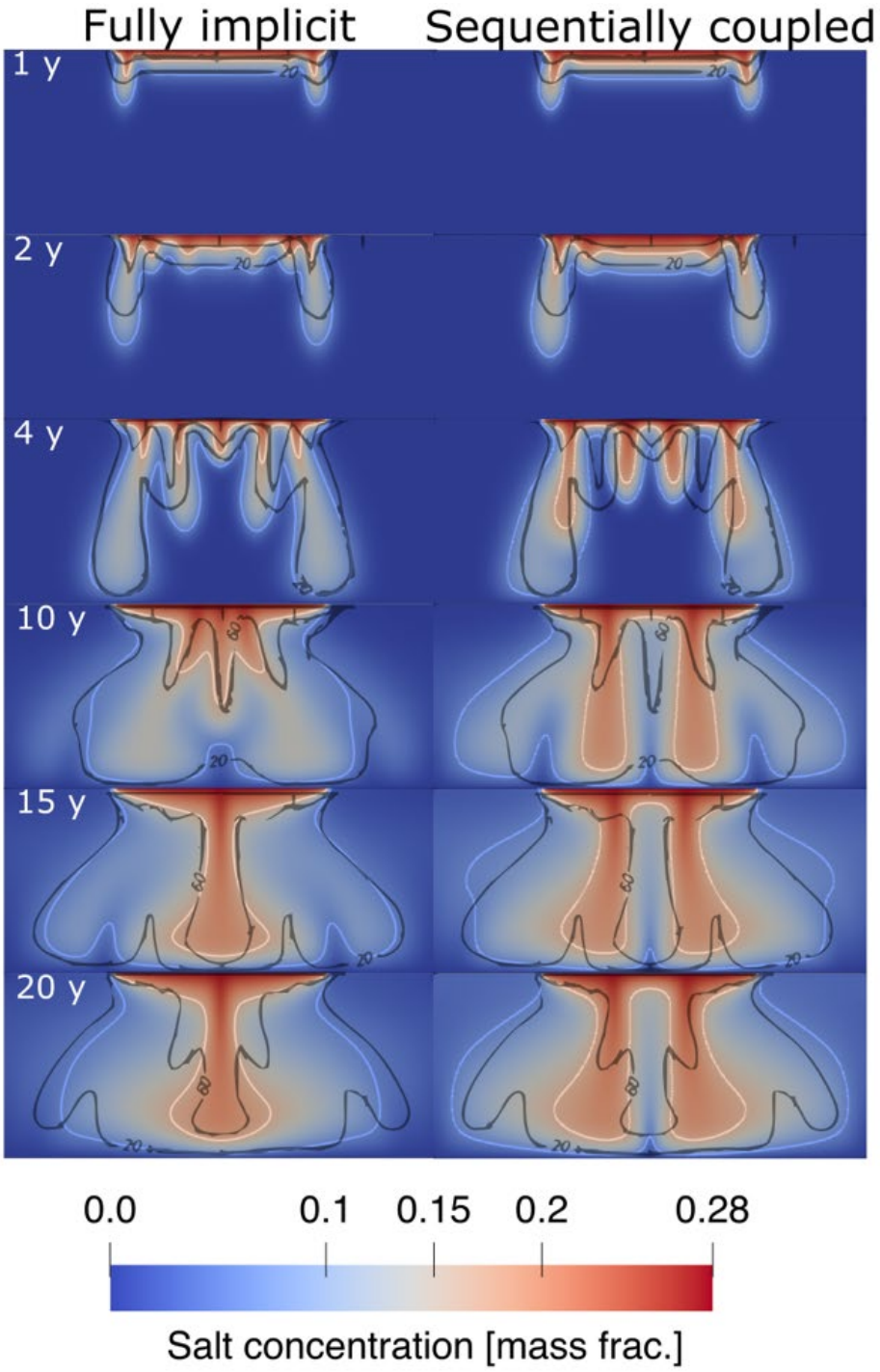

Figure 4-2 **Comparison of Elder problem results for fully implicit and sequentially coupled implementations. Voss and Souza (1987) concentration contours of 60% and 20% of the maximum concentration (black) are compared to the corresponding concentration contours (yellow and blue, respectively) of the PFLOTRAN simulations.**

4.1.2.4 Stairstep Correction for Fracture Path Upscaling

In the crystalline reference case and other GDSA simulations involving discrete fracture networks (DFNs), DFNs are upscaled to space-filling meshes. When DFNs are upscaled to hexagonal meshes, sloped fracture planes are converted into coarsely pixilated stairsteps. Stairsteps effectively result in longer path lengths and longer solute travel times.

To counter the longer path lengths generated by upscaling, a stairstep correction was implemented in mapdfn.py. The correction is derived from Sweeney et al. (2020) where the amount of correction needed is determined by the dot product between each fracture in the grid cell and the normal vector to each coordinate axis. The factor is applied based on the fracture in the cell whose angle is closest to 45°. Initial testing indicates the implementation was successful, but additional verification is needed.

4.1.3 Model Capability Development

4.1.3.1 Strategy for Model Capability Development

In FY 2020, a general strategy was developed to facilitate a streamlined quality-controlled process of integrating models into PFLOTRAN (Mariner et al. 2020a, Section 3.1.3). The approach uses the Jira issue and project tracking software discussed in Section 4.1.1.1. Requests for a code enhancement or a new process model implementation are submitted as Jira issues, along with details describing what is needed and the overall importance of the enhancements. In FY 2022, the approach was refined and used for the proposed development of the buffer erosion and waste package degradation model (Section 4.1.3.2). A summary of the refined approach is provided here.

1. To qualify for the attention of the PFLOTRAN developers, requestors must:
    a. Provide a summary of the model and general ideas for how it will be used
    b. Justify why the model is needed
        i. Is the model expected to have significant effects on important repository performance metrics or otherwise support GDSA Framework objectives?
    c. Identify all model input and output requirements including valid ranges of input values and valid combinations of input values (Detailed requirements on inputs and outputs are listed in Section 3.1.3 of Mariner et al. (2020a).)
    d. State relevant model assumptions and limitations
    e. Provide an example simulation/calculation of the model along with plots or tables of outputs
    f. Address the following questions
        i. Are all relevant model assumptions acceptable, and do the valid ranges of input values extend beyond the envelope of acceptable inputs for the intended use? If not, explain.
        ii. Are there other models or approaches with more defensible assumptions that could cover the same or larger range of applicability?
        iii. Does the standalone model converge and produce sensible results over the entire (potentially multi-dimensional) input sample space requested?
2. The developers must then:
    a. Verify that the requestor has provided the necessary information and justification

b. Decide whether the model is ready for implementation

c. Seek work package manager approval as needed to ensure support

d. Accept or reject request, documenting reasons (and management approval as needed)

Upon acceptance, the Jira issue is prioritized and, depending on whether it is high enough priority level, the Scrum Master designs a series of tasks and assigns them to the appropriate PFLOTRAN developer(s). Once assigned, the developer works with the requestor to identify the best implementation approach. Depending on the complexity of the model, the developer may establish regular meetings with the requestor during implementation.

This general approach was followed for the buffer erosion and waste package corrosion model. The requestor prepared a Microsoft (MS) Word file that addressed in detail all the information listed above, including example simulations in Mathcad and results of the calculations. The PFLOTRAN developers were satisfied with the request and because it would involve a significant effort, they shared it with the work package manager to ensure support for the implementation. The implementation has since been assigned to a developer and has been scheduled to begin in late FY 2022.

4.1.3.2 Buffer Erosion and Waste Package Degradation

Copper, due to its high chemical stability under crystalline repository conditions, continues to be a prime candidate as a waste package outer barrier material in the U.S. repository program and in the programs of many countries. In FY 2021, a concerted planning effort was made to implement buffer erosion and copper corrosion models into PFLOTRAN. The models are based on the models developed and used by SKB and Posiva for the Forsmark and Olkiluoto repositories. Adding this type of modeling capability to PFLOTRAN is expected to be useful not only for simulating buffer erosion and waste package corrosion processes in the U.S. program but also potentially to facilitate adoption and testing of PFLOTRAN for repository applications outside the U.S. The basic models are summarized in Mariner et al. (2021) and Nole et al. (2022). The conceptual buffer erosion model is illustrated in Figure 4-3.

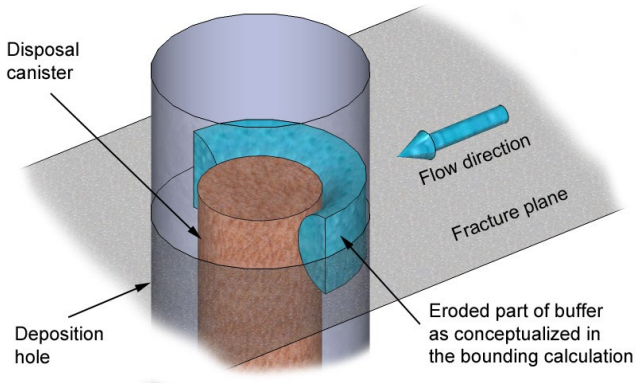

Figure 4-3 Conceptual model of buffer erosion due to a flowing fracture (Fig 6-108, Posiva 2013)

In FY 2022, with the general implementation conceptualized the year before, a MS Word file was prepared to accompany the Jira request. That file carefully described the conceptual model, inputs and outputs, the ranges of model validity for the inputs, assumptions, limitations, and the mathematical model. In addition, it provided a printout of a Mathcad model developed to show how the model worked, and it provided an application that verified that the model produced the expected results. Further, it addressed the various questions asked of a requestor when making a Jira request (Section 4.1.3.1).

The request was accepted, and the implementation is underway. A summary of the various model components and how they will be implemented is provided in Nole et al. (2022).

4.1.3.3 Fuel Matrix Degradation (FMD)

The FMD model is the uranium dioxide (UO_2) matrix degradation process model of GDSA Framework. It was developed collaboratively at Argonne National Laboratory and Pacific Northwest National Laboratory (Jerden et al. 2015b). The model, coded in MATLAB, calculates spent fuel degradation rates as a function of radiolysis, electro-kinetic reactions, alteration layer growth, and diffusion of reactants through the alteration layer. In more recent versions of the model, steel corrosion is included to provide a source of hydrogen (Jerden et al. 2018).

In FY 2015 a version of the FMD process model that excludes steel corrosion was coded in Fortran (Jerden et al. 2015a). That Fortran code was coupled to PFLOTRAN and was successfully demonstrated (Mariner et al. 2015). Apart from the computational results, the demonstration indicated that the coupled model was highly demanding computationally. Mechanistic simulation of the FMD model processes requires many calculations at each time step. For a probabilistic repository PA calculation with thousands of WPs and hundreds of realizations, the coupled Fortran code from 2015 is too expensive. Further, the is does not allow for dynamic time stepping and was not written for parallel computing.

In FY 2019 and FY 2020, two approaches were undertaken to include the FMD process model in GDSA Framework. One approach, described in the first subsection below, was to develop a new Fortran code utilizing rapid solvers and flexible time steps for a more powerful standalone FMD process model that smoothly couples to PFLOTRAN. The other approach, summarized in the second subsection, was to use Machine Learning (ML) techniques to develop surrogate models of the FMD process model for accurate and rapid emulation in PFLOTRAN.

Fortran Process Model

In FY 2019, GDSA Framework developers began building a new Fortran code to simulate the FMD process model. The objectives of the new code are a faster design, HPC-compatible, improved convergence, and improved coupling with PFLOTRAN. Also, to make the new process model more flexible than the original MATLAB code, an additional objective is to add the capability of using dynamically changing chemical and temperature inputs over time. The code will be open source.

Appendix B documents progress in FY 2022. Efforts this year concentrated on implementing the interfacial reactions of the MATLAB code. As discussed in Appendix B, interfacial reactions are implemented in a non-standard way in the MATLAB code. The MATLAB code is implemented recursively which makes reading the code more challenging. Appendix B outlines the algorithm in which the corrosion potentials are solved first and then the concentrations are updated. It also details the planned approach for improving the iterative process as the interfacial reactions are implemented.

Radiolysis has been implemented in the Fortran code using a constant value for $G_{H_2O_2}$, the primary alpha radiolysis yield of H_2O_2. For a constant value, the implementation is working as expected. A demonstration that includes diffusion is shown in Figure 4-4. A more complex model for $G_{H_2O_2}$ is needed when concentrations of H_2 are high and O_2 low (Buck et al. 2013); that model will be implemented in the future. The initial focus, however, is on implementing the interfacial reactions to complete the first overall objective, which is to develop a flexible, efficient, HPC-compatible Fortran code that reproduces the processes implemented in the MATLAB code.

A summary of recent work on this Fortran code development will appear in the proceedings of the 2022 American Nuclear Society International High-Level Radioactive Waste Management Conference. The

title of the paper is, “Development of an Efficient Version of the Fuel Matrix Degradation Model” (Harvey et al. 2022).

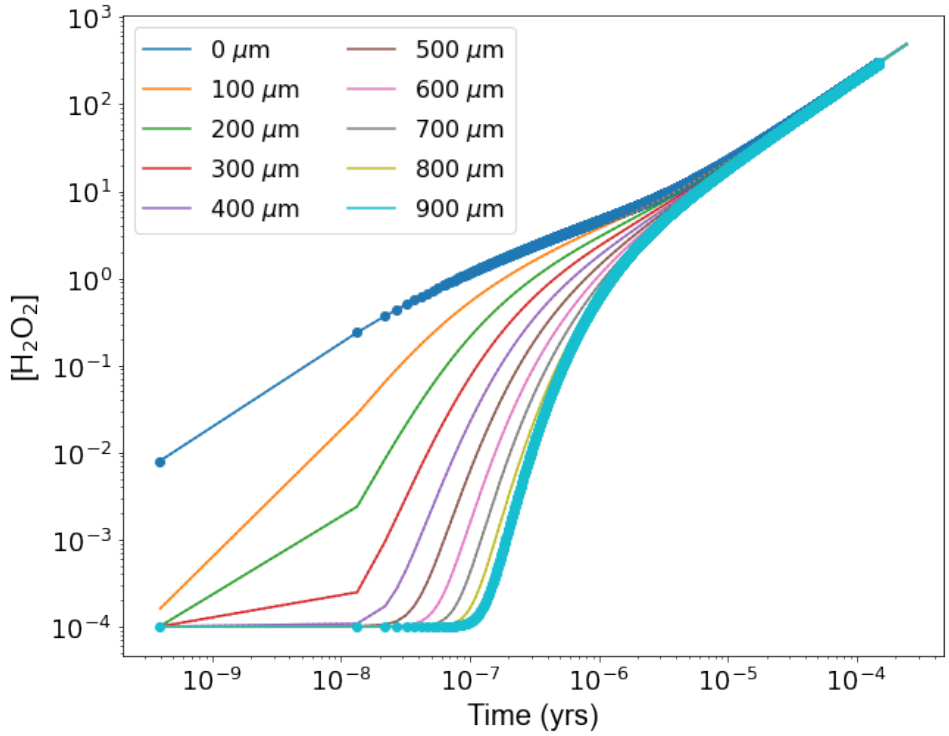

Figure 4-4 Concentration of H_2O_2 as a function of time for various distances from the fuel surface.

FMD Surrogate Models

In FY 2020, an Artificial Neural Network (ANN) surrogate model and a k-Nearest-Neighbors regression (kNNr) surrogate model were implemented in PFLOTRAN for the FMD process model (Mariner et al. 2020b). The ANN surrogate is a parametric model that utilizes a network of artificial neurons with nonlinear activation functions. The kNNr surrogate is a nonparametric model that uses an advanced interpolation approach to approximate a model response using the set of closest neighboring training points in a multidimensional database of training points.

In FY 2022, a major advance in the surrogate approach was developed and tested. The thickness of the corrosion layer on the fuel surface was built into a new version of the kNNr surrogate model. The corrosion layer thickness (CLT) – a valuable dynamic indicator of system state – grows as the fuel degrades. Importantly, CLT physically affects the fuel matrix degradation rate. Secondarily, it qualitatively indicates how long the fuel has been degrading.

To test the idea, CLT was added as an input variable to a branch of the kNNr FMD surrogate model. A new machine-learned surrogate was developed to predict both the CLT and fuel degradation rate at the current time. It was trained on a) the inputs of the original kNNr surrogate model, b) the CLT from the previous time step, and c) the time step length. In a repository reference case simulation, the predicted current CLT provides the CLT input for the kNNr surrogate model at the next time step.

Figure 4-5 and Figure 4-6 show preliminary kNNr surrogate predictions for 50 randomly sampled trajectories of the Matlab FMD process model. Aside from some deviations early in time, the CLT predictions are highly accurate, generally within 1-2% of the Matlab FMD process model “true” values.

The fuel degradation rate (UO_2 flux) prediction is noisy as it is a local prediction, drawing information only from 10 nearest neighbors to each query point in the training sample space.

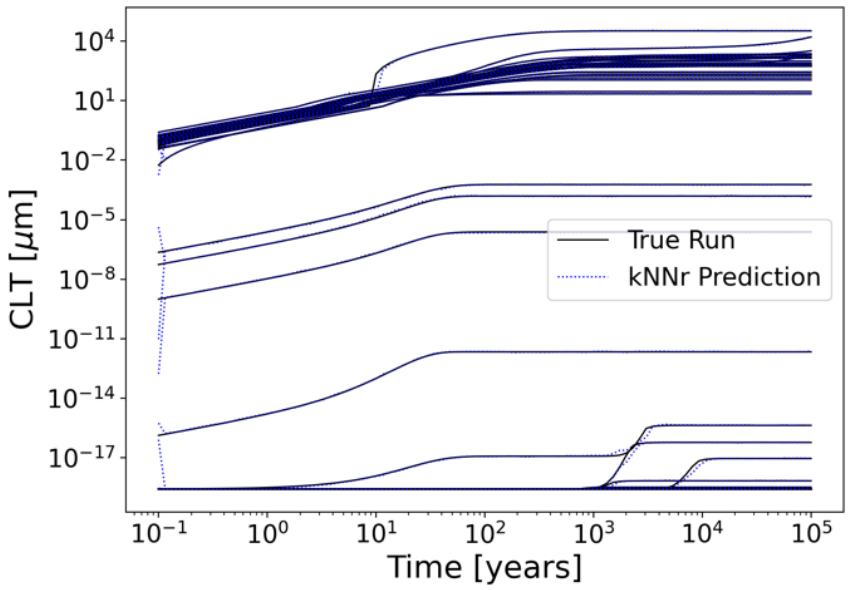

Figure 4-5 Comparison of the True and kNNr prediction of the CLT for 50 randomly selected runs in the testing data.

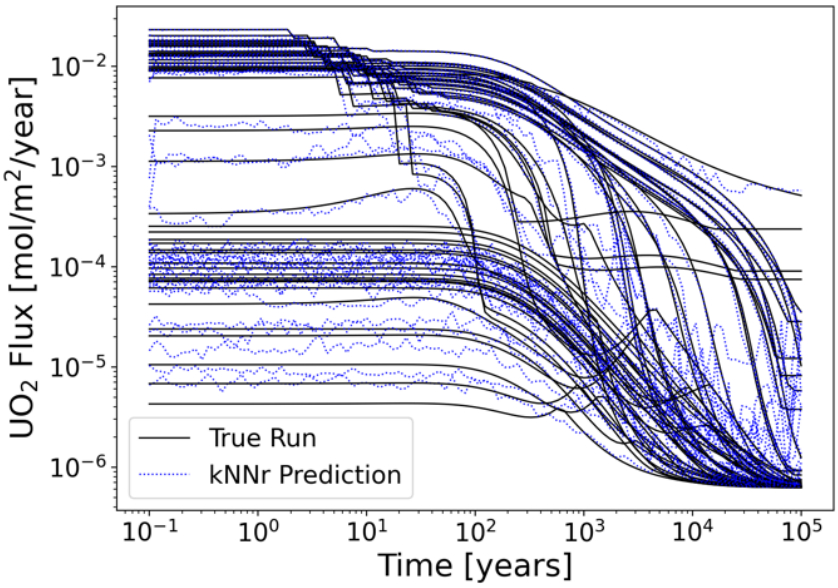

Figure 4-6 Comparison of the True and kNNr prediction of the UO2 flux for 50 randomly selected runs in the testing data.

Overall, with this kNNr configuration and 23 million training samples, the prediction of the fuel degradation rate shows a normalized root mean squared error ($nrmse$) of 0.11, and a mean absolute percentage error ($mape$) of 29%. Even without extensive tuning of the kNNr metaparameters, this is a significant improvement from the $nrmse$ error of 0.48 and $mape$ error of 44% of a well-tuned kNNr

surrogate case where no CLT information was used. A detailed account of this work is provided in Appendix C.

In addition to model development, two papers on FMD surrogate modeling were written this year. The first, "Machine Learning Surrogate Process Models for Efficient Performance Assessment of a Nuclear Waste Repository," presents the model development summarized above and fully described in Appendix C (Debusschere et al. 2022). It will appear in the proceedings of the 2022 American Nuclear Society International High-Level Radioactive Waste Management Conference. The second, "Machine Learning Surrogates of a Fuel Matrix Degradation Process Model for Performance Assessment of a Nuclear Waste Repository," describes the development and testing of the kNNr and ANN FMD surrogate models implemented in GDSA Framework. It was submitted to the Journal of Nuclear Technology in September of 2022.

4.1.3.4 Multi-Continuum Transport

PFLOTRAN's multi-continuum model simulates disconnected secondary (matrix) continua connected to a primary (fracture) continuum. It is referred to as the DCDM (Dual Continuum Disconnected Matrix) model (Lichtner, 2000). Each primary cell hosts its own disconnected one-dimensional secondary continuum.

There were several improvements and activities involving the DCDM capability in FY 2022:

- Improvements were made to user friendliness including the addition of an extensive error messaging system (Nole et al. 2022, Section 2.2.3.1).
- The ability to use log grid spacing was added for grid cells adjacent to the primary continuum (Nole et al. 2022, Section 2.2.3.2).
- The model was exercised for ^{241}Am decaying to ^{237}Np using the UFD Decay Process Model of PFLOTRAN (Nole et al. 2022, Section 2.2.3.3).
- Unsaturated applications that focused on gas transport and diffusion were successfully tested against two analytical solutions and an explicit unstructured grid solution (Nole et al. 2022, Section 2.2.6).

4.1.3.5 Material Transform Process Model

Events and processes such as a criticality event or high heat loads can cause material properties to suddenly or gradually change. In FY 2022, a material transform process model was developed for PFLOTRAN to effect these changes in a computationally efficient way.

The material transform process model was refactored from the smectite-to-illite model (Nole et al. 2021) into a general-use module so that multiple processes could affect the material and transport properties of a cell. For example, the properties of buffer cells can be affected by smectite-to-illite transition processes as well as buffer erosion processes. This new model was set up such that it can make use of its own time-stepper if iterations are needed for convergence.

The new capability was tested on a 1D smectite-to-illite transition sample problem for two different transition models. In each case, calculation of smectite fraction, permeability, and sorption coefficients as a function of time matched the analytical solutions. Figure 4-7 compares the analytical solutions of the cesium sorption coefficient changes over time versus the two different models tested. A more detailed

discussion of the new materials transform process model and its verification are provided in Nole et al. (2022).

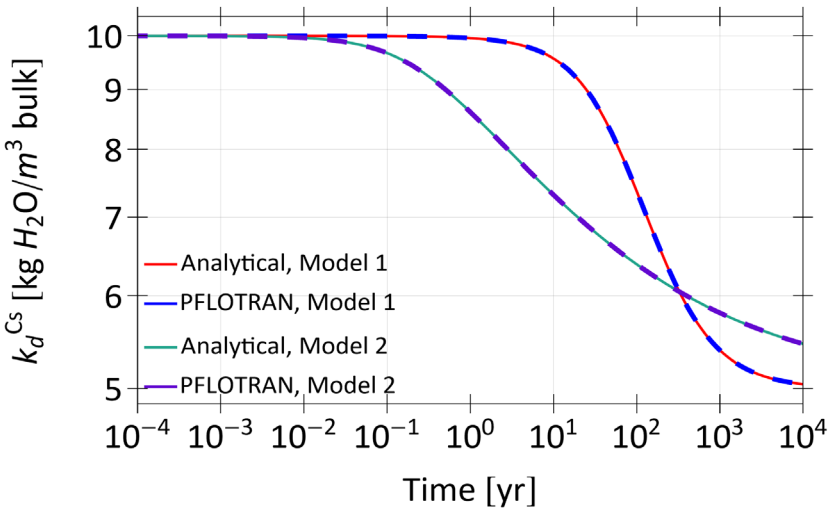

Figure 4-7 Cesium sorption coefficient (K_D) as a function of time using the Huang et al. (1993) model (1) and the Cuadros and Linares (1996) model (2).

4.1.3.6 Lookup Table Interpolation

Three-dimensional lookup table interpolation is another capability added to PFLOTRAN this year. This capability is useful for interpolating user-provided three-dimensional response surfaces having three independent variables.

Two methods were implemented:

- LookupTableInterpolate3DLP: Lagrange polynomials (the default) as applied to three axes, or
- LookupTableInterpolate3DTrilinear: Trilinear method, an extension of linear interpolation in three dimensions.

This new capability is demonstrated in Nole et al. (2022) for two criticality applications.

4.1.3.7 Salt Effects and Salt Transport

There were three major advances in PFLOTRAN's ability to account for salt content in the calculation of flow and transport this year:

- Salinity-dependent equations of state were implemented, as summarized in the first subsection below. These equations are used to calculate the density, viscosity, vapor pressure, and enthalpy of the liquid phase as a function of the amount of aqueous sodium chloride.
- Solute mass balance equations that use the salinity-dependent equations of state were fully coupled with the flow solution (Section 4.1.2.3).
- The ability to dissolve and precipitate the solid matrix based on solubility limits was added to the solute mass balance equations for the GENERAL mode of PFLOTRAN (two/three-component,

multi-phase air/water flow), as demonstrated in the second subsection below. This capability is useful when the rock matrix is salt.

Salinity-Dependent Equations of State

Sodium chloride is often the dominant salt in groundwater. In FY 2022, a new set of equations of state for sodium chloride solutions was built into PFLOTRAN. These equations of state improve the accuracy of PFLOTRAN calculations of the density, viscosity, saturation pressure, and enthalpy of sodium chloride solutions, especially for brines.

The set of sodium-chloride-dependent equations of state includes formulations for:

- Aqueous solubility of sodium chloride as a function of temperature (Sparrow 2003)
- Fluid mass density as a function of temperature and sodium chloride mass fraction (Sparrow 2003) or as a function of temperature, pressure, and salt concentration (Batzle and Wang 1992)
- Vapor pressure as a function of temperature and sodium chloride mass fraction (Sparrow 2003) or as a function of pure water temperature at the same pressure and sodium chloride molality (Haas 1976)
- Liquid enthalpy as a function of temperature and sodium chloride mass fraction (Sparrow 2003)

The response surface for the enthalpy relationship is shown in Figure 4-8. The full set of sodium-chloride-dependent equations of state and their response surfaces are documented in Nole et al. (2022).

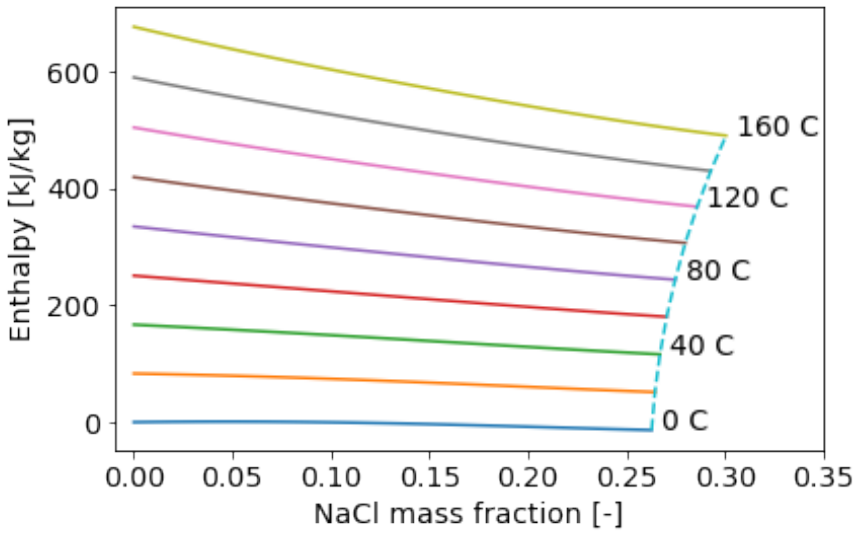

Figure 4-8 Specific enthalpy as a function of salt concentration

Implicitly-Solved Precipitation and Dissolution

A solubility-controlled solid phase was included as an additional component in the solute mass balance equations of the GENERAL mode of PFLOTRAN. This solid phase can form in the pore space of an insoluble matrix (e.g., sandstone), or can form the solid rock matrix of a soluble material (e.g., salt). For a salt formation, if the groundwater in the salt becomes undersaturated with respect to the salt for any

reason (e.g., changes in temperature), a portion of the salt matrix will dissolve, raising the groundwater salinity and increasing porosity. By incorporating a solubility-controlled solid phase in the solute mass balance equations, GENERAL mode can now be used to adjust cell porosities as needed to maintain mass balance of salt in the domain while also maintaining chemical saturation with salt. The new solute mass balance equations are presented and described in Nole et al. (2022, Section 2.2.9).

There are two major benefits of this new fully implicit solution. The first is that there are convergence issues when the flow problem and reactive transport problem are solved sequentially. For that type of problem, the Courant–Friedrichs–Lewy (CFL) condition must be met to prevent convergence on an oscillatory/improper solution. The CFL condition is based on the grid discretization, magnitude of the fluid velocity, and the timestep (CFL=dt*velocity/dx), so meeting this condition usually involves reducing the timestep. The fully implicit solution is unconditionally stable, so it does not require the CFL condition to be met and allows larger timesteps. The second major benefit is related to being able to entirely dissolve the rock matrix in a partially saturated system. Because the porosity becomes a primary variable, as porosity decreases, the gas phase is compressed and the gas pressure increases.

To demonstrate this new capability, along with the other new salt-related capabilities implemented this year (see the beginning of Section 4.1.3.7), a common benchmark problem by Olivella et al. (1994) was simulated: a one-dimensional multi-phase fluid flow problem through salt. The initial porosity is 30%, and the initial water saturation is 30%. The temperature is held constant at 85 °C on the left and 5 °C on the right. During the simulation, the high temperature on the left causes water to evaporate, salt to precipitate, porosity to decrease, and water vapor to flow to the right. Toward the right, where temperatures are cooler, vapor condenses, a small portion of the salt matrix dissolves to maintain chemical saturation, and porosity increases.

The calculated porosity profiles over time are shown in Figure 4-9. They successfully demonstrate the expected trends. Calculated profiles of gas velocities and liquid velocities are also calculated but not shown here. They are shown in Section 2.2.9.2 of Nole et al. (2022) where this demonstration is fully described.

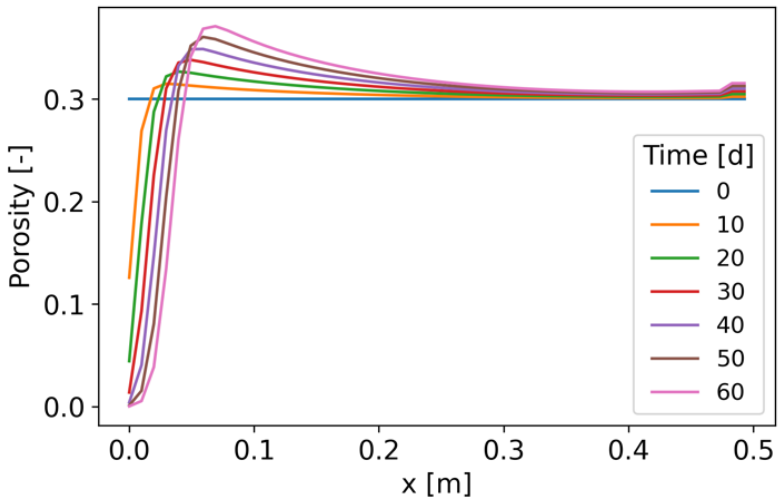

Figure 4-9 Porosity evolution in the Olivella et al. (2011) benchmark problem

4.1.3.8 Groundwater Evolution

The concentrations of dissolved species in groundwater affect many processes important to repository performance. Affected processes include fuel matrix degradation, buffer erosion, canister corrosion, in-package material degradation, alteration of smectite in buffer materials, multiphase flow, colloid stability, radionuclide solubility, and radionuclide sorption. The GDSA Framework salt reference case may soon begin to incorporate salt effects (Section 4.1.3.7), but otherwise, GDSA Framework reference cases have not yet included aqueous groundwater chemistry.

This year, development of a hydrogeochemical reactive transport model was initiated for the crystalline reference case. Studies performed at the Onkalo spent nuclear fuel repository (Posiva 2021) are used to guide development. The Onkalo spent nuclear fuel repository is a mined repository located on the island of Olkiluoto in Eurajoki, Finland. The host rock is gneiss and granite.

In the performance assessment for the Onkalo repository, groundwater salinity and concentrations of sulfide are important. A decrease in groundwater salinity, due to deep percolation from melting ice after a glacial period, could potentially cause significant erosion of buffer around a copper waste canister if there is a flowing fracture intersecting the emplacement borehole. If buffer erosion is extensive and exposes a canister to groundwater flow, sulfide in the groundwater could potentially corrode enough copper to breach it.

Calculations were performed using PHREEQC to reproduce groundwater compositions at Olkiluoto by mixing and equilibrating four depth-dependent water endmembers. PHREEQC is an aqueous geochemical code developed by the U.S. Geological Survey (www.usgs.gov/software/phreeqc-version-3). In addition, a one-dimensional reactive transport model is being developed using PHREEQC to simulate the processes and chemical reactions hypothesized to produce the groundwater compositions observed with depth. A major reaction in the Posiva model is the reduction of sulfate by hydrogen gas diffusing from the matrix. The PHREEQC calculations, chemical reactions, and general chemical model are described in detail in Appendix D. Incorporation of chemistry into the GDSA Framework crystalline reference case is expected to begin next year.

4.1.3.9 Biosphere

The current biosphere model implemented in PFLOTRAN consists of an ingestion dose model from drinking contaminated well water (Mariner et al. 2017, Section 3.2.3). That model can be used to simulate Example Reference Biospheres 1A and 1B of the International Atomic Energy Agency (IAEA 2003) and can explicitly include the special enhancement effects of highly-mobile short-lived radionuclides like radon-222.

In FY 2020, Pacific Northwest National Laboratory (PNNL) began developing a comprehensive biosphere model for GDSA Framework. The general requirements of the model are that it be generic, flexible, open source, compatible with PFLOTRAN, and consistent with international recommendations and guidance for such models built for deep geological repositories. Features and processes include multiple pathways, components, interactions, and radionuclide decay and ingrowth. Figure 4-10 shows a schematic diagram of the various pathways planned for inclusion.

This fiscal year, a software design document was developed and finalized. In addition, twelve new exposure pathways were added for a human receptor. A detailed description of these accomplishments and planned next steps is provided in Ghosh et al. (2022).

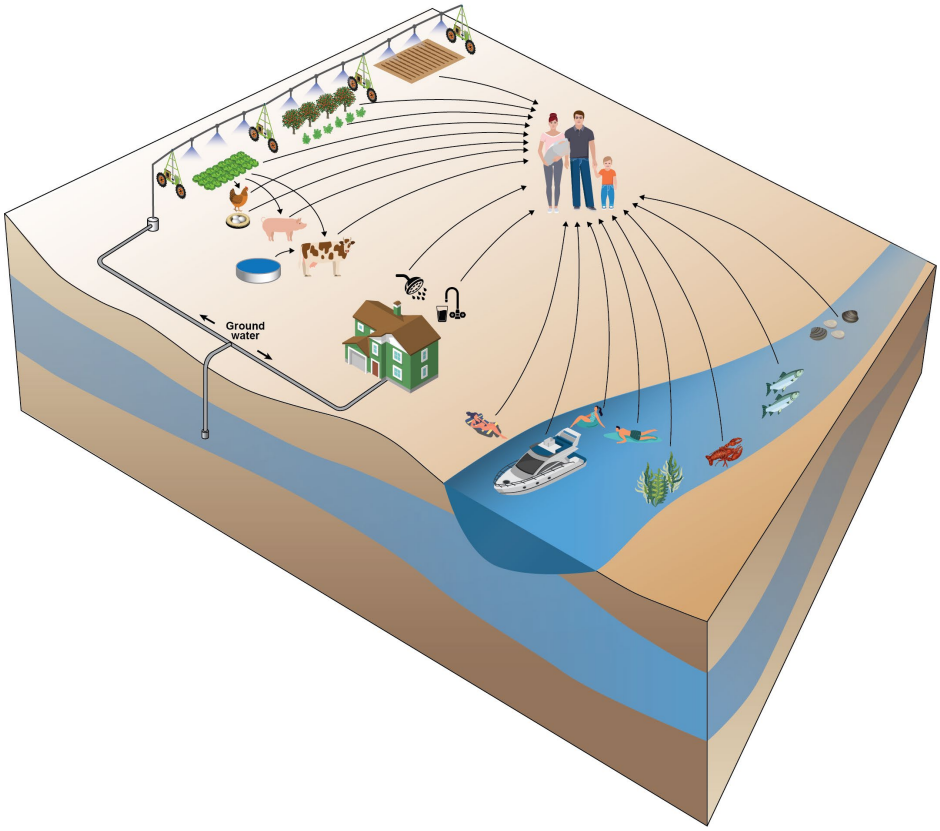

Figure 4-10 Schematic diagram of potential pathways in new biosphere model being developed for GDSA Framework (graphic from Condon et al. 2020)

4.2 Other GDSA Framework Development

In addition to development of the PFLOTRAN code (Section 4.1), there were advances in other GDSA Framework codes. There were also advances in GDSA Framework reference cases and documentation of model capabilities and calculations. These advances include development of:

- Next Generation Workflow graphical interface for GDSA Framework simulations (Section 4.2.1)
- Geologic Framework Model application to crystalline rock (Section 4.2.2)
- An open-source version of VoroCrust-Meshing and a simplified PA model using VoroCrust (Section 4.2.3)
- Uncertainty and sensitivity analysis applications and methods (Section 4.2.4)
- International generic performance assessment models (Section 4.2.5)
- Improved generic reference case models (Section 4.2.6)
- GDSA model and calculation documentation (Section 4.2.7)

4.2.1 GDSA Workflow

In FY 2020, the GDSA team began developing automated analysis workflows using the Next-Generation Workflow (NGW) capability of Dakota to improve automation, reproducibility, and traceability for GDSA Framework simulations. The NGW capability is a graphical, node-based interface that includes

many pre-programmed support functions. As part of the GDSA Framework, NGW is used to autonomously collect inputs from multiple sources, modify the PFLOTRAN input files based on the inputs collected, run the PFLOTRAN simulations, and run a post-processing script to collect and visualize results and calculate additional quantities of interest. NGW is available within the Dakota Graphical User Interface (GUI) (Ridgway 2020) and is thus available to the GDSA analysis community.

Development of NGW workflows for GDSA Framework aims to:

- Reduce the learning curve for new users to set up and run new simulations
- Speed up analysis workflow execution time
- Eliminate/reduce the need for manual intervention
- Allow for automated monitoring
- Reduce the potential for human errors
- Increase traceability and reproducibility

The eventual goal is to develop an analysis workflow library that can be made available to the GDSA analysis community. A full demonstration of a probabilistic GDSA Framework workflow is provided in Appendix C of Mariner et al. (2020a).

In FY 2021, a "Crystalline Reference Case UA Nested Workflow" was developed and run to support uncertainty propagation and sensitivity analysis of the GDSA Framework crystalline reference case. The advantages and benefits were found to include:

- Quicker turnaround enabling two full studies in one year
- Easy handoff of workflows to new analysts
- Increased development of scripts supporting final production runs
- Increased robustness against HPC outages during production runs

A notional view of the detailed structure of the crystalline reference case uncertainty analysis (UA) Nested Workflow is shown in Figure 4-11. A detailed description of each of the elements of this workflow along with an overall description of this structure is given in Swiler et al. (2021).

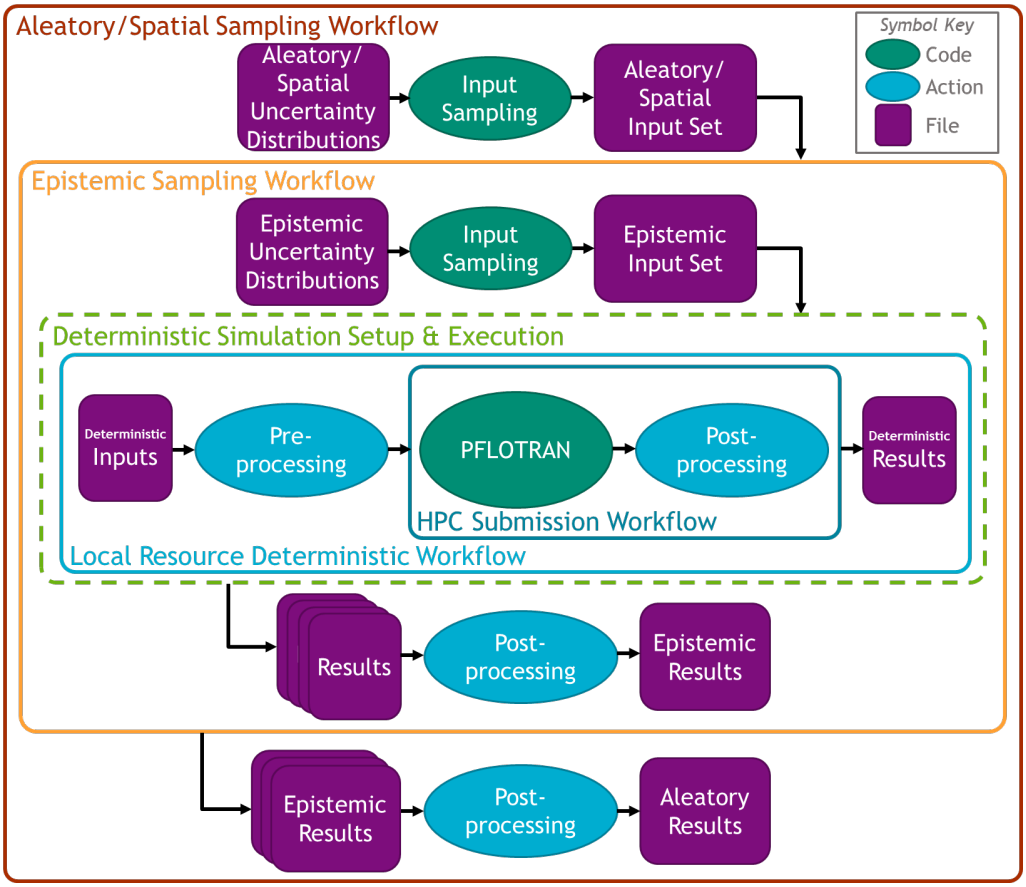

Figure 4-11 Detailed notional view of the Crystalline Reference Case UA Nested Workflow structure showing the workflows along with important files, actions, and codes that are employed for each.

In FY 2022, the NGW capability became referred to as GDSA Workflow. In addition to supporting two new probabilistic crystalline reference case simulations, it was extended to support the DECOVALEX Task F1 work discussed in Section 4.2.5.1 (Swiler et al. 2022).

Adapting the GDSA Workflow to the DECOVALEX reference case required editing input files, updating run directories and job submission scripts, and updating selected outputs and post-processing scripts. To help with future conversions, analysts developed a checklist of steps to take when an established workflow is converted to a new reference case.

4.2.2 Geologic Framework Model – Geology and Hydrology of Glacial Deposits to Support Biosphere Modeling in a Crystalline Rock Environment

Host-rock models for the crystalline reference case have focused on a generic representation of the geosphere based partly on features of crystalline rock (e.g., fracture systems) that have been well documented at the Forsmark site in Sweden (Mariner et al. 2016). In FY 2021, we developed a conceptual model of the shallow geosphere (within ~100 meters of the surface) based on features of crystalline basement rocks and glacial deposits in the northeastern US (LaForce et al. 2021). Glacial deposits ("overburden") represented in the conceptual model are glacial till, glaciofluvial ("outwash") sand and gravel deposits and glaciomarine silts and clays. In FY 2022, we use this information and data obtained from an example watershed in New England to begin development of a test case for biosphere modeling

that focuses on the groundwater contribution to streams and the irrigation needs and water sources for crops. This effort is summarized here and described in detail in LaForce et al. (2022).

Pacific Northwest National Laboratory (PNNL) is developing a biosphere model to evaluate dose to human receptors as part of GDSA disposal system modeling (Condon et al. 2020). The biosphere model will be broadly applicable to geologic media and environments being considered in the GDSA generic reference cases (Mariner et al. 2021, Section 3.2.6). Unconsolidated glacial deposits overlie crystalline basement rocks in many areas of the northern US that were glaciated during the Quaternary Period. This geologic environment is therefore of interest when evaluating geosphere-biosphere interactions as part of development of the biosphere model.

Common pathways for movement of radionuclides into the biosphere are through extraction of groundwater from wells and groundwater discharge to surface water features (Condon et al. 2020). In the case of groundwater discharge, radionuclide concentrations in surface waters depend partly on the properties of the near-surface geosphere features (e.g., permeability of glacial deposits) and the degree of mixing that occurs between radionuclide-contaminated groundwater and surface streams or lakes.

In this section we summarize data from a representative watershed in New England that is intended to provide a basis for development of initial biosphere test case scenarios in a crystalline environment. The watershed used as an example for this study was chosen based on geology that is representative of the region. The geology and hydrology of the glacial deposits within the watershed are intended to represent a simplified and generalized ("generic") example of a geologic features that can be found in other areas of the northern US.

4.2.2.1 Description of the Example Watershed

The example watershed is located within a few kilometers of the coast of Maine. The lower portion of the watershed nearest the coast lies on a flat coastal plain (Figure 3-1A). Further inland, the watershed transitions to a broadly sloping plateau that is incised by the primary stream and its tributaries (Nielsen and Locke 2015; Figure 3-1A). The elevation difference from the top to the bottom of the watershed is about 110 meters. Total length of the watershed is about 15 km with an approximate width that is between 2 and 3 km, for a total area of approximately 40 km^2.

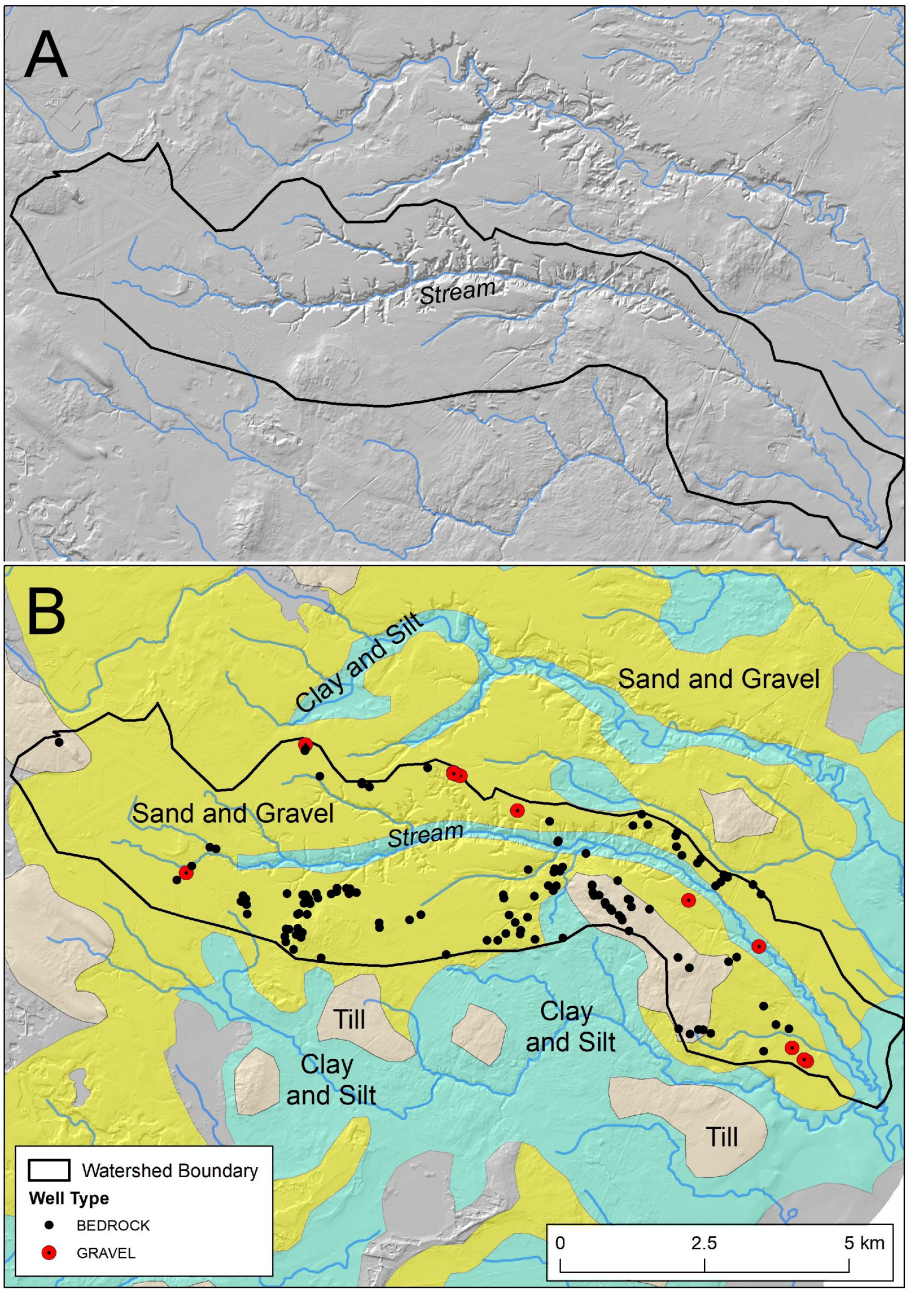

Figure 4-12 Shaded relief map showing the boundary of the watershed and the incision of the glacial deposits by the main stream and its tributaries (streams shown in blue). B. Simplified geologic map of glacial deposits within the region of the watershed and distribution of water wells within the watershed

Glacial deposits that overlie the crystalline basement rocks can be divided into three major units (Figures 3-1B and 3-2). The lowermost unit, directly draping crystalline bedrock, is glacial till with a thickness of up to 7 meters. Clay and silt deposits of the glaciomarine Presumpscot Formation overlie glacial till with a typical thickness of 5-20 meters. The Presumpscot Formation is the most extensive glacial deposit in the area of the watershed. Due to its low permeability, it is a regional aquitard that limits groundwater flow to overlying and underlying units. The youngest glacial deposits within the watershed are sand and gravel glacial outwash deposits that form the shallow aquifer of the area. Sand and gravel deposits have typical

thicknesses of 5-20 meters. In most areas of the watershed, the main stream has incised through the sand and gravel deposits into the underlying Presumpscot Formation. Tributaries of the stream are generally less incised and only incise the overlying sand and gravel deposits. Because to their high permeability, sand and gravel deposits are the main pathway for groundwater discharge to the tributaries that supply water to the main stream (Nielsen and Locke 2015).

Groundwater flow within the watershed is from west to east and follows the topographic gradient (Nielsen and Locke 2015). Groundwater flows from local topographic highs within sand and gravel units to the nearest discharge points at streams. Participation in the region of the watershed averages between 115-140 cm (45-55 inches) per year (National Weather Service 2022; Nielsen and Locke 2015). Rainfall amounts in the region are fairly consistent from month to month ranging from about 9 to 13 cm. For the May-September growing season, average precipitation is about 10 cm per month with a range in the average of 9.7 to 11.6 cm.

Recharge to the uppermost permeable sand and gravel deposits in the watershed is approximately 50-60% of total precipitation (Nielson and Locke 2015). For use in biosphere models, we assign a recharge rate of 70 cm per year to the sand and gravel deposits and the overlying soils. The underlying Presumpscot Formation, which is a regional confining unit, has a recharge rate estimated at 1 to 5 cm per year (Nielsen and Locke 2015). We assign the Presumpscot Formation a recharge rate of 2 cm per year. We assign a recharge rate of 12 cm per year for both till and underlying fractured bedrock, based on values reported in Nielsen and Locke (2015).

4.2.2.2 Water Well Characteristics

A total of 126 water wells are located within the watershed (Figure 3-1B). A large majority of these wells (116) are within the crystalline bedrock and ten are shallow wells within gravel deposits. All of the bedrock wells are for domestic use, and most have yields of less than 20 gallons per minute (GPM). Nine of the ten gravel wells are also for domestic use with the highest yielding well (150 GPM) for municipal use. The average depth of bedrock wells is 91 meters with an average yield of 18 GPM. The average depth of bedrock wells falls within the depth range of high-permeability horizontal fracture zones typical of crystalline rock environments (LaForce et al. 2021). Based on a much smaller sample size, sand and gravel wells have an average depth of 15 meters and an average yield of 27 GPM.

4.2.2.3 Groundwater Contribution to Streams

The groundwater contribution to streams is controlled largely by the permeability of underlying geologic units. Groundwater contributions are highest where streams are in contact with high-permeability units (Winter et al. 1998; Figure 3-2). Nielsen and Locke (2015) modeled groundwater and surface water flow to understand potential streamflow depletion from well withdrawals. Our interest is in how base flow values for the main stream (representing groundwater contribution to stream flow) compare to the overall stream flow. Stream flow is at its lowest in the summer when calculated streamflow values overlap calculated base flow values of 15-20 ft^3/s (Nielson and Locke 2015), indicating that a high percentage of the summer streamflow between precipitation events is due to base flow. Based on these estimates, we assign a groundwater contribution of 90% (by volume) to total stream flow during the growing season with the groundwater derived dominantly from the sand and gravel deposits (Figure 3-2). This estimate is consistent with results presented by Winter et al. (1998) showing groundwater contribution to streams is controlled by the permeability of underlying geologic formations with the highest contributions from unconsolidated sand and gravel deposits.

Although we can estimate the contribution of groundwater as a percentage of stream flow, radionuclide concentrations in the groundwater that contributes to streamflow will require PFLOTRAN modeling. Modeling will allow estimates of radionuclide concentrations in surface waters when combined with

estimates of groundwater contributions to streams. Given the high amount of surface recharge into the shallow aquifer and the possibility of limited flow from below due to the presence of the clay and silt confining unit, it is likely that radionuclides in the sand and gravel aquifer will have significantly lower radionuclide concentrations compared to water flowing through bedrock fractures.

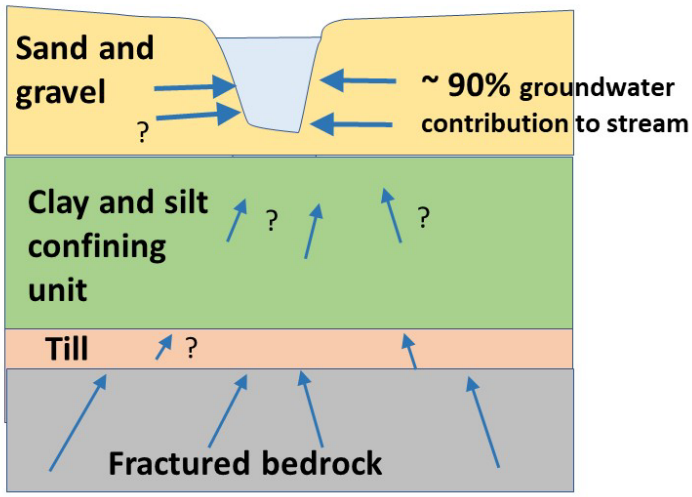

Figure 4-13 Schematic representation of stratigraphy and groundwater flow in a watershed with three types of glacial deposits (not to scale). Groundwater flow from the upper sand and gravel aquifer contributes approximately 90% of the water to the total streamflow. Arrows are general indicators of flow velocities based on differences in permeability. Question marks indicate uncertainty in flow and transport in glacial deposits.

4.2.2.4 Agricultural Framework

The climate and soils of southern Maine support a variety of crops including leafy vegetables, root vegetables, fruit trees and berries (Central Aroostook Soil and Water Conservation District 2005). The growing season is from May through September and can be extended by the use of greenhouses and other enclosed growing facilities. Average rainfall during the growing season (10 cm per month) typically supplies at least half the water needs for most crops with irrigation supplying the rest.

Water Sources

Water sources for agriculture are described in Central Aroostook Soil and Water Conservation District (2005). Water sources in southern Maine include streams, lakes, man-made impoundments (ponds), springs and wells (Central Aroostook Soil and Water Conservation District 2005). The sources considered for input to the biosphere model in this test case scenario are wells and streams. Water from wells in crystalline bedrock, sand and gravel aquifers and surface streams would be expected to have decreasing concentrations of radionuclides. In general, streams are not a reliable water source for irrigation because irrigation demands are greatest in August and September when stream levels are at their lowest (Central Aroostook Soil and Water Conservation District 2005). It is important to be able to estimate radionuclide concentration in streams however due to their potential use for irrigation and impact on downstream natural habitats or other users.

Water Requirements

Most crops in the region require about 2.5 cm of water per week and possibly more during critical growing periods. Precipitation during the growing season is approximately equal to the water needs of crops but water needs may not be reliably met on a week-by-week basis or during drier years. Because of high precipitation rates in Maine, irrigation is not employed on all farms or for all crops grown on a farm. In order to include an irrigation component in scenarios for the biosphere model, we assume the upper range of water needs and calculate the possible shortfall based on monthly average precipitation rates. Based on these assumptions, irrigation is needed to supply up to an additional 2.5 cm of water per week consistently across most crops. For sandy soils of the watershed, irrigation would be applied at a rate of between 1-2 cm per hour (intake rate of the soil) to prevent ponding and runoff (Central Aroostook Soil and Water Conservation District 2005). In general, the total amount of water available for crops (precipitation plus irrigation) would be sufficient to maintain a soil moisture content of 50-100% (Central Aroostook Soil and Water Conservation District 2005). Concentrations of radionuclides in irrigation water will be based on PFLOTRAN modeling of radionuclide concentrations in well water from either crystalline basement or the sand and gravel aquifers, along with estimates of groundwater contributions to streams that possibly supply irrigation water.

4.2.3 Voronoi Meshing and Simulation

Two significant developments have been achieved in the Voronoi meshing and simulation this year:

- Creation and release of an open-source version of VoroCrust (Abdelkader et al. 2020) called "VoroCrust-Meshing" that contains the capability necessary for simulation in PFLOTRAN (Lichtner et al. 2020) and visualization of the results in ParaView 5.9 (Ahrens et al. 2005).
- Development of a simplified shale performance assessment (PA) case using PFLOTRAN simulations on VoroCrust meshes that includes an uncertain geological structure.

4.2.3.1 Improvements to VoroCrust

In FY 2022 the VoroCrust team will release the meshing part of the software as an open-source code on GitHub. This effort required completely redesigning the architecture of the VoroCrust framework to strip out prototype and patented code. An open-source license had to be applied for and awarded. Prior to release it was also necessary to develop a GitHub repository, conduct extensive code testing on Linux, Windows, and macOS operating systems, and recruit a small group of experienced and inexperienced users to beta-test the release version of the code.

4.2.3.2 Shale Performance Assessment

LaForce et al. (2022) Section 7.2 presents a detailed discussion of a simplified shale PA case utilizing VoroCrust-Meshing to include geological uncertainty in a prototype analysis. The shale geological framework model (GFM) from Sevougian et al. (2019c) is used as the basis for development of the uncertain models. This work represents the first time a GFM has been directly used in a GDSA Framework simulation and is a critical first step towards incorporating geological realism into PA calculations.

The geological models for simulating the shale repository are clipped out of the GFM and deterministic and uncertain parameters consistent with previous shale cases (Mariner et al. 2017; Sevougian et al. 2019c; Swiler et al. 2019). The example PA case is simplified significantly from the previous shale PA cases in three ways: first the entire repository and surrounding disturbed rock zone are represented as a single, rectangular source term having the material properties of bentonite buffer; second, the system is assumed to be isothermal; and third, the source term is represented by two tracers with properties

representative of ^{129}I released at the beginning of the simulation. The simplicity of the prototype model allowed for generation of ten realizations in Dakota and simulation in PFLOTRAN.

Development of the simulation model is discussed in detail in LaForce et al. (2022) Section 7.2. Figure 4-14 shows a single realization of the PA-scale model, while Figure 4-15 shows Tracer 1 in the reservoir for this model at several snapshots in time. Flow is from left to right, and tracer concentration is monitored in the repository and at three observation points 5 km downstream of the repository in geological strata that represent potential flow paths to the biosphere. Figure 4-15 shows that transport of Tracer 1 in the host shale is largely diffusive and that transport in the Overburden and Limestone Aquifer is advective, which is consistent with the current understanding of the geological system and previous simulation results (Sevougian et al. 2019c; Swiler et al. 2019).

Figure 4-16 shows the tracer breakthrough curves for all ten realizations at the three downstream observation points. Ten realizations is not a large enough sample to perform a quantitative statistical analysis; however, the spread and magnitude of the Tracer 1 breakthrough curves appear to be qualitatively consistent with previous shale PA cases (Mariner et al. 2017; Swiler et al. 2019). Proposed future work is to fully-automate the model building and simulation process using the Sandia next generation workflow (NGW) (Mariner et al. 2021) and run a sufficiently large number of simulations to perform a quantitative statistical analysis on the results.

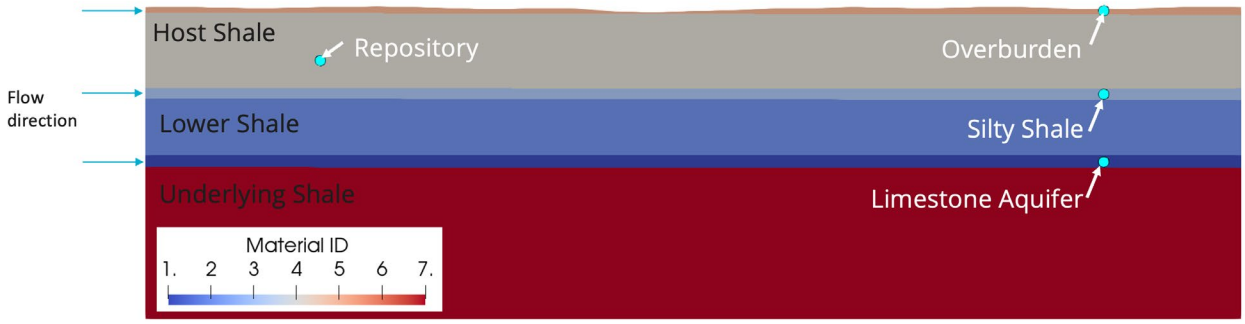

Figure 4-14 Sideview of one realization of the PA-scale simulation showing the realized variation in thickness of each layer in space. Observation points are denoted by blue circles. Blue arrows indicate that the flow direction is from left to right.

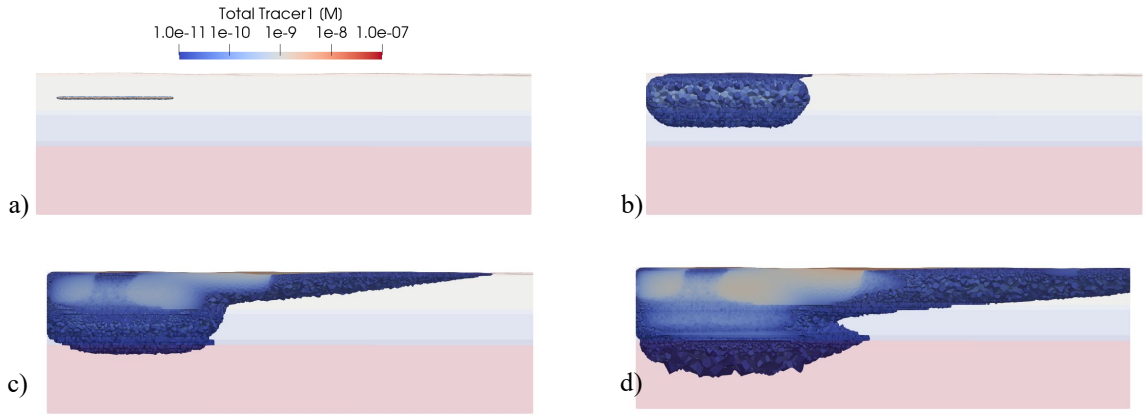

Figure 4-15 Tracer concentrations above 1×10^{-11} M for a central slice of the domain for one realization at a) 1 year; b) 100,000 years; c) 500,000 years; d) 1,000,000 years.

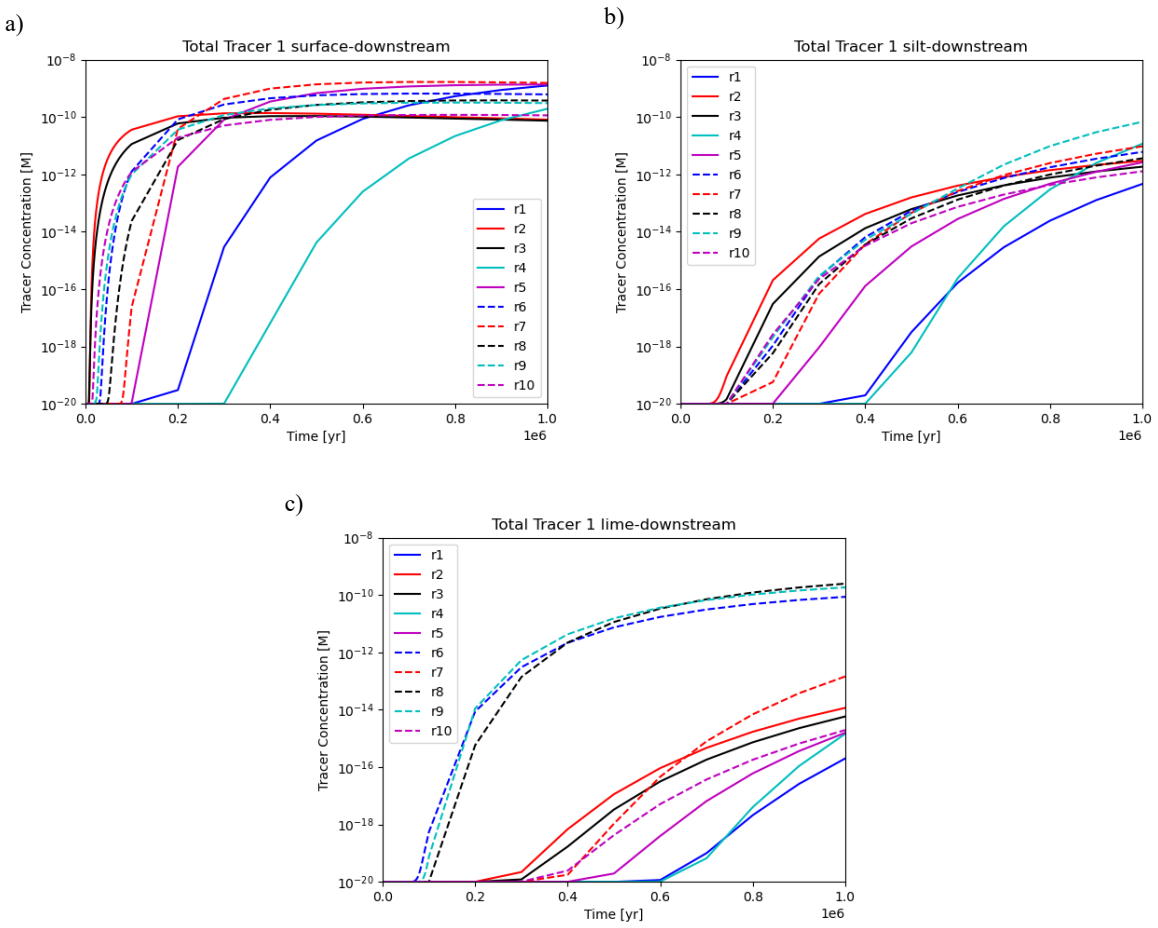

Figure 4-16 Concentration of Tracer 1 for all ten realizations over time at the observation points in a) the overburden, b) silty shale, and c) limestone aquifer.

4.2.4 Uncertainty and Sensitivity Analysis

The report *Uncertainty and Sensitivity Analysis Methods and Applications in GDSA Framework (FY2022)* (Swiler et al. 2022) describes the work done on uncertainty quantification and sensitivity analysis (UQ/SA) in detail. This section provides a summary of that work.

This year, the GDSA UQ/SA team focused on four areas: multifidelity UQ methods, surrogate accuracy and its effect on sensitivity indices, discrete fracture network analysis, and sensitivity analysis case studies involving a generic crystalline reference case and the DECOVALEX crystalline reference case. These are summarized in the sections below.

4.2.4.1 Multifidelity UQ methods

The main idea in multifidelity UQ is to extract information from a limited number of high-fidelity model evaluations and complement them with a much larger number of a set of lower fidelity evaluations. The final result is an estimator of the mean response with a lower variance: a more accurate and reliable estimator can be obtained at lower computational cost. We demonstrated the use of multifidelity (MF) methods to explore how much variance reduction can be achieved by using MF UQ methods on a representative problem for GDSA Framework. Section 2 of Swiler et al. (2022) presents MF results involving models at multiple levels of fidelity applied to a simplified version of the crystalline reference case. This simplified reference case retains many of the key qualities of the full reference case. The multifidelity analysis showed that the variance in a key quantity of interest (QoI), peak ^{129}I concentration, could be reduced by almost an order of magnitude using a set of runs at different fidelities which had the same cost as 500 high fidelity runs.

4.2.4.2 Surrogate accuracy and effect on Sensitivity Indices

A major challenge in the Sobol' sensitivity index calculation is computational cost of calculating the sensitivity indices. Surrogate models are often used to overcome this, but surrogates have not captured the effect of spatial heterogeneity very well. To investigate these issues, we structured an analysis to compare Sobol' indices calculated by directly sampling the model and Sobol' indices estimated using surrogate modeling. This analysis was performed on a simplified version of the crystalline reference case so we could generate thousands of samples required for this investigation.

Section 3 of Swiler et al. (2022) presents this comparison using the simplified crystalline reference case. A Sobol' index calculation was performed for 7 variables involving 9000 sample runs, where each run involved a DFN generated by dfnWorks and PFLOTRAN. This entire workflow was repeated five times to generate five entire replicate sets. This allowed detailed comparison of surrogate models within and across replicates. It also allowed comparison of the sensitivity indices using only the samples and using surrogates based on the samples. We take the "samples only" case as the better estimate because the direct effect of DFNs can be obtained. Surrogates required a proxy metric for the DFN spatial heterogeneity to be calculated and used as an independent predictor in the surrogate.

We found that surrogate choice has some effect on the sensitivity analysis results, but it is minimal for most QoI. All surrogate models included in these studies demonstrated overfitting behavior. A significant finding was that the calculation of the Sobol' indices based on samples only vs. using the surrogates resulted in significant difference in the actual sensitivity index values and in their ranking. Typically, the sample-only calculation of the sensitivity indices ranked the effect of spatial heterogeneity much higher than the surrogate-based calculations. This is likely due to proxies or metrics for the DFNs that do not completely capture their spatial heterogeneity. We considered the following proxies: y-location of peak ^{129}I, number of intersections between the repository and aquifer, shortest travel time, and number of intersections in the entire discrete fracture network. The graph metrics proved to be our best tool to date

for improving surrogate model performance but are demonstrably incomplete tools. These studies showed that improvement in our treatment of spatial heterogeneity is the most promising avenue for accomplishing better surrogate models.

4.2.4.3 Discrete Fracture Network (DFN) analysis

We continue to study various aspects of the Discrete Fracture Networks (Swiler et al. 2022, Section 4). This year, we performed a detailed study involving 100 DFNs each modeling two transmissivity relationships: correlated constant vs. correlated depth-dependent transmissivity. The purpose was to determine if a correlated depth-dependent transmissivity relationship produces a significant change in the performance quantities for the flow and transport simulations of nuclear repositories in subsurface rock as compared to a correlated constant transmissivity. The findings showed that the main QoI, the maximum ^{129}I concentration in the aquifer at 1 Ma, was not significantly different but the timing of the peak ^{129}I concentration did differ. Other QoI such as median residence time and mass fluxes did show statistically significant differences between the two transmissivities. We also observed that the maximum ^{129}I in the aquifer showed no real correlation with any graph metric for either relationship.

The study highlighted differences with respect to the mass flow rates (specifically the rock to east boundary flow rate) as shown in Figure 4-17. Figure 4-17 displays the time-histories of the rock to east boundary mass flow rate based on the 100 DFNs used for each transmissivity relationship. Figure 4-17 indicates that there is a significant difference in the means from each transmissivity: the mean mass flow rate for the correlated constant relationship is a little less than 90,000 kg/yr and the mean mass flow rate for the correlated depth-dependent relationships is around 1,000,000 kg/yr. This information indicates an increase in downstream flow towards the east boundary for the correlated depth-dependent transmissivity relationship. The increased flushing behavior for the correlated depth-dependent relationship is worth investigating further.

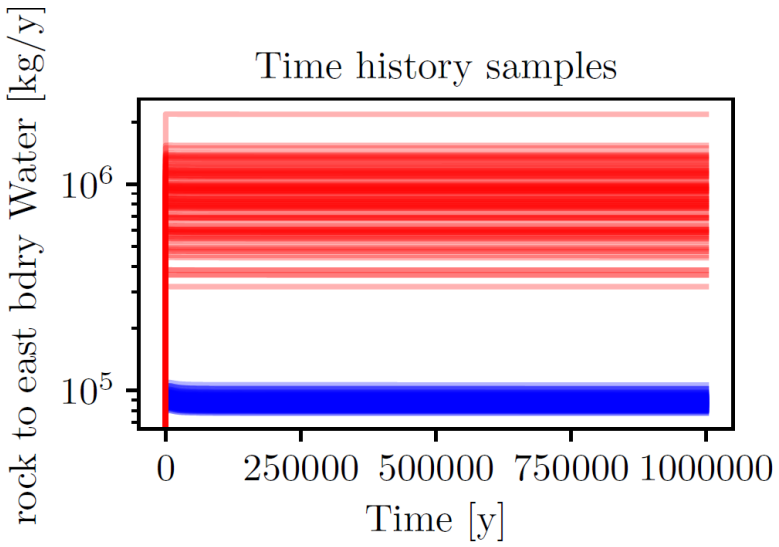

Figure 4-17 Mass flow rate (kg/yr) from the rock to east boundary over time: red is correlated depth-dependent and blue is correlated constant transmissivity

4.2.4.4 Sensitivity analysis of reference cases

This year, we extended the sensitivity analysis of the generic GDSA crystalline reference case performed in FY 2021 (Swiler et al. 2021). The FY 2022 analysis uses the FY 2021 crystalline case and adds another dimension to the sensitivity analysis: that of model form. The FY 2022 analysis addresses uncertainty

from spatial heterogeneity represented by DFNs, epistemic parameter uncertainty, and model form uncertainty in the treatment of fuel matrix degradation (FMD). Two alternatives for FMD are investigated: a fractional dissolution rate (FDR) model and an Artificial Neural Network (ANN) surrogate model of the FMD model.

Comparison between the sensitivity analyses for the crystalline reference case simulations with either the FDR alternative model or the ANN alternative model for FMD showed that the choice of FMD model alternative has a minimal effect on most QoI (Swiler et al. 2022, Section 5). An example is shown in Figure 4-18, where the maximum ^{129}I concentration in the aquifer is plotted over time for simulations with the FDR model (black) and with the ANN surrogate (pink). The concentrations are very similar between the simulations with the two alternatives to the FMD model, but some differences are apparent towards the end of the simulation where there is more variability in concentrations for the FDR model simulations. The mean and standard deviation of the concentrations at 1 million years are 3.66×10^{-9} M and 6.74×10^{-9} M respectively for the FDR simulations and 3.41×10^{-9} M and 5.00×10^{-9} M respectively for the ANN simulations.

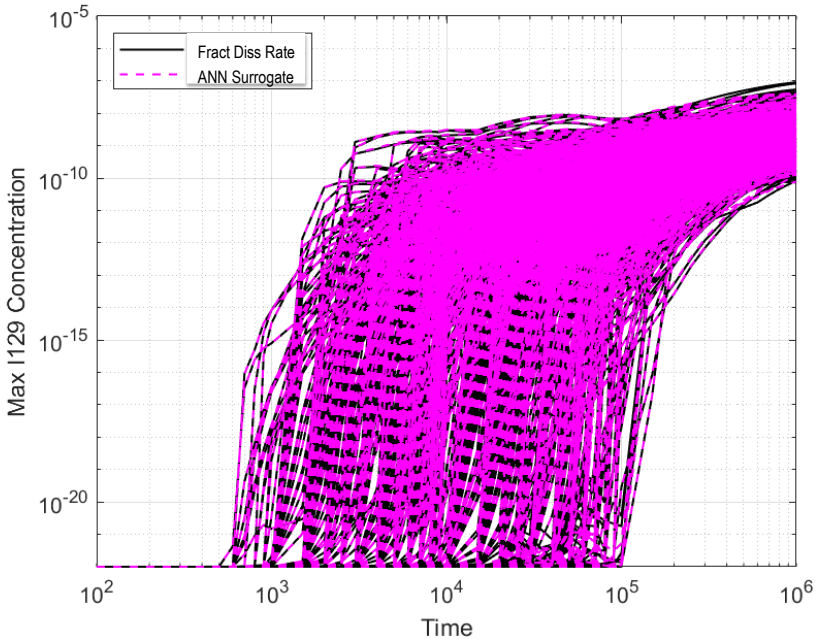

Figure 4-18 Maximum ^{129}I concentrations [M] comparison between the simulations with the ANN and FDR model

The increased variation of the maximum ^{129}I concentrations at late times with the FDR model is likely due to the incorporation of uncertainty in the FDR model via the *rateUNF* parameter; no comparable parametric uncertainty is currently included in the ANN model. The effect of FMD model choice was also small because of the significance of the instantaneous release fraction (*IRF*) up until around 200,000 years. Time-dependent sensitivity analysis showed that, among the parametric uncertainties, the mean waste package degradation rate (*meanWPrate*) dominates early, then *IRF* and *kGlacial* become significant, and *rateUNF* only gains importance after most waste packages have breached. Future analysis may incorporate additional uncertainty into the ANN surrogate model so that it is more directly comparable to the FDR model. Additionally, the *IRF* uncertainty is fairly high, so reductions in that uncertainty could also influence how early the FMD model alternative becomes important.

The sensitivity analyses of the FY 2022 crystalline reference case again highlighted the important effect that spatial heterogeneity has on the QoI, including on the behavior of ^{129}I. This spatial heterogeneity also interacts significantly with the parameter uncertainties. Again, we saw that spatial heterogeneity presents the most significant challenge for our use of surrogate modeling SA. This conclusion motivates further advancement to our treatment of spatial heterogeneity to improve SA accuracy in performance assessment with the GDSA Framework.

Also this year, in addition to the GDSA Framework crystalline reference case, we utilized the GDSA Workflow (Section 4.2.1) to perform a sensitivity analysis on the DECOVALEX crystalline reference case (Section 4.2.5.1). Preliminary results are discussed in Section 6 of Swiler et al. (2022). We note that these results need further investigation, but it was interesting to see that the permeabilities and porosities of both the buffer and the backfill had very little influence on the QoI which were water fluxes at different surface locations and tracer concentrations. Only the *rateUNF* dissolution rate parameter had a significant effect on the Tracer2 concentrations: the uncertainty in most of the QoI was entirely due to spatial heterogeneity as seen by the effect of the DFNs. We plan to extend this analysis as the DECOVALEX case develops further.

4.2.5 DECOVALEX-2023 Task F

The DECOVALEX project is an international research and model comparison collaboration for advancing the understanding and modeling of coupled THMC processes in geological systems (decovalex.org). Task F of DECOVALEX-2023 is a task that focuses on comparison of models and methods used for post-closure PA. Members of the GDSA Framework development team at SNL are leading this effort. The goal of this work is to test and build confidence in the models, methods, and software used for post-closure PA and to identify additional research and development needed to improve PA methodologies.

In Task F, two hypothetical repositories are being developed, one in crystalline rock and the other in salt. In 2020, the first year of the four-year task, nine teams from six countries participated in the crystalline repository and benchmarking exercises, and three teams from three countries defined a generic salt repository reference case. In the second year, each focus group gained one additional team.

To date, Task F has provided and will continue to provide numerous opportunities for learning new modeling approaches, developing new models for use in PA simulations, testing uncertainty and sensitivity analysis methods, comparing PA methods, and exchanging ideas with modelers in other programs. Several accomplishments in the past year are highlighted below.

4.2.5.1 Crystalline

The primary focus of the crystalline group of Task F in the first two years (2020 and 2021) was the testing and comparison of codes used to simulate flow and transport through fractured rock. Several benchmark cases, detailed in LaForce et al. (2021, Section 2.1), were simulated by participating teams. The exercise allowed participants to examine differences in model implementation, types of model outputs, and the influence of modeling choices. Benchmark problems included analytical solutions for single fracture problems and a 4-fracture discrete network fracture (DFN) problem with and without stochastic fractures. Several teams modeled the 4-fracture problem as an equivalent continuous porous medium (ECPM), some teams applied multiple models, and two teams applied particle tracking. Work on the benchmark problems is ongoing as the teams work to ensure initial conditions, boundary conditions, and tracer introduction methods are interpreted consistently and implemented accordingly.

This year the primary focus was on the development of a generic crystalline repository reference case. Task participants chose a fractured rock domain 5 km in length, 2 km in width, and 1 km in depth. A

vertical profile is shown in Figure 4-19. All sides of the domain are flat except the top, which has a flat section on the west (x < 1700 m), a flat section on the east (x > 3700 m) 20 m lower than the west section, and a gradual hillslope connecting the two. The pressure head boundary at the surface tracks the surface elevation. With no-flow boundaries assigned to the other five sides of the domain, the pressure head distribution at the top surface causes downward groundwater flow in the west and upward flow in the east. Conceptually, the east surface is a wetland such that all mass flowing out of the top layer no longer interacts with the system.

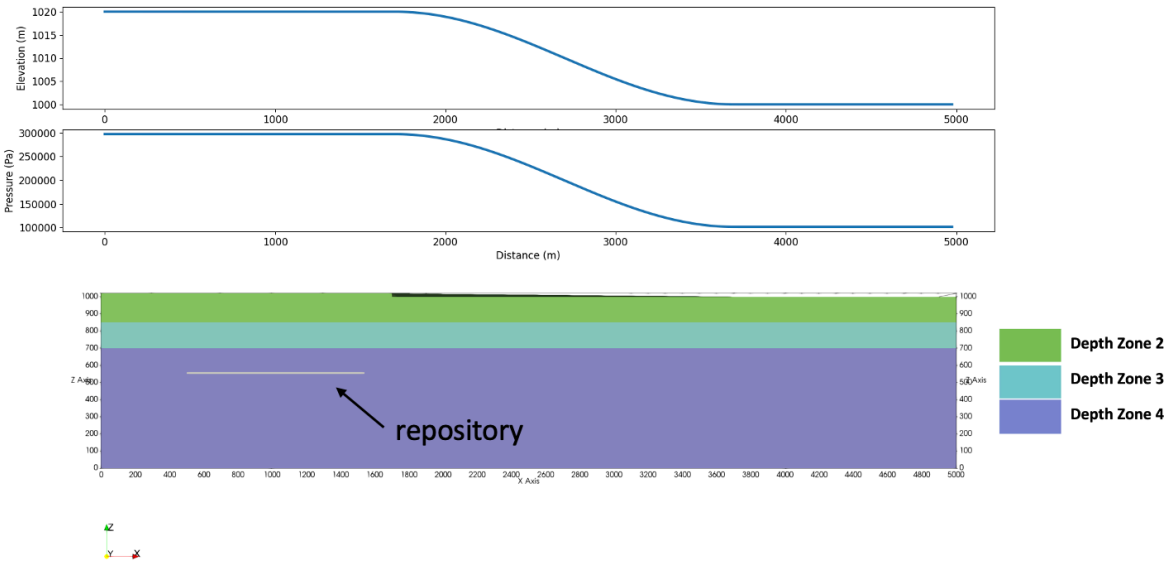

Figure 4-19 Elevation and pressure head profiles at the surface of the domain in the x direction (top) and a vertical slice of the domain showing depth zones and the repository location (bottom)

The reference case utilizes the KBS-3V repository concept. Waste package canisters are copper and are individually placed, surrounded with bentonite, in deposition holes drilled 6 m apart center-to-center into the drift floors. The repository, located at a depth of 450 m, has 50 deposition drifts of length 306 m spaced 40 m apart center-to-center. In total, the layout accommodates 2500 waste packages. Further details and figures of the repository layout and engineered barrier system are provided in LaForce et al. (2022b, Section 3).

The rock domain hosts six deformation zones (Figure 4-20). Additionally, three depth zones have unique fracture families for three primary orientations, each defined statistically in terms of trend, plunge, size, and intensity. Fracture density decreases with depth as does fracture transmissivity. A realization of the fracture families is shown in Figure 4-21.

Five teams are implementing the reference case. All five are upscaling stochastically generated fracture networks to ECPM. Three are conforming their meshes to the deterministic deformation zones and two (including SNL) are including the properties of the deformation zones when upscaling to meshes composed primarily of hexahedrons.

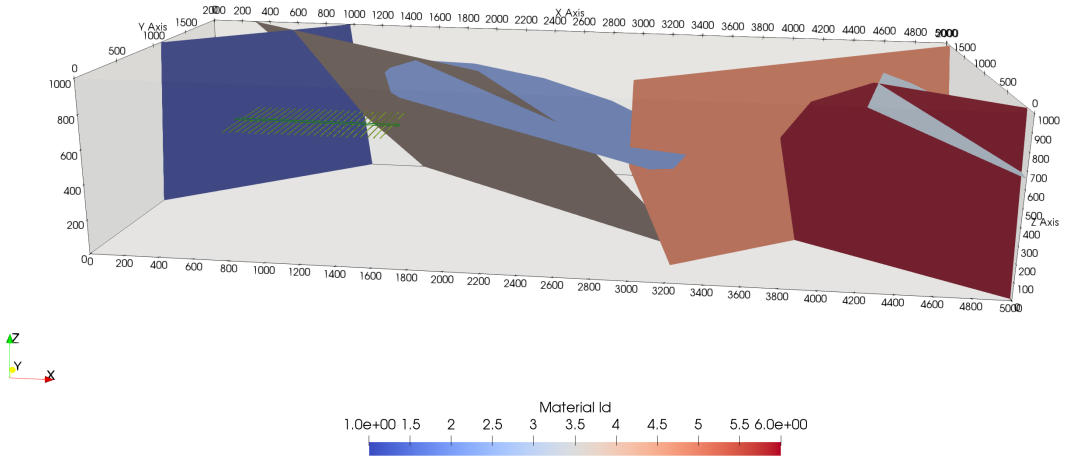

Figure 4-20 Deterministic fractures in the model domain.

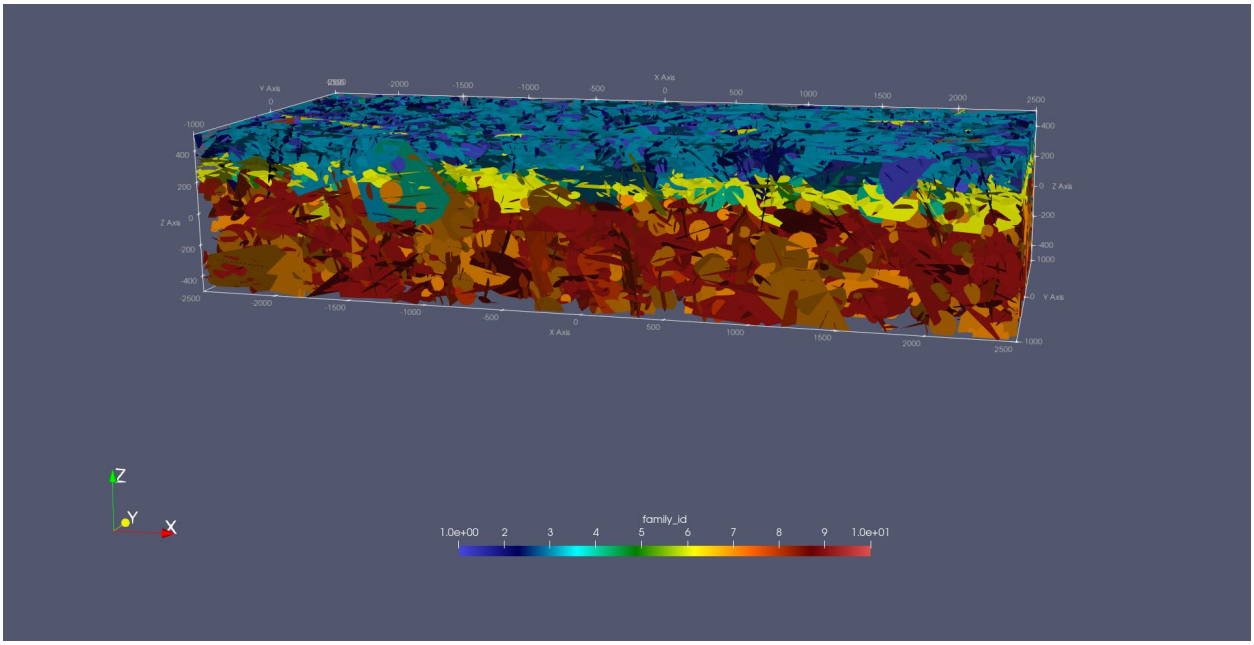

Figure 4-21 One realization of the stochastic fractures, colored by fracture family. Depth zones correspond to different colors.

For the initial reference case simulations, two tracers were chosen. Both are conservative and placed at the locations of the waste packages at the beginning of the simulations. Tracer 1 is 10% of the total tracer mass and is released completely at the beginning of the simulation. Tracer 2 is released slowly over time at a fractional rate of 10^{-7}/yr. With these properties, Tracer 1 acts like an instant release fraction compared to Tracer 2, which is modeled as if it is being released from a slowly degrading UO_2 waste form. For these simulations, there is no cladding and no waste package barriers.

The Tracer 1 plume is shown in Figure 4-22 for a SNL simulation at 100 years. Tracer is initially transported downward and eastward from the repository primarily through fractures. The plume surfaces

at the base of the hill and farther to the east, spreading laterally with increasing distance from the repository. Tracer 2 shows similar trends but at much lower concentrations due to its slow release.

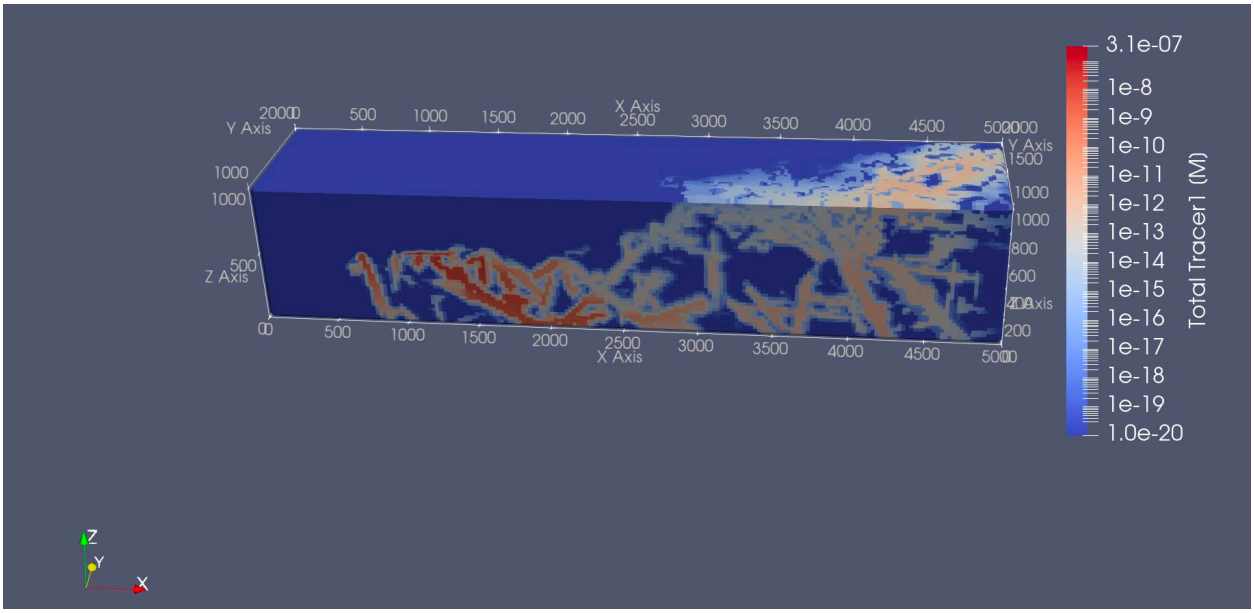

Figure 4-22 Tracer 1 plume at 100 years along the central vertical west-east plane and the north half of the surface boundary for Realization 1.

At 100,000 yr, the SNL model calculates that approximately 95% of Tracer 1 remains in the repository region. Hydraulic containment of conservative solutes in the repository region is aided by low fracture intensities, low fracture transmissivities, low pressure gradients, and low buffer permeability. Additional preliminary results and details are documented in LaForce et al. (2022, Section 2.1).

4.2.5.2 Salt

In FY 2022, the salt group of DECOVALEX-2023 Task F developed additional scenarios for the salt repository reference case. The general setting is a generic salt dome as shown in Figure 4-23. The repository is located at a depth of 850 m and is accessed by two vertical shafts. The spacing of waste was chosen to ensure that temperatures on the waste package surface will not exceed 100°C. Detailed information on the repository design and natural barrier system is presented in LaForce et al. (2022). One important change was that a new layered shaft seal option was added.

The SNL team developed a model of a large block of the salt dome near the repository (2000 m × 2000 m × 2000 m) using Voronoi meshing and half symmetry. Voronoi elements are optimal for finite volume simulators like PFLOTRAN. Drifts are meshed but not individual waste packages. In the simulations, pressure and liquid saturation in the repository and shaft slowly increase over time, as shown in Figure 4-24. Additional results and more detailed discussion are provided in LaForce et al. (2022).

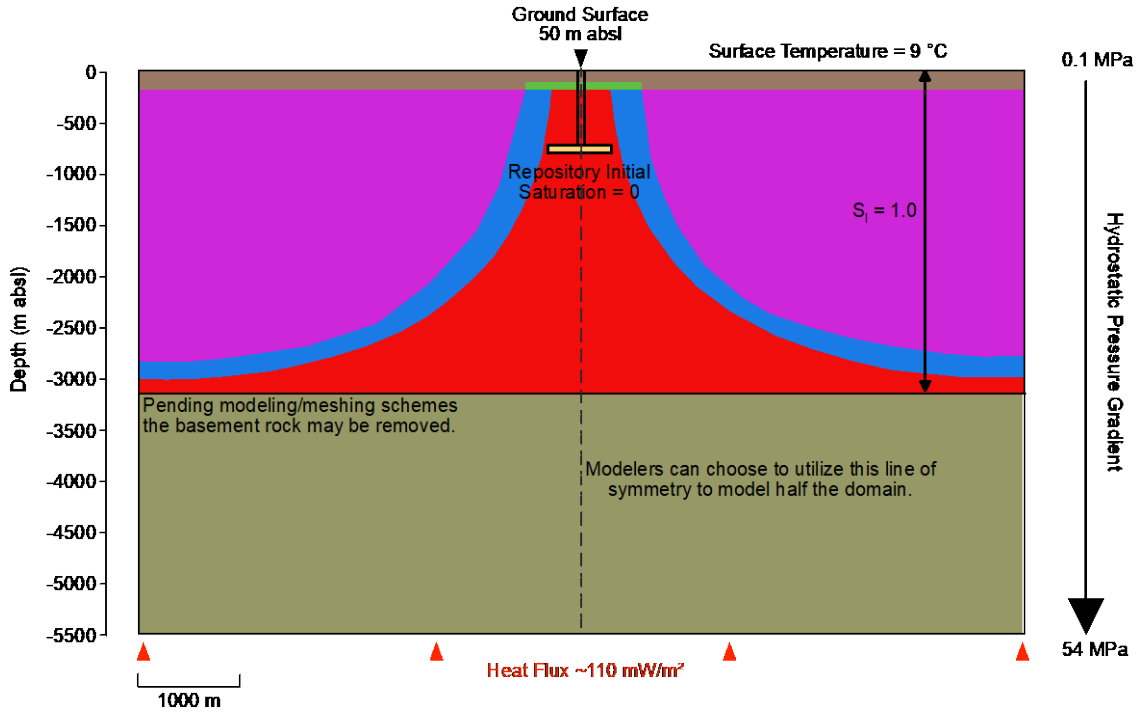

Color Legend	Geologic Unit
	Higher permeability Overburden
	Caprock
	Lower permeability sediment basin fill
	Anhydrite/Potash Ash/Crystal Lump Salt/Grey Salt
	Domal Salt
	Basement Rock

Figure 4-23 Geologic cross-section of salt reference case for Task F

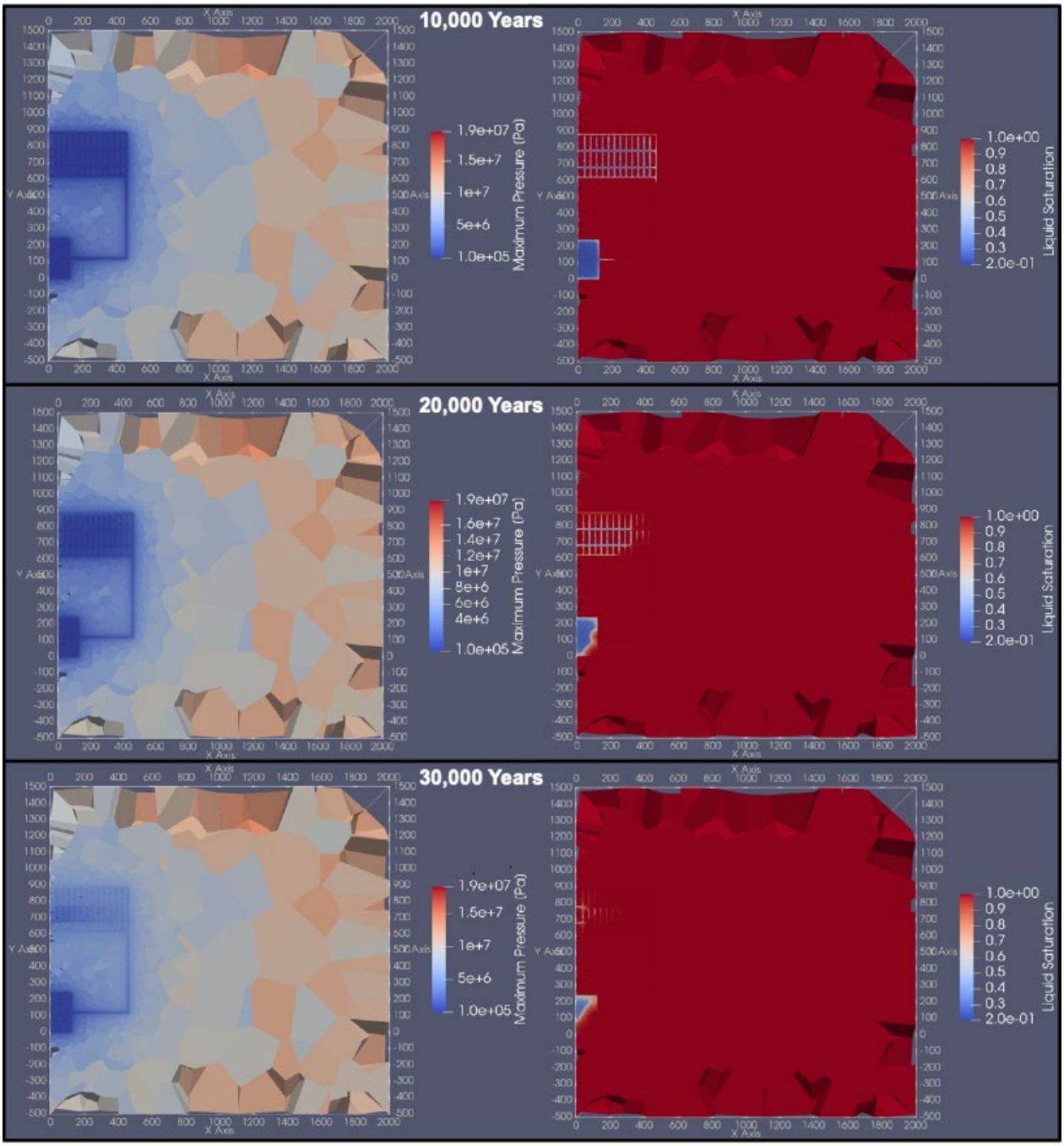

Figure 4-24 Overhead view of DECOVALEX salt reference case simulation results at the repository level showing pressure (left) and liquid saturation (right) at 10,000, 20,000, and 30,000 years

4.2.6 Repository Reference Cases

Over the past decade, generic repository reference cases have been simulated using GDSA Framework for many host rocks and repository designs. Table 4-1 identifies the core reference cases, their conceptual models, and their recent applications. Two more conceptual models, one in crystalline rock and one in salt, were included in the table this year to reflect the reference cases developed for Task F of DECOVALEX-2023 (Section 4.2.5).

Table 4-1 Repository concepts and generic (inventory) reference cases implemented with GDSA Framework

Repository Concepts and Inventory(s)	Conceptual Models	Model Application Reports
Argillite/shale repository		
SNF ranging from 4-PWR waste packages to 37-PWR dual purpose canisters (DPCs) High-temperature shale repository	Jové Colón et al. (2014); Zheng et al. (2014) Stein et al. (2020)	Mariner et al. (2017); Sevougian et al. (2019) Stein et al. (2020)
Crystalline repository		
Commercial SNF DOE managed waste (cancelled by DOE in 2017)	Wang et al. (2014); LaForce et al. (2022b)	Mariner et al. (2016); Swiler et al. (2019, 2020, 2021, 2022) Sevougian et al. (2016)
Salt repository		
Commercial SNF DOE managed waste (cancelled by DOE in 2017)	Sevougian et al. (2012); Freeze et al. (2013); LaForce et al. (2022b)	Sevougian et al. (2016); LaForce et al. (2020, 2022) Sevougian et al. (2019)
Alluvium repository, unsaturated conditions		
SNF ranging from 12-PWR waste packages to 37-PWR DPCs	Mariner et al. (2018)	Mariner et al. (2018); Sevougian et al. (2019); LaForce et al. (2021, 2022)
Dual purpose canister (DPC)		
24- to 37-PWR DPCs and 68- to 80-BWR DPCs	Price et al. (2019a)	Price et al. (2019b)
Deep borehole disposal		
Various waste types, including Cs/Sr capsules	Brady et al. (2009)	Freeze et al. (2016, 2019)

4.2.7 GDSA Framework Documentation

4.2.7.1 Model Information Database

GDSA Framework is a framework of conceptual models, mathematical models, and coded model capabilities constructed to produce applied system models. Coded model capabilities include coded models like buffer erosion, fuel degradation, temperature-dependent solubility, etc. Applied system models include repository reference case models and specific models for subdomains of those systems.

Each year GDSA developers build or improve conceptual and mathematical models and implement mathematical models in PFLOTRAN or elsewhere in GDSA Framework. While such accomplishments

get summarized in annual reports, they generally do not get documented in model-specific living documents or in a centralized model information database. Annual progress reports include calculations produced from new or revised coded model capabilities and applied system models. Selected information on evolving models is provided in annual reports, and certain user information is added to online PFLOTRAN documentation. However, individual model products (with model version numbers) are not produced.

In a regulatory environment, applied model calculations require a qualified model as input. The SFWST campaign does not operate in a regulatory environment, so GDSA Framework developers currently do not have NQA-1 documentation obligations. The R&D environment has allowed GDSA Framework developers to be quite prolific in producing model capabilities and systems models.

GDSA Framework is adding model capabilities at a rapid rate. An important part of the framework is supporting code and model documentation. Therefore, in FY 2022, a centralized GDSA model information database was initiated.

The model information database is currently in the form of a SharePoint site with a separate Word file for each model capability. Each Word file is a template in which descriptions or lists of specific information are requested. Requested information includes: model name, model version, model purpose, conceptual model, FEPs included, mathematical model, alternative models, software, input/output parameters, assumptions, limitations, input ranges of validity, model verification/demonstration, model validation, ideas for future improvement, references, developer(s), and reviewer(s). With this information in the database, a user will be able to quickly learn about the model capability and decide whether it is appropriate for the intended use or what improvements are needed. Also, with versioning it will be easier to determine the capabilities of a model for an application produced using a specific PFLOTRAN build.

Developing the database will take time. Table 4-2 lists the first ten model capabilities in the database. Two have been fully entered and reviewed (MDL-101 and MDL-110) and two others are currently underway (MDL-104 and MDL-107). A potential eventual format for this database is wiki or HTML. In the meantime, data entry into Word files will proceed.

Table 4-2 Model capabilities defined in the GDSA Framework model information database

Model ID	Model Capability
MDL-101	Buffer erosion canister corrosion
MDL-102	Waste package general corrosion
MDL-103	Fuel matrix degradation (FMD)
MDL-104	HLW glass degradation
MDL-105	Fuel matrix fractional degradation rate
MDL-106	Radioactive decay and ingrowth
MDL-107	FMD surrogate - kNNr
MDL-108	FMD surrogate - neural network
MDL-109	Isotope partitioning
MDL-110	Fracture network modeling in a space-filling mesh

4.2.7.2 Calculation Archive

In FY 2021, the GDSA Framework development team established a GDSA calculation archive, a centralized (gitlab) repository of GDSA calculations. The archive targets all GDSA milestone calculations and their supporting input files, codes, and workflow.

The main purpose of the archive is for improved internal communication and knowledge capture. The primary goals are:

- To document and archive GDSA calculations in a secure, centralized location
- To allow autonomous sharing of these calculations among GDSA team members
- To provide R&A technical reviewers easy access to supporting materials and calculations
- To provide a springboard for new calculations

In FY 2022, complications caused by large binary files prompted a new approach to the archive. Calculations that involve large binary files were relegated to a special hard drive on a common GDSA server. Calculations that do not contain large binary files remain in the gitlab repository.

4.2.7.3 SFWST Document Archive

The GDSA team continues to support the SFWST Document Archive (SDA), a document repository available to all SFWD participants. The SDA is a restricted-access SharePoint website that serves as an online library for reports generated in:

- NE 81, Office of SFWST
  - Disposal Research (DR)
  - Storage and Transportation (S&T)
- NE 82, Office of Integrated Waste Management (IWM)

Additionally, it contains presentations from past SFWD Annual Meetings.

4.3 Outreach

This section reviews important outreach activities supported by the GDSA Framework development work package and how they benefit nuclear waste repository performance assessment.

4.3.1 International Involvement

Much can be learned from the research and accomplishments of nuclear waste programs around the world. Interaction and collaboration with scientists involved in these programs is beneficial to the US program.

Opportunities for SFWST participants to interact and collaborate directly arise from participation in:

- International research projects, e.g., DECOVALEX and underground research facility studies
- International clubs, e.g., clay, salt, and crystalline clubs of the Nuclear Energy Agency (NEA)
- International conferences and journals

- International PFLOTRAN short courses (Nole et al. 2022, Section 2.4.5)

A detailed account of SFWST involvement in international research projects is presented in Birkholzer et al. (2020).

Like other SFWST work packages, GDSA work packages are deeply committed to international participation. For example, in FY 2022, participants in the GDSA Framework development work package (SF-22SN01030409) 1) took the lead of Task F of DECOVALEX-2023, 2) presented research at the 5th NEA Crystalline Club meeting in Dresden, Germany, 3) proposed a 2023-2024 program-of-work for the Crystalline Club, 4) wrote several papers (three for the 2022 International High Level Radioactive Waste Management Conference, one for the Journal of Nuclear Technology (Section 4.1.3.3)), and 5) reviewed a paper on fracture flow modeling for the Journal of Nuclear Technology. Many other international research activities, club meetings, conferences, and papers were supported by other GDSA work packages.

4.3.2 Open-Source Software

GDSA Framework is being developed for DOE and its subcontractors. Most of the software components of GDSA Framework are open source, including PFLOTRAN, Dakota, and dfnWorks. These codes are utilized by a community of users from around the world for work related to, and unrelated to, repository performance assessment (e.g., Hammond and Lichtner 2010; Chen et al. 2013; de Vries et al. 2013; Karra et al. 2014; Gardner et al. 2015; Kumar et al. 2016; Zachara et al. 2016; Avasarala et al. 2017; Trinchero et al. 2017; Shuai et al. 2019).

Open-source software licensing governs the free distribution of source code and/or binaries among a group of software developers and users. PFLOTRAN utilizes the GNU LGPL (lesser general public license) which states that the code may be distributed and modified as desired, but any changes to the original source code must be free and publicly available. LGPL also allows anyone to link a proprietary third-party library to the code or develop a graphical user interface on top of the code for profit. Further details are provided in Mariner et al. (2019, Section 2.3.4.1).

There are many benefits to open-source collaboration, especially when taxpayer funds support much of the code development. First, it encourages collaboration among a diverse team of developers. This collaboration pushes the code to the users who can help test and debug the code while providing feedback regarding user interaction. Open source provides transparency that exposes implementation details that are often critical for scientific reproducibility and quality assurance. These details are often deliberately or unintentionally omitted from user documentation, journal publications and reports. From a financial standpoint, open source allows developers to pool funds across a diverse set of projects funded in academia, government laboratories or the private sector. In addition, funding that would be spent on licensing fees can be redirected towards development. Finally, although the most fit codes can survive under any licensing option, open source may provide a more level playing field for natural selection to run its course.

PFLOTRAN's open-source licensing and accessible distribution facilitate collaboration amongst a broader U.S. and international community. This broad user community enhances the development of PFLOTRAN by sharing conceptual models, incorporating novel physicochemical algorithms, optimizing code performance, debugging problematic issues, and generating grass-roots publicity, all of which benefit DOE in return.

The PFLOTRAN website at www.pflotran.org directs interested parties to the online documentation and the Bitbucket repository (including source code and documentation build status and code coverage). Developer and user mailing lists are managed through Google Groups.

Estimating the size and extent of the PFLOTRAN user community is relatively difficult due to the inability to track downloads on Bitbucket. However, through Google Analytics, the hits on the PFLOTRAN website are tracked which provides a qualitative estimate (Figure 4-25) and demonstrates that the PFLOTRAN user base is multi-national.

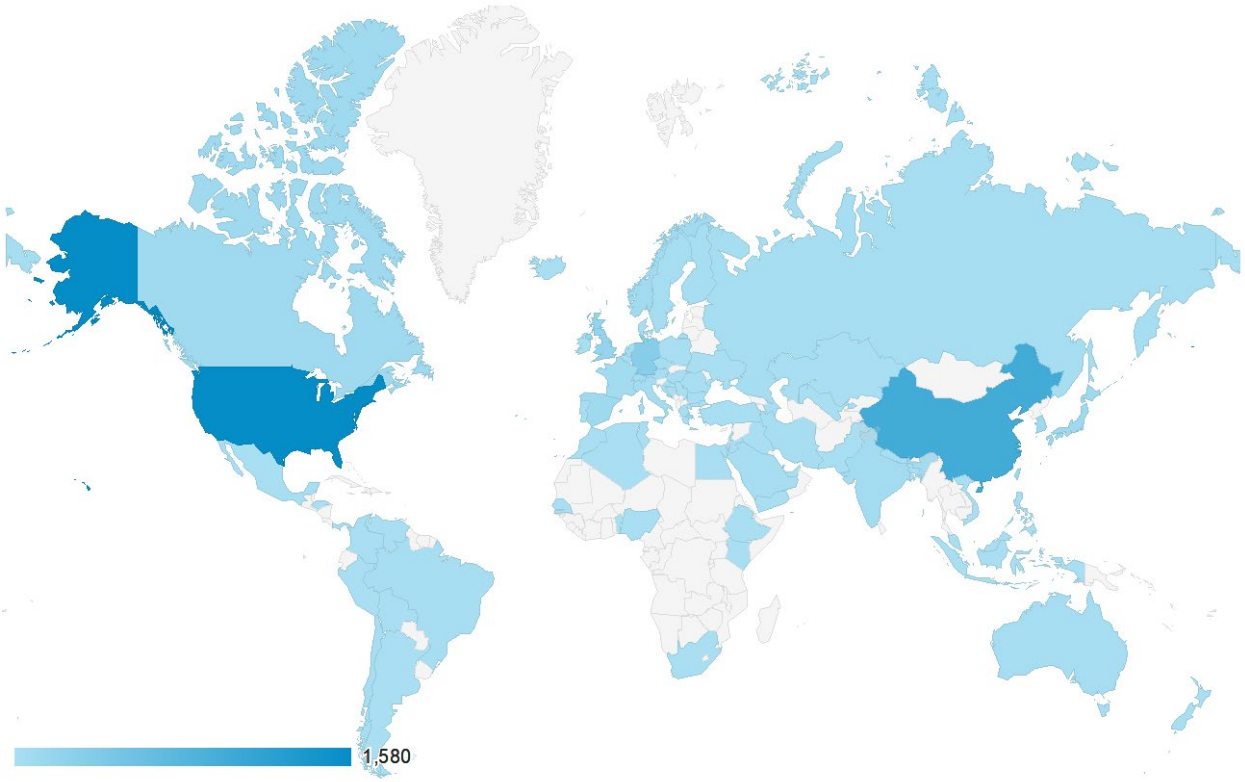

Figure 4-25 Total global hits to the PFLOTRAN website from individual users between May 1, 2021 to April 30, 2022 (Nole et al. 2022)

4.3.3 GDSA Framework Website

The GDSA team continues to support and develop the public GDSA Framework website at http://pa.sandia.gov/. The home page is shown in Figure 4-26.

The purpose of the website is to:

- Describe GDSA Framework, its capabilities, and the objectives behind its development
- Provide related reports for downloading
- Provide links to software used in GDSA Framework (e.g., PFLOTRAN, Dakota, dfnWorks)
- Identify collaborators involved in GDSA Framework development
- Announce upcoming events (e.g., PFLOTRAN short courses)

- Provide contact information

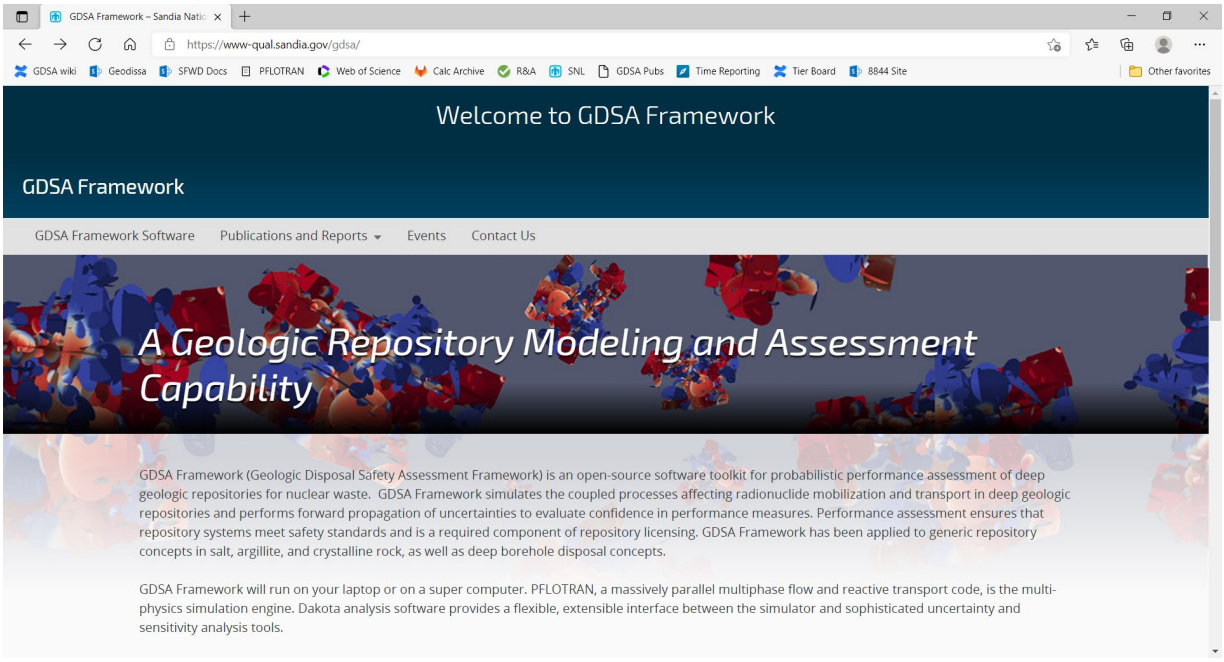

Figure 4-26 GDSA Framework website (http://pa.sandia.gov/)

5. CONCLUSIONS

This report describes FY 2022 advances of the Geologic Disposal Safety Assessment (GDSA) performance assessment (PA) development groups of the SFWST Campaign. The common mission of these groups is to develop a geologic disposal system modeling capability for nuclear waste that can be used to assess probabilistically the performance of generic disposal options and generic sites. The developing capability, called GDSA Framework, employs high-performance computing capable codes PFLOTRAN and Dakota.

The advances in GDSA Framework modeling capabilities in FY 2022 allow for improved fluid transport under saline conditions, improved emulation of fuel matrix degradation in repository simulations, automated material property changes to porous media over time, improved PFLOTRAN convergence for multiphase systems and dry out, and more detailed sensitivity analysis of system performance. New innovative methods implemented in PFLOTRAN allow for direct reactive transport of soluble porous media (salt) and improved simulation of the interactions of fractures and the matrix. A new correction factor implemented in mapdfn.py allows for improved upscaling of fracture properties to reference case meshes. New modeling approaches include the development and use of Voronoi meshing, advanced plans for simulating buffer erosion, and a finalized software design document for a comprehensive biosphere model. Continued advances in simulation workflow, quality assurance workflow, process model coupling workflow, and other forms of supporting infrastructure are expected to further facilitate future model development and user adoption.

An important responsibility of the GDSA Framework development team is to integrate with disposal R&D activities across the SFWST Campaign to ensure that R&D activities support the parts of the generic safety cases being developed. In FY 2022, the team continued to participate with other scientists and engineers at LANL, LBNL, PNNL, ORNL, INL, ANL, DOE, and SNL in the development of discrete fracture network modeling, multi-continuum modeling, Geologic Framework Models, fuel matrix degradation process modeling, machine-learning surrogate models, DECOVALEX-2023 Task F performance assessment, and advanced biosphere modeling.

Each year, GDSA Framework improves as additional modelers and programmers from around the world use, apply, and contribute to its development. GDSA Framework can be shared because the primary codes, PFLOTRAN and Dakota, are open source, available for free download, and have supporting documentation online. Outreach and collaborations support a primary objective of the GDSA Framework Development work package by facilitating testing of, and feedback on, PFLOTRAN and GDSA Framework and by increasing the likelihood outside users will contribute directly to code development in the future.

The ability to simulate increasingly complex repository reference cases continues to affirm that HPC-capable codes can be used to simulate important multi-physics couplings directly in a total system safety assessment demonstration. Reference-case-repository applications show that PFLOTRAN and its coupled codes can simulate complex coupled processes in a multi-kilometer domain while simultaneously simulating sub-meter-scale coupled behavior in the vicinity of each modeled waste package. Continued development will further enhance the preparedness of GDSA Framework for application in the future when transitioning to a program with potential sites.

6. REFERENCES

Abdelkader, A., Bajaj, C.L., Ebeida, M.S., Mahmoud, A.H., Mitchell, S.A., Owens, J.D., & Rushdi, A.A. (2020). VoroCrust: Voronoi meshing without clipping. ACM Transactions on Graphics (TOG) 39(3):1–16.

Adams, B.M., K.R. Dalbey, M.S. Eldred, L.P. Swiler, W.J. Bohnhoff, J.P. Eddy, D.M. Vigil, P.D. Hough and S. Lefantzi (2012). DAKOTA, A Multilevel Parallel Object-Oriented Framework for Design Optimization, Parameter Estimation, Uncertainty Quantification, and Sensitivity Analysis: Version 5.2+ User's Manual. Sandia National Laboratories, Albuquerque, New Mexico.

Adams, B.M., M.S. Ebeida, M.S. Eldred, J.D. Jakeman, L.P. Swiler, W.J. Bohnhoff, K.R. Dalbey, J.P. Eddy, K.T. Hu, D.M. Vigil, L.E. Baumann and P.D. Hough (2013). Dakota, a Multilevel Parallel Object-Oriented Framework for Design Optimization, Parameter Estimation, Uncertainty Quantification, and Sensitivity Analysis, Version 5.3.1+ Theory Manual. Sandia National Laboratories, Albuquerque, New Mexico.

Ahrens, J., Geveci, B., and Law, C. (2005). ParaView: An End-User Tool for Large Data Visualization, Visualization Handbook. Elsevier

Avasarala, S., P.C. Lichtner, A. . S. Ali, R. Gonzalez-Pinzon, J.M. Blake and J.M. Cerrato (2017). "Reactive Transport of U and V from Abandoned Uranium Mine Wastes." Environmental Science & Technology 51(21): 12385-12393.

Balay, S., J. Brown, K. Buschelman, V. Eijkhout, W.D. Gropp, D. Kaushik, M.G. Knepley, L. Curfman McInnes, B.F. Smith and H. Zhang (2013). PETSc Users Manual. Argonne, Illinois, Argonne National Laboratory.

Batzle, M., & Wang, Z. (1992). Seismic properties of pore fluids. Geophysics, 57(11), 1396–1408. https://doi.org/10.1190/1.1443207.

Birkholzer, J., B. Faybishenck, Y. Guglielme, J. Rutqvist, L. Zheng, F. Caporuscio, H. Viswanathan, C. Jove-colon, Y. Wang, M. Zavarin, and S. Asmussen (2020). International Collaboration Activities in Geologic Disposal Research: FY20 Progress. LBNL-2001353. Lawrence Berkeley National Laboratory, Berkeley, California.

Brady, P.V., B.W. Arnold, G.A. Freeze, P.N. Swift, S.J. Bauer, J.L. Kanney, R.P. Rechard, and J.S. Stein (2009). Deep borehole disposal of high-level radioactive waste. SAND2009-4401. Sandia National Laboratories, Albuquerque, New Mexico.

Buck, E., J. L. Jerden, Jr., W. L. Ebert and R. S. Wittmann (2013). Coupling the Mixed Potential and Radiolysis Models for Used Fuel Degradation. Washington D.C., U.S. Department of Energy.

Central Aroostook Soil and Water Conservation District, Maine Irrigation Guide 2005. Linda Alverson, Executive Director, Presque Isle.

Chen, X., G. Hammond, C. Murray, M. Rockhold, V. Vermeul and J. Zachara (2013). "Applications of ensemble-based data assimilation techniques for aquifer characterization using tracer data at Hanford 300 area." Water Resources Research 49: 7064-7076.

Chen, X., H. Murakami, M. Hahn, G. E. Hammond, M.L. Rockhold, J.M. Zachara and Y. Rubin (2012). "Three-Dimensional Bayesian Geostatistical Aquifer Characterization at the Hanford 300 Area using Tracer Test Data." Water Resources Research 48.

Condon C. A., Napier, B. A., Ghosh, S., Weaver, W. C., Varnum-Lowry, C. B., 2020. GDSA Biospherr Model Software Requirements Document. M3SF-20PN010304091, PNNL-30280. Pacific Northwest National Laboratory. Richland, Washington.

de Vries, L. M., J. Molinero, H. Ebrahimi, U. Svensson, P. Lichtner and E. Abarca (2013). Regional Scale HPC Reactive Transport Simulation of Nuclear Spent Fuel Repository in Forsmark, Sweden. Joint 8th International Conference on Supercomputing in Nuclear Applications (SNA) / 4th Monte Carlo Meeting (MC), Paris, France.

Debusschere, B.J., D.T. Seidl, T.M. Berg, K.W. Chang, R.C. Leone, L.P. Swiler, & P.E. Mariner (2022). Machine Learning Surrogate Process Models for Efficient Performance Assessment of a Nuclear

Waste Repository. Proceedings of the 2022 International High-Level Radioactive Waste Management Conference, American Nuclear Society, Phoenix, Arizona (SAND2022- 10696 C.Sandia National Laboratories, Albuquerque, New Mexico).

DOE (2012). Used Fuel Disposition Campaign Disposal Research and Development Roadmap. Washington, DC, Fuel Cycle Technologies, Office of Nuclear Energy, US Department of Energy.

DOE (2013). Strategy for the Management and Disposal of Used Nuclear Fuel and High-Level Radioactive Waste, January 2013. Washington, DC. http://energy.gov/downloads/strategy-management-and-disposalused-nuclear-fuel-and-high-level-radioactive-waste, U.S. Department of Energy.

Freeze, G., P.E. Mariner, J.A. Blink, F.A. Caporuscio, J.E. Houseworth and J.C. Cunnane (2011). Disposal System Features, Events, and Processes (FEPs): FY11 Progress Report. Sandia National Laboratories, Albuquerque, New Mexico.

Freeze, G., Stein, E.R., Brady, P.V., Lopez, C., Sassani, D. (2019). Deep Borehole Disposal Safety Case SAND2019-1915. Sandia National Laboratories, Albuquerque, New Mexico.

Freeze, G., Stein, E.R., Price, L., MacKinnon, R., and Tillman, J. (2016). Deep Borehole Disposal Safety Analysis. FCRD-UFD-2016-000075, SAND2016-10949R. Sandia National Laboratories, Albuquerque, New Mexico.

Freeze, G., W.P. Gardner, P. Vaughn, S.D. Sevougian, P. Mariner, V. Mousseau and G. Hammond (2013). Enhancements to the Generic Disposal System Modeling Capabilities. Sandia National Laboratories, Albuquerque, New Mexico.

Gardner, W.P., G. Hammond and P. Lichtner (2015). "High Performance Simulation of Environmental Tracers in Heterogeneous Domains." Groundwater 53: 71-80.

Ghosh, S., C.A. Condon, B.A. Napier, G. Hammond, S. Snyder, and T. Bailie (2022). GDSA Biosphere Model Design Document. M3SF- 22PN010304071. PNNL-32062. Rev. 1. Pacific Northwest National Laboratory, Richland, Washington.

Haas, J. L. (1976). Physical properties of the coexisting phases and thermochemical properties of the H2O component in boiling NaCl solutions. US Geol. Surv. Bull., 1421, 1–73.

Hammond, G., P. Lichtner and C. Lu (2007). "Subsurface multiphase flow and multicomponent reactive transport modeling using high performance computing." Journal of Physics: Conference Series 78: 1-10.

Hammond, G.E. and P. Lichtner (2010). "Field-scale modeling for the natural attenuation of uranium at the Hanford 300 area using high performance computing." Water Resources Research 46.

Hammond, G.E., P.C. Lichtner and M.L. Rockhold (2011b). "Stochastic simulation of uranium migration at the Hanford 300 Area." Journal of Contaminant Hydrology 120-121: 115-128.

Hammond, G.E., P.C. Lichtner, C. Lu and R.T. Mills (2011a). PFLOTRAN: Reactive Flow and Transport Code for Use on Laptops to Leadership-Class Supercomputers. Groundwater Reactive Transport Models. F. Zhang, G. T. Yeh and J. Parker, Bentham Science Publishers.

Hammond, G.E., P.C. Lichtner, R.T. Mills and C. Lu (2008). "Toward petascale computing in geosciences: application to the Hanford 300 Area." Journal of Physics Conference Series 125: 12051-12051.

Harvey, J.A., A.M. Taconi, & P.E. Mariner (2022). Development of an Efficient Version of the Fuel Matrix Degradation Model. Proceedings of the 2022 International High-Level Radioactive Waste Management Conference, American Nuclear Society, Phoenix, Arizona (SAND2022-8791 C, Sandia National Laboratories, Albuquerque, New Mexico).

Huang, W.L., Longo, J.M., & Pevear, D.R. (1993). An experimentally derived kinetic model for smectite-to-illite conversion and its use as a geothermometer. Clays and Clay Minerals, 41(2), 162-177.

IAEA (2003). Reference Biospheres for Solid Radioactive Waste Disposal. Vienna, Austria, International Atomic Energy Agency.

IAEA (2006). Geological Disposal of Radioactive Waste. Safety Requirements No. WS-R-4. Vienna, Austria, International Atomic Energy Agency.

Jerden, J., G. Hammond, J. M. Copple, T. Cruse and W. Ebert (2015b). Fuel Matrix Degradation Model: Integration with Performance Assessment and Canister Corrosion Model Development. Washington, DC, US Department of Energy.

Jerden, J., J.M. Copple, K. E. Frey and W. Ebert (2015a). Mixed Potential Model for Used Fuel Dissolution - Fortran Code. O. o. U. N. F. Disposition. Washington, DC, US Department of Energy.

Jerden, J., V.K. Gattu and W. Ebert (2018). Update on Validation and Incorporationof a New Steel Corrosion Module into Fuel Matrix Degradation Model. Illinois, Argonne National Laboratory.

Jove Colon, C.F., P. Weck, L. Zheng, J. Rutqvist, C.I. Steefel, K. Kim, S. Nakagawa, J. Houseworth, J. Birkholzer, F.A. Caporuscio, M. Cheshire, M.S. Rearick, M.K. McCarney, M. Zavarin, A.B. Benedicto, M.S. Kersting, J.L. Jerden, K.E. Frey, J.M. Copple, and W.L. Ebert (2014). Evaluation of Used Fuel Disposition in Clay-Bearing Rock. FCRD-UFD-2014-000056. SAND2014-18303R. Sandia National Laboratories, Albuquerque, New Mexico.

Karra, S., S.L. Painter and P.C. Lichtner (2014). "Three-phase numerical model for subsurface hydrology in permafrost-affected regions (PFLOTRAN-ICE v1.0)." Cryosphere 8(5): 1935-1950.

Kumar, J., N. Collier, G. Bisht, R. T. Mills, P. E. Thornton, C. M. Iversen and V. Romanovsky (2016). "Modeling the spatiotemporal variability in subsurface thermal regimes across a low-relief polygonal tundra landscape." Cryosphere 10(5): 2241-2274.

LaForce, T., Basurto, E., Chang, K.W., Ebeida, M., Eymold, W., Faucett, C., Jayne, R., Kucinski, N., Leone, R., Mariner, P., Perry, F.V. (2022, in progress). GDSA Repository Systems Analysis Investigations in FY 2022. SAND2022-xxxx R, Sandia National Laboratories, Albuquerque, NM

LaForce, T., Chang, K.W., Perry, F.V., Lowry, T.S., Basurto, E., Jayne, R., Brooks, D., Jordan, S., Stein, E.R., Leone, R., Nole, M. (2020) GDSA Repository Systems Analysis Investigations in FY 2020. SAND2020-12028 R. Sandia National Laboratories, Albuquerque, New Mexico.

LaForce, T., E. Basurto, K.W. Chang, R. Jayne, R. Leone, M. Nole, F.V. Perry, and E. Stein (2021). GDSA Repository Systems Analysis Investigations in FY2021. SAND2021-11691-R, Sandia National Laboratories, Albuquerque, New Mexico.

LaForce, T., R.S. Jayne, R. Leone, Stein, E., Nguyen, S. (2022b). DECOVALEX-2023 Task F Specification Revision 8. SAND2022-6944 R. Sandia National Laboratories, Albuquerque, NM.

Lichtner, P. C., Hammond, G. E., Lu C., Karra, S., Bisht, G., Andre, B., Mills, R. T., Kumar, J., Frederick, J. M. (2020) PFLOTRAN Web page. http://www.pflotran.org

Lichtner, P.C. (2000). Critique of Dual Continuum Formulations of Multicomponent Reactive Transport in Fractured Porous Media, Ed. Boris Faybishenko, Dynamics of Fluids in Fractured Rock, Geophysical Monograph 122, 281–298.

Lichtner, P.C. and G.E. Hammond (2012). Quick Reference Guide: PFLOTRAN 2.0 (LA-CC-09-047) Multiphase-Multicomponent-Multiscale Massively Parallel Reactive Transport Code. Los Alamos, New Mexico, Los Alamos National Laboratory.

Lu, C. and P. C. Lichtner (2007). "High resolution numerical investigation on the effect of convective instability on long term CO2 storage in saline aquifers." Journal of Physics Conference Series 78: U320-U325.

Mariner, P. E., E. R. Stein, J. M. Frederick, S. D. Sevougian and G. E. Hammond (2017). Advances in Geologic Disposal System Modeling and Shale Reference Cases. SFWD-SFWST-2017-000044, SAND2017-10304 R. Sandia National Laboratories, Albuquerque, New Mexico.

Mariner, P. E., E. R. Stein, J. M. Frederick, S. D. Sevougian, G. E. Hammond and D. G. Fascitelli (2016). Advances in Geologic Disposal System Modeling and Application to Crystalline Rock. FCRD-UFD-2016-000440, SAND2016-9610 R. Sandia National Laboratories, Albuquerque, New Mexico.

Mariner, P. E., E. R. Stein, S. D. Sevougian, L. J. Cunningham, J. M. Frederick, G. E. Hammond, T. S. Lowry, S. Jordan and E. Basurto (2018). Advances in Geologic Disposal Safety Assessment and an Unsaturated Alluvium Reference Case. SFWD-SFWST-2018-000509, SAND2018-11858 R. Sandia National Laboratories, Albuquerque, New Mexico.

Mariner, P. E., L. A. Connolly, L. J. Cunningham, B. J. Debusschere, D. C. Dobson, J. M. Frederick, G. E. Hammond, S. H. Jordan, T. C. LaForce, M. A. Nole, H. D. Park, F. V. Perry, R. D. Rogers, D. T. Seidl, S. D. Sevougian, E. R. Stein, P. N. Swift, L. P. Swiler, J. Vo and M. G. Wallace (2019). Progress in Deep Geologic Disposal Safety Assessment in the U.S. since 2010. SAND2019-12001 R. Sandia National Laboratories, Albuquerque, New Mexico.

Mariner, P. E., T. M. Berg, K. W. Chang, B. J. Debusschere, R. C. Leone and D. T. Seidl (2020b). Surrogate Model Development of Spent Fuel Degradation for Repository Performance Assessment. SAND2020-10797 R. Sandia National Laboratories, Albuquerque, New Mexico.

Mariner, P. E., W. P. Gardner, G. E. Hammond, S. D. Sevougian and E. R. Stein (2015). Application of Generic Disposal System Models. FCRD-UFD-2015-000126, SAND2015-10037R. Sandia National Laboratories, Albuquerque, New Mexico.

Mariner, P.E., M.A. Nole, E. Basurto, T.M. Berg, K.W. Chang, B.J. Debusschere, A.C. Eckert, M.S. Ebeida, M. Gross, G.E. Hammond, J. Harvey, S.H. Jordan, K.L. Kuhlman, T.C. LaForce, R.C. Leone, W.C. McLendon III, M.M. Mills, H.D. Park, F.V. Perry, A. Salazar III, D.T. Seidl, S.D. Sevougian, E.R. Stein, and L.P. Swiler (2020a). Advances in GDSA Framework Development and Process Model Integration. M2SF-20SN010304042. SAND2020-10787 R. Sandia National Laboratories, Albuquerque, New Mexico.

Mariner, P.E., T.M. Berg, K.W. Chang, B.J. Debusschere, A.C. Eckert, J. Harvey, T.C. LaForce, R.C. Leone, M.M. Mills, M.A. Nole, H.D. Park, F.V. Perry, D.T. Seidl, L.P. Swiler (2021). GDSA Framework Development and Process Model Integration FY 2021. M2SF-21SN010304053, SAND2021-12626 R. Sandia National Laboratories, Albuquerque, New Mexico.

Meacham, P. G., D. R. Anderson, E. J. Bonano and M. G. Marietta (2011). Sandia National Laboratories Performance Assessment Methodology for Long-Term Environmental Programs: The History of Nuclear Waste Management. Sandia National Laboratories, Albuquerque, New Mexico.

Mills, R., C. Lu, P. C. Lichtner and G. Hammond (2007). Simulating subsurface flow and transport on ultrascale computers using PFLOTRAN. 3rd Annual Scientific Discovery through Advanced Computing Conference (SciDAC 2007), Boston, Journal of Physics Conference Series.

National Weather Service (2022). https://www.weather.gov/wrh/Climate?wfo=gyx

Navarre-Sitchler, A., R. M. Maxwell, E. R. Siirila, G. E. Hammond and P. C. Lichtner (2013). Elucidating geochemical response of shallow heterogeneous aquifers to CO2 leakage using high-performance computing: implications for monitoring CO2 sequestration. Advances in Water Resources 53: 44-55.

Nielsen, M.G., and Locke, D.B. 2015. Simulation of groundwater flow and streamflow depletion in the Branch Brook, Merriland River, and parts of the Mousam River watersheds in southern Maine: U.S. Geological Survey Scientific Investigations Report 2014–5235. 78 p.

Nole, M., G.D. Beskardes, D. Fukuyama, R.C. Leone, P. Mariner, H.D. Park, M. Paul, A. Salazar, G.E. Hammond, and P.C. Lichtner (2021). PFLOTRAN Development FY2022. M3SF-22SN010304112. SAND2022-10526 R. Sandia National Laboratories, Albuquerque, New Mexico.

Nole, M., R.C. Leone, H.D. Park, M. Paul, A. Salazar, G.E. Hammond, and P.C. Lichtner (2021). PFLOTRAN Development FY2021. M3SF-21SN010304072. SAND2021-8709 R. Sandia National Laboratories, Albuquerque, New Mexico.

OECD (2004). Post-Closure Safety Case for Geological Repositories Nature and Purpose. Paris, France, Organisation for Economic Co-Operation and Development, Nuclear Energy Agency.

Olivella, S., Carrera, J., Gens, A., & Alonso, E. (1994). Nonisothermal multiphase flow of brine and gas through saline media. Transport in Porous Media, 15(3), 271–293.

Olivella, S., Castagna, S., Alonso, E., & Lloret, A. (2011). Porosity variations in saline media induced by temperature gradients: Experimental evidences and modelling. Transport in Porous Media, 90(3), 763–777.

Posiva (2013). Safety Case for the Disposal of Spent Nuclear Fuel at Olkiluoto - Models and Data for the Repository System 2012. POSIVA 2013-01. Posiva Oy, Eurajoki, Finland.

Posiva (2021). Sulfide Fluxes and Concentrations in the Spent Nuclear Fuel Repository at Olkiluoto – 2021 Update. Working Report 2021-07. Posiva Oy, Eurajoki, Finland.

Price, L.L., A.A. Alsaed, A. Barela, P.V. Brady, F. Gelbard, M.B. Gross, M. Nole, J.L. Prouty, K. Banerjee, S. Bhatt, G.G. Davidson, Z. Fang, R. Howard, S.R. Johnson, S.L. Painter, and M. Swinney (2019b). Preliminary Analysis of Postclosure DPC Criticality Consequences. M2SF-20SN010305061. SAND2020-4106. Sandia National Laboratories, Albuquerque, New Mexico.

Price, L.L., A.A. Alsaed, P.V. Brady, M.B. Gross, E.L. Hardin, M. Nole, J.L. Prouty, K. Banerjee and G.G. Davidson (2019a). Postclosure Criticality Consequence Analysis—Scoping Phase. M3SF-19SN010305061. Sandia National Laboratories, Albuquerque, New Mexico.

Rechard, R.P. (1995). Performance Assessment of the Direct Disposal in Unsaturated Tuff of Spent Nuclear Fuel And High-Level Waste Owned by US Department of Energy. Sandia National Laboratories, Albuquerque, New Mexico. 1, 2, and 3.

Rechard, R.P. (2002). General approach used in the performance assessment for the Waste Isolation Pilot Plant. Scientific Basis for Nuclear Waste Management XXV, Boston, Massachussetts, Materials Research Society.

Rechard, R.P. and C.T. Stockman (2014). "Waste degradation and mobilization in performance assessments of the Yucca Mountain disposal system for spent nuclear fuel and high-level radioactive waste." Reliability Engineering and System Safety 122(2): 165-188.

Rechard, R.P. and M.S. Tierney (2005). "Assignment of probability distributions for parameters in the 1996 performance assessment for the Waste Isolation Pilot Plant, Part 1: Description of process." Reliability Engineering and System Safety 88(1): 1-32.

Ridgway, E.M. (2020). Dakota. GUI Version 6.12 User Manual – Next-Gen Workflow. https://dakota.sandia.gov/content/next-gen-workflow. Accessed August 5, 2020.

Sassani, D., J. Birkholzer, R. Camphouse, G. Freeze and E. Stein (2021). SFWST Disposal Research R&D 5-Year Plan – FY2021 Update. Draft Report. M2SF-21SN010304054. Draft Report - SAND2021-12491 R. Sandia National Laboratories, Albuquerque, New Mexico.

Sevougian, S. D., E. R. Stein, T. LaForce, F. V. Perry, T. S. Lowry, L. J. Cunningham, M. Nole, C. B. Haukwa, K. W. Chang and P. E. Mariner (2019b). GDSA Repository Systems Analysis Progress Report. SAND2019-5189 R. Sandia National Laboratories, Albuquerque, New Mexico.

Sevougian, S. D., G. A. Freeze, P. Vaughn, P. Mariner and W. P. Gardner (2013). Update to the Salt R&D Reference Case. FCRD-UFD-2013-000368. SAND2013-8255P. Sandia National Laboratories, Albuquerque, New Mexico.

Sevougian, S. D., G. A. Freeze, W. P. Gardner, G. E. Hammond and P. E. Mariner (2014). Performance Assessment Modeling and Sensitivity Analyses of Generic Disposal System Concepts. Sandia National Laboratories, Albuquerque, New Mexico.

Sevougian, S. D., P. E. Mariner, L. A. Connolly, R. J. MacKinnon, R. D. Rogers, D. C. Dobson and J. L. Prouty (2019a). DOE SFWST Campaign R&D Roadmap Update, Rev. 1. SAND2019-9033R. Sandia National Laboratories, Albuquerque, New Mexico.

Sevougian, S. D., Stein, E. R., LaForce, T., Perry, F. V., Nole, M., Haukwa, C. B., and Chang, K. W. (2019c). GDSA Repository Systems Analysis FY19 Update. SAND2019-11942R. Sandia National Laboratories, Albuquerque, NM.

Sevougian, S.D., G.A. Freeze, M.B. Gross, J. Lee, C.D. Leigh, P. Mariner, R.J. MacKinnon, and P. Vaughn (2012). TSPA Model Development and Sensitivity Analysis of Processes Affecting Performance of a Salt Repository for Disposal of Heat-Generating Nuclear Waste. FCRD-UFD-2012-000320 Rev. 0. U.S. Department of Energy, Office of Nuclear Energy, Used Nuclear Fuel Disposition, Washington, D.C.

Sevougian, S.D., Stein, E.R., Gross, M.B., Hammond, G.E., Frederick, J.M., and Mariner, P.E. (2016). Status of Progress Made Toward Safety Analysis and Technical Site Evaluations for DOE Managed HLW and SNF. FCRD-UFD-2016-000082. SAND2016-11232R. Sandia National Laboratories, Albuquerque, New Mexico.

Shuai, P., X. Y. Chen, X. H. Song, G. E. Hammond, J. Zachara, P. Royer, H. Y. Ren, W. A. Perkins, M. C. Richmond and M. Y. Huang (2019). "Dam Operations and Subsurface Hydrogeology Control Dynamics of Hydrologic Exchange Flows in a Regulated River Reach." Water Resources Research 55(4): 2593-2612.

Sparrow, B. S. (2003). Empirical equations for the thermodynamic properties of aqueous sodium chloride. Desalination, 159(2), 161–170.

Stein, E.R., C. Bryan, D.C. Dobson, E.L. Hardin, C. Jové-Colón, C.M. Lopez, E.N. Matteo, S. Mohanty, M. Pendleton, F.V. Perry, J.L. Prouty, D.C. Sassani, Y. Wang, J. Rutqvist, L. Zheng, K.B. Sauer, F. Caporuscio, R. Howard, A. Adeniyi, K. Banerjee, and R. Josep (2020). Disposal Concepts for a High-Temperature Repository in Shale. M3SF-21SN010304064. SAND2020-12471 R. Sandia National Laboratories, Albuquerque, New Mexico.

Sweeney, M. R., Gable, C. W., Karra, S., Stauffer, P. H., Pawar, R. J., & Hyman, J. D. (2020). Upscaled discrete fracture matrix model (UDFM): an octree-refined continuum representation of fractured porous media. Computational Geosciences, 24(1), 293–310. https://doi.org/10.1007/s10596-019-09921-9

Swiler, L. P., E. Basurto, D. M. Brooks, A. C. Eckert, P. E. Mariner, T. Portone and E. R. Stein (2020). Status Report on Uncertainty Quantification and Sensitivity Analysis Tools in the Geologic Disposal Safety Assessment (GDSA) Framework. SAND2020-10802 R. Sandia National Laboratories, Albuquerque, New Mexico.

Swiler, L. P., J. C. Helton, E. Basurto, D. M. Brooks, P. E. Mariner, L. M. Moore, S. Mohanty, S. D. Sevougian and E. R. Stein (2019). Status Report on Uncertainty Quantification and Sensitivity Analysis Tools in the Geologic Disposal Safety Assessment (GDSA) Framework. SAND2019-13835 R. Sandia National Laboratories, Albuquerque, New Mexico.

Swiler, L.P., E. Basurto, D.M. Brooks, A.C. Eckert, R. Leone, P.E. Mariner, T. Portone, M. L. Smith and E.R. Stein (2021). Uncertainty and Sensitivity Analysis Methods and Applications in the GDSA Framework (FY2021). M3SF-21SN010304042. SAND2021-9903R. Sandia National Laboratories, Albuquerque, New Mexico.

Swiler, L.P., E. Basurto, D.M. Brooks, A.C. Eckert, R. Leone, P.E. Mariner, T. Portone, and M. L. Smith. "Uncertainty and Sensitivity Analysis Methods and Applications in the GDSA Framework (FY2022)." M3SF- 22SN010304082. SAND2022-11220 R. Sandia National Laboratories, Albuquerque, New Mexico

Trinchero, P., I. Puigdomenech, J. Molinero, H. Ebrahimi, B. Gylling, U. Svensson, D. Bosbach and G. Deissmann (2017). "Continuum-based DFN-consistent numerical framework for the simulation of oxygen infiltration into fractured crystalline rocks." Journal of Contaminant Hydrology 200: 60-69.

Voss, C. I., & Souza, W. R. (1987). Variable density flow and solute transport simulation of regional aquifers containing a narrow freshwater-saltwater transition zone. Water Resources Research, 23(10), 1851–1866.

Wang, Y., E. N. Matteo, J. Rutqvist, J. A. Davis, L. Zheng, J. Houseworth, J. Birkholzer, T. Dittrich, C. W. Gable, S. Karra, N. Makedonska, S. Chu, D. Harp, S. L. Painter, P. W. Reimus, F. V. Perry, P. Zhao, J. Begg, M. Zavarin, S. J. Tumey, Z. Dai, A. B. Kersting, J. L. Jerden, K. E. Frey, J. M. Copple, and W. L. Ebert (2014). Used Fuel Disposal in Crystalline Rocks Status and FY14 Progress. FCRD-UFD-2014-000060. SAND2014-17992 R. Sandia National Laboratories, Albuquerque, New Mexico.

Winter, T. & Harvey, J. & Franke, O. & Alley, William. 1998. Ground water and surface water: a single resource. U.S. Geological Survey Circular 1139. 87 p.

Zachara, J. M., X. Y. Chen, C. Murray and G. Hammond (2016). "River stage influences on uranium transport in a hydrologically dynamic groundwater-surface water transition zone." Water Resources Research 52(3): 1568-1590.

Zheng, L. C. Jové Colón, M. Bianchi, and J. Birkholzer (2014). Generic Argillite/Shale Disposal Reference Case. FCRD-UFDC-2014-000319. LBNL-6709E. Lawrence Berkeley National Laboratory, Berkeley, California.

Appendix A. NEAR-TERM GDSA THRUSTS IN THE DISPOSAL RESEARCH R&D 5-YEAR PLAN UPDATE

APPENDIX A. NEAR-TERM GDSA THRUSTS IN THE DISPOSAL RESEARCH R&D 5-YEAR PLAN UPDATE

Disposal Research 5-Year Plan Thrusts: Near Term FY21

Thrust	Description	Tech. Area	Term
	Geologic Disposal Safety Assessment		
G01	*Advanced simulation capability*	*GDSA*	*Near*
	Near term advancements in PFLOTRAN capability will continue to focus on high priority topical areas identified in the 2019 Disposal Research R&D Roadmap Reassessment while building on previous accomplishments. These efforts will include continuing to advance high-temperature simulation capability, implementing material-specific waste package degradation models, and addressing the coupled thermo-hydro-mechanical (THM) processes affecting buffer evolution, and the coupled thermo-hydro-chemical (THC) processes affecting radionuclide transport. Multi-fidelity model implementation, including mechanistic models derived from detailed process understanding, reduced order models, and machine learning emulators, enhances computational efficiency and dovetails with integration of advanced UQ/SA methods. Other software development tasks will include ongoing development of open-source biosphere simulation software; addition of capability to dfnWorks (Hyman et al. 2015), software for generating discrete fracture networks and simulating particle transport; and release of an open source version of Vorocrust (Abdelkader et al. 2020), an automated meshing tool for generating conforming meshes of complex engineered and geologic features.		
G02	*Uncertainty and sensitivity analysis*	*GDSA*	*Near*
	Uncertainty quantification and sensitivity analysis (UQ/SA) methods in GDSA Framework will be advanced in two ways. First, the team will continue to identify and demonstrate methods consistent with the current standard of practice that add value to deep geologic repository performance assessment such as surrogate (meta) modeling, variance decomposition, multifidelity analysis, and evaluation of model form uncertainty. The team will continue to take a leadership role in international collaboration on these topics. Second, the team will begin to evaluate the reliability of methods dependent on surrogate models through techniques such as cross-validation and development of quantitative metrics for assessing goodness of surrogates.		

Thrust	Description	Tech. Area	Term
	Geologic Disposal Safety Assessment		
G03	*Workflow* Transparent, traceable workflows increase stakeholder confidence and user-friendliness. In the next 1 to 2 years, GDSA automation will be further developed using NGW and two additional important workflows will be established: an open source framework (scripted in Python) that automates software (PFLOTRAN) verification testing; and a workflow that streamlines data transfer from the geologic model to the meshing software and ultimately to the simulator. Integration of GDSA Framework with the Online Waste Library will be initiated. This integration will provide quality-assured radionuclide inventories for simulations involving defense-related waste streams.	*GDSA*	*Near*
G04	*Repository systems analysis* In the next 1 to 2 years, a main priority will be simulation and analysis of the salt and crystalline reference cases developed for the DECOVALEX2023 task. This task will drive development of models of bentonite backfill evolution and waste package degradation (crystalline) and of salt consolidation and creep; and advance understanding of uncertainties associated with simulation and analysis methods. GDSA will continue to integrate with other technical areas to advance analyses of direct disposal of DPCs, understanding of high-temperature FEPs, and scenario development methodology.	*GDSA*	*Near*
G05	*Geologic modeling* Geologic modeling involves two primary efforts: generation of representative 3-dimensional (3D) regional geology models that inform reference case concepts and simulations, and development of an interactive web-based application (https://gis1.inl.gov/regionalgeology/) for visualizing argillite, salt, and crystalline formations in the US. In the next 1 to 2 years, geologic models of a generic unsaturated alluvial basin and of regional argillite stratigraphy will be linked into the meshing workflow described above; and 3D subsurface visualization tools will be developed within the web application.	*GDSA*	*Near*

(This page is intentionally blank.)

Appendix B. FUEL MATRIX DEGRADATION PROCESS MODEL CODE DEVELOPMENT IN FORTRAN

APPENDIX B. FUEL MATRIX DEGRADATION PROCESS MODEL CODE DEVELOPMENT IN FORTRAN

INTRODUCTION

Modeling the degradation of stored spent nuclear fuel (UO_2) in a breached waste package is useful for performance assessment (PA) simulations. Currently, the Fuel Matrix Degradation (FMD) model is the capability under development by the Spent Fuel and Waste Science and Technology (SFWST) campaign of the U.S. Department of Energy (DOE). Recent results have indicated that machine learned surrogate models could be used as accurate replacements for full process models. The surrogate models provide a significant speed up in computational time and are much better suited to handle the large number of simulations that are routinely performed in PA activities. Surrogate models are currently trained on data generated from the full process model, therefore the need for an accurate process model still exists such that new surrogate models can be developed in the event of new processes or new machine learning techniques are deployed. The current version of the FMD process model exists as a suite of MATLAB functions and subroutines which can be challenging to update and modify. Herein we describe the current and on-going efforts to develop a working Fortran model that reproduces the MATLAB version. We provide a brief overview of the FMD process model with a focus on the radiolysis model for H_2O_2 generation and interfacial reactions. Results to date are presented, and future directions are discussed.

FMD PROCESS MODEL

The broader FMD process model has been discussed in great length in several recent reports (Jerden, et al., 2012; Jerden, et al., 2018). The goal of the FMD model is to predict UO_2 fuel dissolution rates in a breached waste package to help calculate radionuclide release rates for PA simulations. The original FMD process model was adapted from Canadian Mixed Potential Model of Shoesmith, King, and Kolar (Shoesmith, et al., 2003) which critically works on two assumptions: (1) electrochemical reactions can be broken into partial oxidation/reduction reactions, and (2) no net accumulation of charge is observed

(Wagner and Traud, 1938). Fuel dissolution occurs via a complex balance between oxidative and chemical processes; therefore the electrochemical reactions are the crux of the FMD model.

While the FMD process model exists as a one-dimensional (1D) reactive-transport column, it should be noted that 2D models are the subject of active research (Liu, et al., 2018). In its current form, the column is broken into three regions depicted in Fig. B-1, namely the fuel region, aqueous region, and steel container region. The spatial region is broken up logarithmically with smaller grid cell spacings implemented near the surface interfacial regions.

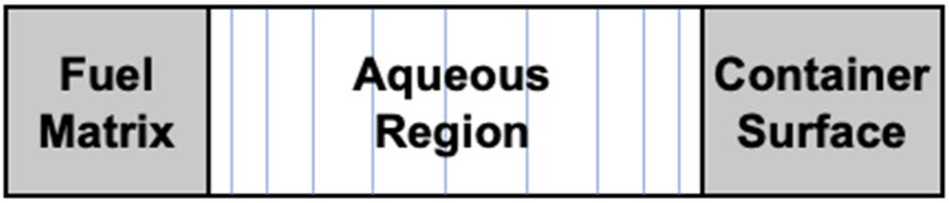

Fig. B-1 Physical depiction of the FMD model which exists as a 1D reactive-transport column. The column is broken into three distinct regions including the fuel surface (left), aqueous region (middle), and steel container surface (right). The spatial region is broken up using a logarithmic scaling with smaller grid cell spacings near the surface interfaces.

The aqueous chemistry reactions included in the model are shown in Tab. B-1. The interfacial, electrochemical reactions are shown in Tab. B-2. The reaction rates and parameters are omitted here for clarity however they can be found in previous reports (Jerden, et al., 2012). In addition to the chemical reactions, the FMD model incorporates the following processes

- Precipitation and dissolution of solid uranium phases at the interfaces which retard diffusion and limit access to the fuel surface
- Alpha radiolysis for the generation of H_2O_2 which acts as the main oxidant of the UO_2 fuel.
- Arrhenius temperature dependences for reaction rates.
- Noble metal particle phases on the fuel surface which catalyze the redox reactions.

Tab. B-1 List of aqueous chemistry reactions incorporated in the FMD model.

Aqueous Chemistry Reactions
$UO_2^{2+} + 2OH^- + H_2O \rightarrow UO_3 \cdot 2H_2O$
$UO_2^{2+} + H_2O_2 + 4H_2O \rightarrow UO_4 \cdot 4H_2O + 2H^+$
$UO_2(CO_3)_2^{2-} + 2OH^- + H_2O \rightarrow UO_3 \cdot 2H_2O + 2CO_3^{2-}$
$UO_3 \cdot 2H_2O + 2CO_3^{2-} \rightarrow UO_2(CO_3)_2^{2-} + 2OH^- + H_2O$
$H_2O_2 + 2Fe^{2+} + 4OH^- \rightarrow 3H_2O + Fe_2O_3$
$O_2 + 4Fe^{2+} + 8OH^- \rightarrow 4H_2O + 2Fe_2O_3$
$UO_2^{2+} + 2Fe^{2+} + 6OH^- \rightarrow UO_{2,(aq)} + 3H_2O + Fe_2O_3$
$UO_2(CO_3)_2^{2-} + 2Fe^{2+} + 6OH^- \rightarrow UO_{2,(aq)} + 2CO_3^{2-} + 3H_2O + Fe_2O_3$
$H_2O_2 \rightarrow H_2O + \frac{1}{2}O_2$
$UO_{2,(s)} \rightarrow UO_{2,(aq)}$
$UO_{2,(aq)} \rightarrow UO_{2,(s)}$

Tab. B-2 Electrochemical reactions incorporated into the FMD model at the fuel, fuel noble metal particle (NMP), and steel (canister) interface.

Surface	Reactions
Fuel	$UO_2 \rightarrow UO_2^{2+} + 2e^-$ $UO_2 + 2CO_3^{2-} \rightarrow UO_2CO_3^{2-} + 2e^-$ $UO_2 \rightarrow UO_{2,(aq)}$ $H_2 + 2OH^- \rightarrow 2H_2O + 2e^-$ $H_2O_2 + 2OH^- \rightarrow O_2 + 2H_2O + 2e^-$ $H_2O_2 + 2e^- \rightarrow 2OH^-$ $O_2 + 2H_2O + 4e^- \rightarrow 4OH^-$
Fuel, NMP	$H_2 + 2OH^- \rightarrow 2H_2O + 2e^-$ $H_2O_2 + 2e^- \rightarrow 2OH^-$ $H_2O_2 + 2OH^- \rightarrow O_2 + 2H_2O + 2e^-$ $O_2 + 2H_2O + 4e^- \rightarrow 4OH^-$
Steel	$Fe \rightarrow Fe^{2+} + 2e^-$ $2H_2O + 2e^- \rightarrow H_2 + 2OH^-$

APPROACH TO IMPLEMENTING THE FMD MODEL IN FORTRAN

Our previous progress has been outlined elsewhere (Harvey et al. 2022; Mariner et al. 2021). Our reactive-transport model is implemented using the standard residual approach, that is

$$f\left(c^{k+1,p}\right) = \frac{c^{k+1,p} - c^{k}}{\Delta t} + L\left(c^{k+1,p}\right) - R(c^{k+1,p}) \quad \text{(B-1)}$$

where c is the concentration of a given species, L is the diffusion operator, and R is the kinetic rate expression. Diffusion is implemented by discretizing the system in space and time using a finite volume approach. Concentrations at each new timestep are updated by solving the non-linear system of equations using a Newton-Rhapson (NR) approach.

$$J\delta C = -f(C^{k+1,i}) \quad \text{(B-2)}$$

In the previous year we implemented all aqueous reactions and incorporated an adaptive time stepping routine. The code is currently stored and version controlled in a gitlab repository.

INTERFACIAL REACTION REGION

The reactions that occur at the interfacial region are integral to the FMD process model. These reactions are not implemented in the standard way that many reactions are implemented in reactive transport models. Instead, the redox reactions are broken into half reactions which contribute to an electrical current. Moreover, the current equations contain multiple unknowns including a new term called a "corrosion potential". For example, reaction 1 in Tab. B-2 ($UO_2 \rightarrow UO_2^{2+} + 2e^-$) is given by

$$i^{UO_2,1} = nF\varepsilon k_{UO_2,1} exp\left[\frac{\alpha_{UO_2,1}F}{RT}\left(E_{corr}^{UO_2} - E_{UO_2,1}^{0}\right)\right] \quad \text{(B-3)}$$

where n is the number of transferred electrons, F is Faraday's constant, ε is the porosity of fuel or steel corrosion layers, $k_{UO_2,1}$ is the reaction rate constant, $\alpha_{UO_2,1}$ is the electrochemical transfer coefficient, R is the universal gas constant, T is the temperature, $E_{corr}^{UO_2}$ is the corrosion potential of the fuel, and $E_{UO_2,1}^{0}$ is the standard potential. The central premise of the FMD model is that there is no net accumulation of charge or current, therefore

$$i_{anode} - i_{cathode} = 0. \quad \text{(B-4)}$$

Considerable effort this FY was spent studying how these reactions are implemented within the MATLAB code. Solving for both the corrosion potentials and the concentrations for a given time step is complicated. The MATLAB code is written "recursively" such that the MATLAB function that solves for the corrosion potentials (AMP_reactFuel) calls itself. The code snippet shown in Fig. B-2 exists in the AMP_reactFuel.m file. What is being performed here is a NR solve for the corrosion potential where the AMP_reactFuel subroutine calls itself on line 65. This causes difficulties in reading the code and understanding the process.

```
56      % Calculate corrosion potential (recursive)
57      if(~oFlg)
58        tic
59        [~,~,~,~,oFun,dFun] = AMP_reactFuel(t,T,conc,eCorr,true);
60        dEcorr            = dFun\oFun;
61        counter=0;
62        while(max(abs(oFun)) > 1e-20 && max(abs(dEcorr)) > 1e-15)
63          counter=counter+1;
64          eCorrNew          = eCorr - dEcorr;
65          [~,~,~,~,oFunT,dFun] = AMP_reactFuel(t,T,conc,eCorrNew,true);
66          if(sum(oFunT.^2) < sum(oFun.^2))
67            eCorr  = eCorrNew;  oFun    = oFunT;
68            dEcorr = dFun\oFun;
69          else
70            dEcorr = dEcorr/2;
71          end
72        end
73        time_corrosion = toc;
74      end
```

Fig. B-2 Code snippet from the MATLAB subroutine that updates corrosion potentials. The recursive nature of the algorithm is shown on line 65 where AMP_reactFuel calls itself.

In Jerden et al. (2015) the FMD model and its implementation is described in detail, specifically stating "For a given simulation, the FMDM solves a set of ordinary differential equations, where the dissolved concentrations are the state variables. Given initial concentrations at the interface with the fuel surface, (the corrosion potential) is calculated such that the total current flow at the fuel surface is zero. This value of (the corrosion potential) is used to determine current densities that represent the individual reaction rates." This makes it clear that the overall process works as follows: (1) given the current concentrations of species that were updated from the previous step using a NR approach, the new corrosion potential is determined (also solved using a NR approach), (2) given the new corrosion potentials the new concentrations are solved for using another NR approach, and (3) for each NR iteration to solve for new concentrations, the corrosion potential is updated. This process is continued until the change in concentrations is below a user-defined threshold. This sequential solve leads to a significant number of NR being performed each time step (Harvey et al. 2022). The MATLAB code was dissected line by line in an effort to ensure we properly understand the interfacial reaction implementation.

We hypothesize that this sequential iteration leads to significant code slowdowns as a typical simulation spends ~30% of the computational time in the AMP_reactFuel subroutine. Herein we suggest a new algorithm that solves for corrosion potentials and new concentrations simultaneously. Imagine a 1D reactive transport system with 3 species (A + B → C) and 3 grid cells. Also assume that species A is accumulated via an electrochemical reaction with an associated corrosion potential (e.g., Eq. B-3). This electrochemical reaction only occurs in the left most grid cell (i.e., fuel surface). A typical matrix representation of the system solved via a finite volume method is shown in Fig. B-3. In the 2nd and 3rd grid cell you observe the standard penta-diagonal structure in which the derivative of the rate expression for A, B, and C is taken with respect to the given species in the center 3 diagonals (e.g., $^{dR(A)}/_{dA}$), and the derivative of the diffusion operator (e.g., $L'(A)$) appears in the center and two off diagonals. The derivative of the standard accumulation term appears in the center diagonal (e.g., $^{1}/_{\Delta t}$). However, now given the need to solve for the corrosion potential and the concentration of A in the left most grid cell, the 3x3 block is transformed to a 4x4 block in the upper right. The 4th column represents the derivative of each reaction equation with respect to the corrosion potential. Note that this is 0 except for the 4th row in which the derivative of the corrosion potential equation is taken. The 4th row therefore has two entries, one in which the derivative of the fuel corrosion equation is taken with respect to the concentration of A

and another where it is taken with respect to the corrosion potential itself. Using this matrix form, the corrosion potential and concentrations can be solved for simultaneously; potentially limiting unnecessary non-linear solver iterations, improving the efficiency of the algorithm, and removing observed discontinuities in the results. Implementing the MATLAB algorithm, as is, is the current focus of our work; however, future efforts will focus on improving the algorithm as described here.

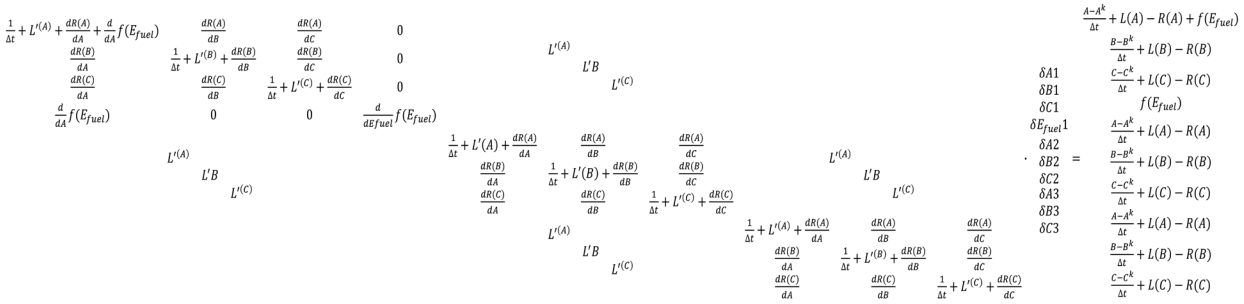

Fig. B-3 Representative proposed matrix for solving for corrosion potentials and new concentrations simultaneously in the FMD model. Here the reaction expressions and their derivatives are given by R, the diffusion operator is given by L, the corrosion potential equation is given by $\mathbf{f(E_{fuel})}$, and the standard accumulation term for each species is $\frac{\mathbf{A-A^k}}{\mathbf{\Delta t}}$.

ALPHA RADIOLYSIS MODEL

The last major component of the FMD model is the alpha radiolysis model which produces the main fuel oxidant (H_2O_2). We have fully implemented the model within the MATLAB code. Here, we will describe the process and show some of our results. Radiolysis is incorporated into the FMD model via a straightforward analytical function which describes the production of H_2O_2 as a function of space and time. It is given by

$$Molar\ Yield\ of\ H_2O_2(x,t) = \left[G_{H_2O_2}\right] * [Dose\ Rate](x,t) * g(x) \qquad \text{(B-5)}$$

where $g(x)$ is a geometrical factor that alters the diffusion of aqueous species through the tortuosity of precipitated UO_2, and $G_{H_2O_2}$ is the primary alpha radiolysis yield of H_2O_2. It should be noted that it is often reported that $G_{H_2O_2}$ is given by the model produced by Buck et al. (2013), which depends on the concentration of H_2 and O_2. However, upon inspection of the MATLAB code a simple constant is used for $G_{H_2O_2}$ instead. It has been shown that $G_{H_2O_2}$ can be significantly smaller at high H_2 and low O_2 concentrations. In these environments we are likely overestimating the fuel dissolution rate as we are overestimating the concentration of H_2O_2 in the system. While, in the future, we would like to implement the Buck et al. (2013) model we are currently focused on producing the MATLAB code as is and thus we have used a constant term for $G_{H_2O_2}$ here.

It should also be stated that several reports discuss three possible regions where radiolysis could occur (Fig. B-4). The assumption here is that radionuclides could be imbedded in the solid uranium phases that form and therefore produce H_2O_2. These regions are as follows, (1) a region where no solid uranium has formed, (2) a region where a solid uranium phase has formed but is less than the penetration depth of the alpha particles, and (3) a region where a solid uranium phase has formed but is longer than the alpha particle penetration depth. Upon inspection of the MATLAB code we discovered that this effect is not

activated and any particles that might be embedded in these solid regions do not contribute to the radiolysis (see Fig. B-5 for the code snippet).

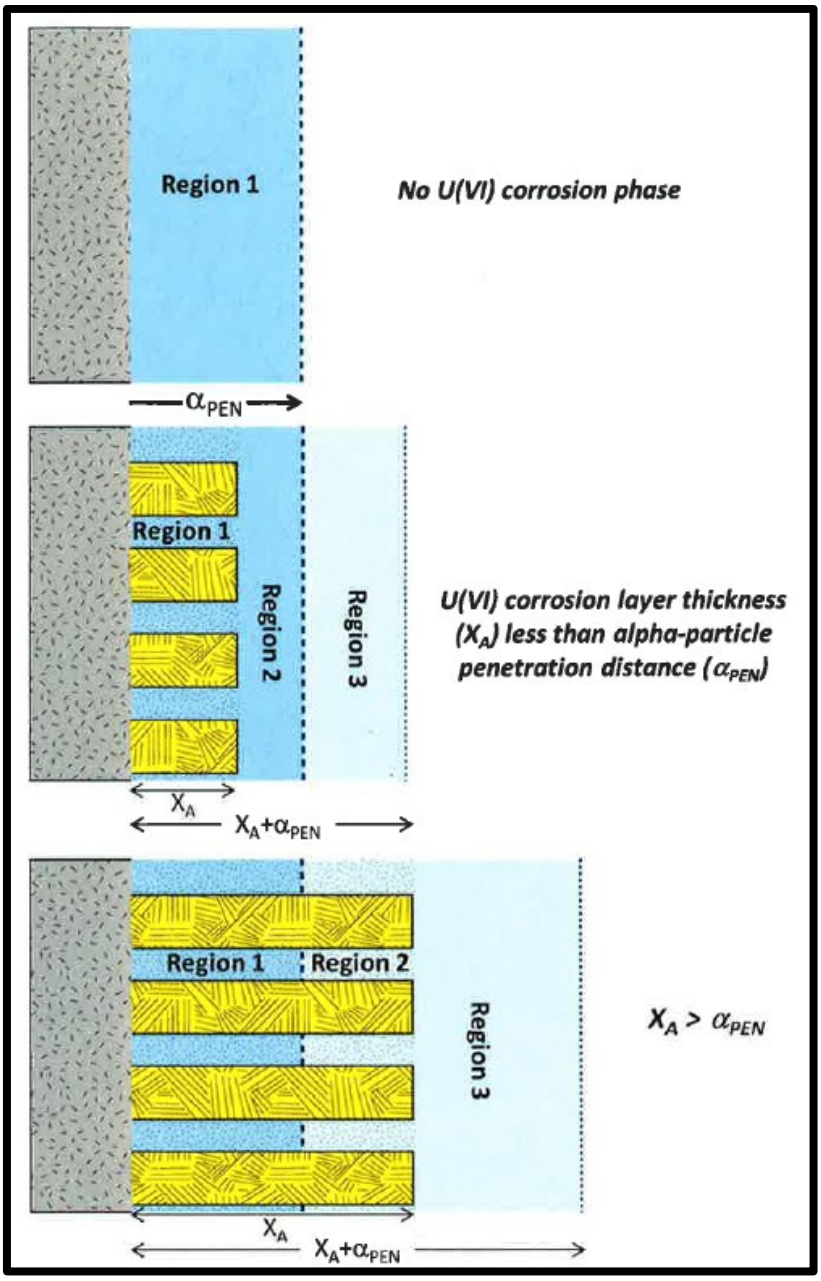

Fig. B-4 **Depiction of 3 regions for radiolysis in which (1) no solid uranium has formed, (2) solid uranium has formed but is less than the length of the alpha particle penetration depth, and (3) solid uranium has formed and is longer than the alpha particle penetration depth.**

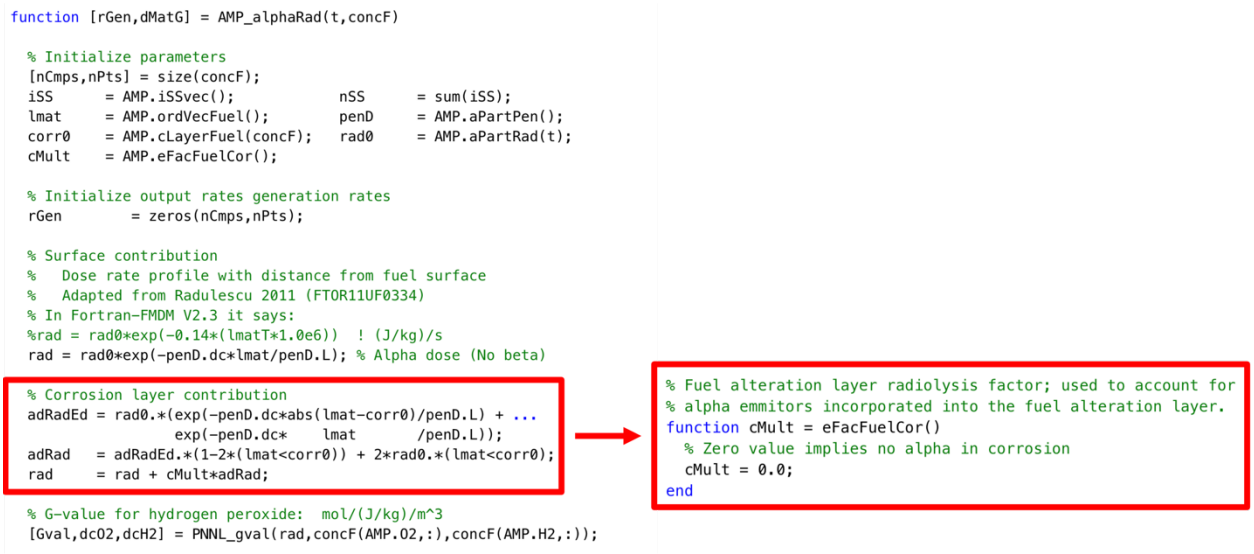

Fig. B-5 Code snippet for the radiolysis model. Contributions to radiolysis from the corrosion layer is indicated in the red box on the left which is eventually multiplied by a factor called "cMult" which is set to 0.0.

Our current working Fortran version has a full grid cell at the left and right boundary of the 1D cell. To implement the radiolysis process, we remove this full grid cell for H_2O_2 to transform it into a hard wall boundary. In simple terms, the radiolysis model acts as the source term for H_2O_2 into the system. The production of H_2O_2 decays exponentially as you move away from the fuel surface. To test our radiolysis implementation, we initially ran a simulation where radiolysis was turned on, but diffusion is turned off. In Fig. B-6 we show the concentration of H_2O_2 as a function of time at various distances from the fuel surface. We observe that past 80 μm, H_2O_2 is not observed which agrees well with the known alpha dose as a function of distance from the fuel surface (Jerden, et al., 2014).

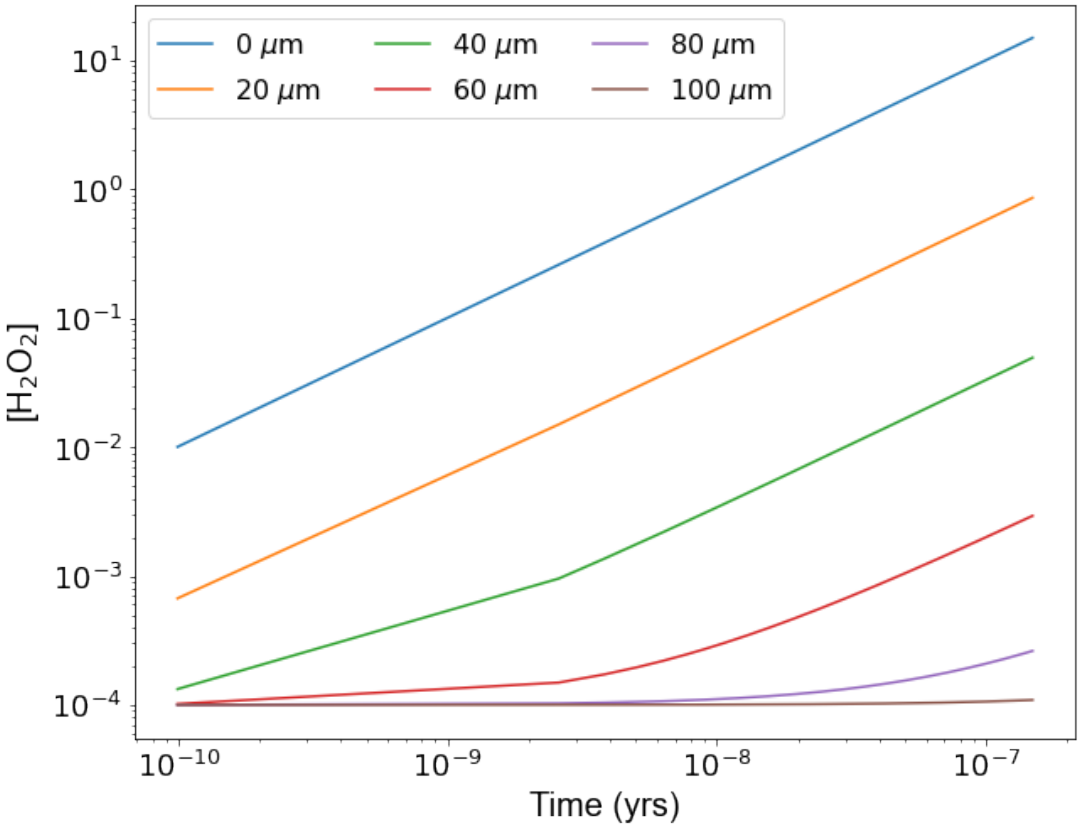

Fig. B-6 The concentration of H_2O_2 as a function of time for various distances from the fuel surface with diffusion turned off. Past 80 µm, H_2O_2 is not observed.

We performed two more tests, both with diffusion turned on (Fig. B-7). In one test we implement the model using the hard wall boundary as described above (lines), while in a second test we keep the full grid cell boundary; however, we turn the boundary concentration to 0 (points). Given the 0 concentration these results should agree exactly with the hard wall boundary, and that is indeed what we observe. Given these results we are confident that the radiolysis model has been implemented correctly.

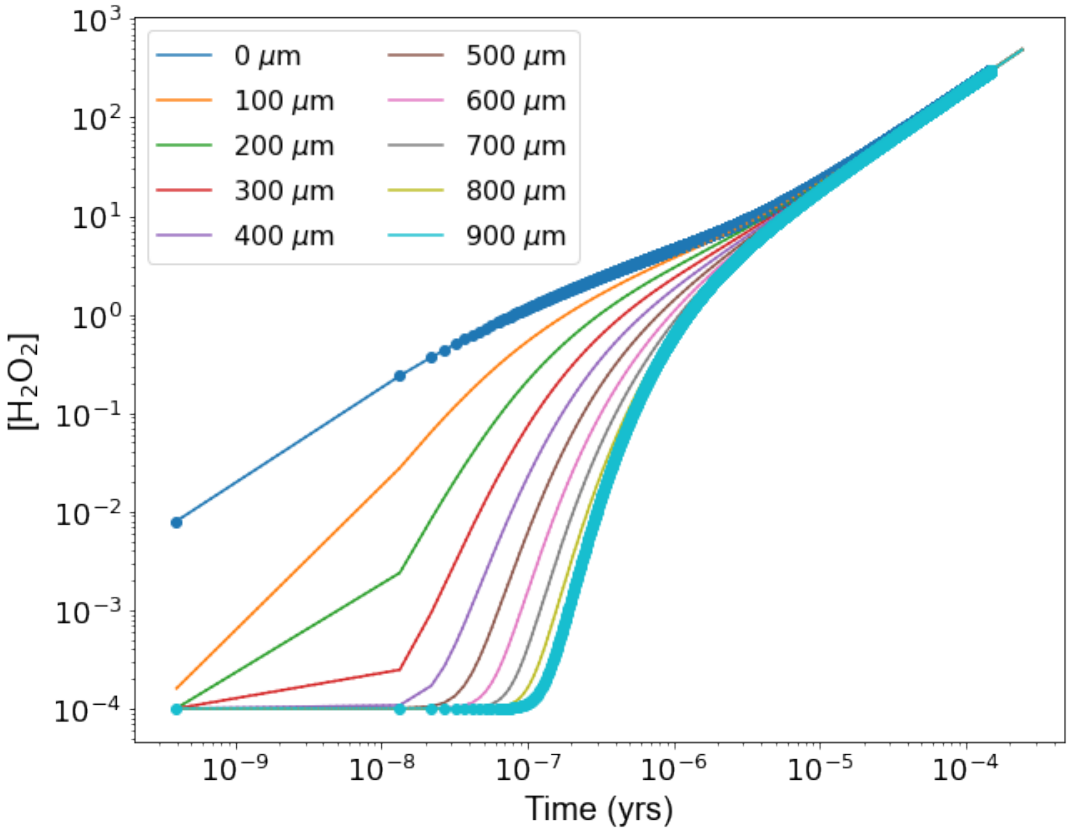

Fig. B-7 Concentration of H_2O_2 as a function of time for various distances from the fuel surface with diffusion turned on

CONCLUSIONS

In this FY we concentrated on implementing the interfacial reactions of the MATLAB code in the Fortran code. As discussed in this report, these reactions are implemented in a non-standard way in the MATLAB code. Additionally, the MATLAB code is implemented recursively which makes reading the code more difficult. We have outlined here the algorithm we are currently working on implementing in which the corrosion potentials are solved first and then the concentrations are updated. We have also outlined in greater detail our hypothesis for improving this sequential iterative process. Currently, radiolysis has been implemented using the simple constant term for $G_{H_2O_2}$, and our results indicate the process is working as expected. However, there is considerable interest in the FMD model user community to implement a more complex model for $G_{H_2O_2}$ which has been shown to be important when concentrations of H_2 are high and O_2 low. We plan on implementing the advanced $G_{H_2O_2}$ model in the future. Our current focus is on implementing the interfacial reactions so that we can achieve our initial goal, which is to reproduce the physical and chemical processes implemented in the MATLAB code.

REFERENCES

Buck, E., Jerden, J., Ebert, W., Wittman, R. (2013), Couple the Mixed Potential and Radiolysis Models for Used Fuel Degradation, FCRD-UFD-2013-000290, Argonne National Laboratory.

Harvey, J.A., A.M. Taconi, & P.E. Mariner (2022). Development of an Efficient Version of the Fuel Matrix Degradation Model. Proceedings of the 2022 International High-Level Radioactive Waste Management Conference, American Nuclear Society, Phoenix, Arizona (SAND2022-8791 C, Sandia National Laboratories, Albuquerque, New Mexico).

Jerden, J., Frey, K., Cruse, T., Ebert, W. (2012), Waste Form Degradation Model Status Report: Electrochemical Model for Used Fuel Matrix Degradation Rate, FCRD-UFD-2012-000169, Argonne National Laboratory.

Jerden, J., Frey, K., Copple, J.M., Ebert, W. (2014), ANL Mixed Potential Model for Used Fuel Degradation: Application to Argillite and Crystalline Rock Environments, FCRD-UFD-2014-000490, Argonne National Laboratory.

Jerden, J., Copple, J.M., Frey, K.E., Ebert, W. (2015), Mixed Potential Model for Used Fuel Dissolution – Fortran Code, FCRD-UFD-2015-000159, Argonne National Laboratory.

Jerden, J., Gattu, V.K., Ebert, W. (2018), Update on Validation and Incorporation of a New Steel Corrosion Module into Fuel Matrix Degradation Model, M4SF-18AN010301017, Argonne National Laboratory.

Liu, N., Zhu, Z., Wu, L., Qin, Z., Noël, J. J., Shoesmith, D.W. (2018), Predicting Radionuclide Release Rates from Spent Nuclear Fuel Inside a Failed Waste Disposal Container Using a Finite Element Model, Corrosion 75: 302-308.

Mariner, P.E., T.M. Berg, K.W. Chang, B.J. Debusschere, A.C. Eckert, J. Harvey, T.C. LaForce, R.C. Leone, M.M. Mills, M.A. Nole, H.D. Park, F.V. Perry, D.T. Seidl, L.P. Swiler, (2021). GDSA Framework Development and Process Model Integration FY2021. M2SF-21SN010304053, SAND2021-12626 R. Sandia National Laboratories, Albuquerque, New Mexico.

Shoesmith, D.W., Kolar, M., King, F. (2003), A Mixed-Potential Model to Predict Fuel (Uranium Dioxide) Corrosion within a Failed Nuclear Waste Container, Corrosion, 59:802-816.

(This page is intentionally blank.)

Appendix C. SURROGATE MODELING OF THE FUEL MATRIX DEGRADATION (FMD) PROCESS MODEL

APPENDIX C. SURROGATE MODELING OF THE FUEL MATRIX DEGRADATION (FMD) PROCESS MODEL

INTRODUCTION

As discussed earlier in this report, the Geologic Disposal Safety Assessment (GDSA) Framework is an open source repository simulation software built around the massively-parallel multi-physics code PFLOTRAN. An important short-term goal of the development of the GDSA Framework (pa.sandia.gov) is to perform probabilistic repository simulations to identify sources of uncertainty to help prioritize future R&D. To achieve this short-term goal with current computer resources, developers must consider ways to include the effects of expensive process models in total system simulations.

High fidelity prediction of waste package and waste form degradation processes for thousands of waste packages in a probabilistic repository performance assessment calculation is expensive. With thousands of waste packages, thousands of time steps, and hundreds of realizations in a simulation to allow for uncertainty quantification, these process models may need to be called a billion times per simulation.

One way to reduce computational expense is to develop response surface surrogate models that can rapidly emulate the mechanistic process models. An ideal response surface surrogate model runs orders of magnitude faster than its parent mechanistic model and provides outputs identical to those of the mechanistic model within a specified range of the model inputs.

Over the past few years, a team of modelers and mathematicians at Sandia National Laboratories has been developing surrogate models for the UO_2 Flux that is predicted by the Fuel Matrix Degradation (FMD) process model (Jerden et al., 2015a). The FMD model has been coupled with PFLOTRAN (Mariner et al., 2015), but the coupled model runs too slowly for a set of probabilistic repository-scale simulations. The surrogate modeling work has examined Machine Learning (ML) approaches such as tabulation with tree-based lookup methods, and artificial neural networks. A key question for obtaining good accuracy with these surrogate models is what information should be used to train the surrogates on. This appendix describes advances made over the past year in incorporating information about the fuel corrosion layer thickness in surrogate model training.

We next describe the FMD process model used to generate results for this appendix followed by a discussion of our general approach for surrogate modeling and the process for generating training data. Next we review some prior results from surrogates that do not use detailed information about the internal state of the waste packages and waste form. After that, we explore the use of surrogate models that estimate, track, and use the growing thickness of the corrosion layer on the fuel surface to help define system state, along with preliminary results.

FUEL DISSOLUTION PROCESS MODEL

The FMD model used for the results in this appendix is a mechanistic spent fuel dissolution model coded in MATLAB and developed at Argonne National Laboratory and Pacific Northwest National Laboratory. The model calculates spent fuel dissolution rates as a function of radiolysis, alteration layer growth, diffusion of reactants through the alteration layer, temperature, and interfacial corrosion potential (Jerden et al., 2015b). It employs a one-dimensional (1D) reactive transport model to simulate diffusion and chemical reactions across this layer over time. The 1D domain, depicted in Fig. B-1, extends 0.05 m from the fuel surface to the bulk water. It is divided into as many as 100 cells with increasing length toward the bulk water boundary cell.

To couple the FMD model with PFLOTRAN, a "coupled" FMD model was coded in Fortran (Mariner et al. 2015). At each time step, PFLOTRAN calls the coupled FMD model to obtain a new dissolution rate. Coupling required PFLOTRAN to keep track of the 1D chemical profiles across the domain from the previous time step. It also required relevant inputs from the main PFLOTRAN simulation, such as temperature, time, and environmental concentrations in the boundary cell. Dose rate is calculated in the coupled FMD model from time and burnup. A full list of FMD model inputs and outputs available for surrogate modeling is presented in Tab. B-1.

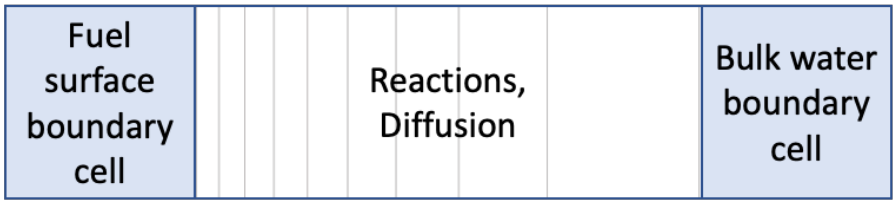

Fig. B-1 FMD Model Domain

Tab. B-1 Inputs/Outputs of Coupled FMD Model

Available Inputs	Outputs
• Initial concentration profiles across 1D corrosion/water layer (UO_2(s), UO_3(s), UO_4(s), H_2O_2, UO_2^{2+}, UCO_3^{2-}, UO_2, CO_3^{2-}, O_2, Fe^{2+}, and H_2) • Initial corrosion layer thickness • Dose rate at fuel surface (= f (time, burnup)) • Temperature • Time and time step length • Environmental concentrations (CO_3^{2-}, O_2, Fe^{2+}, and H_2)	• Final concentration profiles across 1D corrosion/water layer • Final corrosion layer thickness • Fuel dissolution rate (UO_2 flux)

The coupled Fortran FMD model was tested on a problem involving a two-dimensional flow field containing 4 rows of 13 breached spent fuel waste packages. The model successfully simulated fuel dissolution for each of the waste packages over 100 time steps (Mariner et al., 2015). Of the 45 minutes of

computational time required to run the simulation, 30 minutes were used calculating the fuel dissolution rates in the coupled FMD model.

SURROGATE MODELING

It is often useful to construct a surrogate model to use in uncertainty and sensitivity analysis of a computational physics model when it is computationally demanding. A surrogate model (sometimes called meta-model, emulator, or response surface model) is an inexpensive input-to-output mapping that replaces a process model. Once constructed, this meta-model is relatively inexpensive to evaluate so it is often used as a surrogate for the physics model in uncertainty propagation, sensitivity analysis, or optimization problems that may require thousands to millions of function evaluations (Simpson et al., 2008).

There are many different types of surrogate models, including neural networks (Pedregosa et al., 2011; Ben-David et al., 2014), k-Nearest Neighbor regression (Ben-David et al., 2014), and polynomial chaos expansions (Xiu, 2010; Ghanem & Spanos, 2002). Another popular approach in the literature is to develop an emulator that is a stationary smooth Gaussian process (Rasmussen & Williams, 2006; Santner et al., 2003). The popularity of Gaussian processes is due to their ability to model complicated functional forms and to provide an uncertainty estimate of their predicted response value at a new input point. There are many good overview articles that compare various meta-model strategies. Various smoothing predictors and nonparametric regression approaches are compared elsewhere (Simpson et al., 2008, Santner et al., 2003, Storlie et al., 2009). Simpson et al. provides an excellent overview not just of various statistical meta-model methods but also approaches that use low-fidelity models as surrogates for high-fidelity models. Haftka and his students developed an approach that uses ensembles of emulators or hybrid emulators (Viana et al., 2009).

Two ML surrogate modeling approaches are used in this work to predict the UO_2 flux resulting from fuel degradation: A k-nearest-neighbors surrogate model and an Artificial Neural Network. The former interpolates between points in a high-dimensional lookup table generated by sampling the FMD model. The latter fits a nonlinear functional representation to the FMD model data. Both approaches require a sufficient amount of training data from the FMD model.

Training Data

We used a standalone MATLAB implementation of the FMD process model to generate training data by randomly sampling the inputs to the model. The training data itself can be very large. For example, we may have millions of samples of FMD, where each sample involves a multi-dimensional vector sample of inputs such as the environmental concentrations, temperature, burnup, etc. (the left-hand quantities in Tab. B-1). The output is also extensive, since each FMD run involves a hundred timesteps with lots of information about the fuel cask state reported at every time step (e.g., the right-hand quantities in Tab. B-1). Note that in this work, we focus on predicting the fuel dissolution rate (UO_2 flux), although the other two output quantities could be treated with a surrogate in similar manner.

A Latin hypercube sampling (LHS) study was performed to generate training and validation data for regression from the standalone FMD process model. LHS is a stratified sampling technique that generates "well-spaced" samples; it typically gives lower variance statistical estimators than plain Monte Carlo sampling (Helton & Davis, 2003). The six-dimensional sample space contained the parameters initial temperature, burnup, and the environmental concentrations of CO_3^{2-}, O_2, Fe^{2+}, and H_2. The probability distributions for each parameter are given in Tab. B-2.

Tab. B-2 Input Parameters and Their Distributions

Parameter	Distribution	Min.	Max.
Init. Temp. (K)	Uniform	300	400
Burnup (Gwd/MTU)	Uniform	40	65
Env. CO_3^{2-} (mol/m^3)	Log-uniform	10^{-3}	2×10^{-2}
Env. O_2 (mol/m^3)	Log-uniform	10^{-7}	10^{-5}
Env. Fe^{2+} (mol/m^3)	Log-uniform	10^{-3}	10^{-2}
Env. H_2 (mol/m^3)	Log-uniform	10^{-5}	2×10^{-2}

The temporal discretization in each problem consists of 101 logarithmically-spaced (base 10) points in time from 0 to 10^5 years. Some FMD runs need to be filtered out if they either get stuck in an infinite loops and never finish or if they show unphysical results, such as the UO_2 surface flux stagnating after 10^4 years, or the Corrosion Layer Thickness (CLT) growing beyond the computational domain of 0.05m.

To assess the accuracy of the models for a specific training data size, we analyzed the normalized root mean squared error ($nrmse$), which is computed over the data set as:

$$nrmse = \frac{\sqrt{\frac{1}{N}\sum_{i=1}^{N}(y_{pred,i}-y_{true,i})^2}}{\frac{1}{N}\sum_{i=1}^{N} y_{true,i}} \quad \text{(B-1)}$$

where N is the total number of data points. In other words, the $nrmse$ is the root mean squared error normalized by the mean of the true data. Another metric is the mean absolute percentage error ($mape$), which is computed as:

$$mape = \frac{1}{N}\sum_{i=1}^{N}\left|\frac{y_{pred,i}-y_{true,i}}{y_{true,i}}\right| \times 100 \quad \text{(B-2)}$$

The $mape$ error, due to its relative nature, does a good job of treating the approximations in all quantities, large or small, with equal importance. On the other hand, the $mape$ can be sensitive to numerical noise, for example when reasonable errors get divided by very small quantities in absolute value. Also, for some applications, the approximation of the larger values is the most important criterion. For these situations, the $nrmse$ is a good overall measure of goodness. For a data set where the Quantity of Interest (QoI) spans many orders of magnitude, it is good to consider both metrics.

k-Nearest Neighbor Regression

The k-Nearest Neighbors regressor (kNNr) is a supervised, non-parametric machine learning method that tabulates data points inside of a domain X with labels Y. The label for a point within the domain but not in the "table" is obtained as a weighted average of the labels of the k nearest neighbors of this new point, where $k \geq 1$ is fixed. The definition of nearest depends on the metric function one uses, though a typical choice is the Minkowski metric $(\sum_{i=1}^{d}|x_i - y_i|^p)^{\frac{1}{p}}$, with $p \geq 1$. The case of $p = 2$ is the popular Euclidean metric, which is used in this work. For efficient look-up in high-dimensional data sets, a K-D Tree tabulation method is used (Pedregosa et al., 2011). The inverse distances from the nearest-neighbor table points to the query point are used as the weight in the interpolation, so that points further away from the query point have less influence than more nearby points.

One of the attractive aspects of kNNr is that it makes predictions based on local information only, and therefore does not require global smoothness over the input space. As each prediction is a weighted average of known table points, the approach is also highly interpretable. On the other hand, the approach requires a sufficiently dense table to get good predictive accuracy, and the cost of table look-ups increases as the table density increases.

For model development and metaparameter tuning, we employed the kNNr implementation from the Python Scikit-Learn module (Pedregosa et al., 2011). For coupling to PFLOTRAN reservoir simulations, we relied on the open source FORTRAN code KDTREE 2 (Kennel, 2004).

Artificial Neural Network

Artificial Neural Network (ANN) models are commonly employed by the machine learning community for regression and classification problems. They can be described as intricate networks of "artificial neurons" that are essentially weighted combinations of (usually simple) nonlinear functions. One motivation for the development of neural networks (Pedregosa et al., 2011; Ben-David et al., 2014; Rasmussen & Williams, 2006) was to create a regression approach for complex functions that avoids the combinatorial growth of the parameter space that occurs in polynomial regression models as more inputs are added.

ANN can be more accurate than kNNr using fewer training data as its functional representation helps to interpolate in areas where fewer training data are available. However, ANN models are not as readily interpretable as kNNr models, and care must be taken to avoid overfitting.

The ANN surrogate was developed in Python using the Tensorflow/Keras module (Abadi et al, 2016). A feed-forward neural network structure was selected with the popular rectified linear unit (ReLU) activation function. All training and metaparameter tuning were done in Python. For coupling to PFLOTRAN reservoir simulations, a Fortran ANN evaluator was written specifically for the selected network configuration. This evaluator reads in the ANN weights that were determined offline in the Python training and tuning scripts.

Surrogates Not Relying on Detailed Internal State Information

While the FMD model tracks detailed information about the internal state of the fuel cask over time, such as the information listed under Outputs in Tab. B-1, most of this information is not readily available when a surrogate model is called in a reservoir simulation. As such, our first approach to surrogate modeling considers only the following 6 inputs:

- Dose rate at fuel surface (= f (time, burnup))
- Temperature
- Environmental concentrations (CO_3^{2-}, O_2, Fe^{2+}, and H_2)

These inputs are either set by the environment (temperature and environmental concentrations) or can be readily computed from global information (dose rate).

As covered in detail in (Debusschere et al., 2022), surrogates using these inputs show a fair agreement with the process model predictions of the UO_2 fluxes. Tab. B-3 shows the $nrmse$ and $mape$ errors on the UO_2 fluxes predicted by the kNNr and ANN surrogates compared to FMD simulations on testing data. In this case, the surrogate models were trained based on 400,000 FMD Matlab runs. The kNNr model used

dose rate, temperature, and the concentrations of CO_3^{2-} and H_2 as inputs. The kNNr table contained 2.28 million samples and 80 Nearest Neighbors were used for interpolation. The ANN model used two hidden layers with 64 nodes each for a total of 4673 parameters and was trained on the same data set using dose rate, temperature, and all 4 environmental concentrations CO_3^{2-}, O_2, Fe^{2+}, and H_2 as inputs.

Tab. B-3 Error metrics for kNNr and ANN surrogates on testing data for the case where no detailed internal fuel cask information is used

Surrogate	nrmse	mape
kNNr	0.48	44%
ANN	0.52	25%

A demonstration on a full-scale shale repository reference case simulation showed that the ANN and kNNr surrogate models enable accounting for more detailed FMD dynamics than when a fractional dissolution rate approximation is used, while keeping the computational cost of reservoir simulations manageable (Debusschere et al., 2022).

Surrogates Using Corrosion Layer Thickness as a System State Indicator

Approach

While the results in (Debusschere et al., 2022) are encouraging, the accuracy of the surrogates is not superb. In this section, we explore the potential of getting more accurate surrogate models by incorporating additional information about the internal fuel cask state. One variable that is a good indicator of the cumulative amount of waste form degradation that has occurred over time is the Corrosion Layer Thickness (CLT). Since this information is not readily available without running a detailed FMD process model, a dual surrogate model approach is followed.

A first surrogate model predicts the CLT at the current time, using the CLT at the previous time step and the time step size as inputs, in addition to the inputs in Tab. B-2. A second surrogate predicts the UO_2 flux, using this same expanded input set. After advancing to the next time step, the CLT predicted by the surrogate in the previous time step becomes part of the inputs for the next time step.

Preliminary Results

This dual surrogate approach was implemented for the kNNr surrogate, using dose rate, temperature, and the concentrations of CO_3^{2-} and H_2 along with CLT at the previous time step and the time step size as inputs. The surrogate was trained using a data set of 1 million FMD Matlab runs sampled from the distributions listed in Table II. After removing unphysical runs, 15% of the data was split off as validation data and 10% was split off as testing data, resulting in about 9.4 million validation data points, 6.3 million testing data points, and 47 million training data points. Following (Debusschere et al., 2022), the training data was downsampled by randomly selecting a given number of samples from each FMD time trajectory.

Fig. B-2 through Fig. B-5 show preliminary results that explore the choice of kNNr metaparameters (amount of training data and the number of Nearest Neighbors, NN) for the CLT and UO_2 Flux predictions. In all of these experiments, the training data was subsampled to 50 time samples per run. The validation data was used for computing the error metrics. As the CLT is initialized at a very small value on the order of 10^{-19} micrometer, the presence of some very small CLT values makes the computation of

the regular *mape* error numerically unstable. To mitigate this effect, we defined a modified "floored" *mape* error metric, which uses a value of 10^{-4} in the *mape* denominator if the CLT at that point is less than 10^{-4} μm. This effectively removes the impact of division by very small CLT values from the computation. This modified *mape* metric here is indicated as mape_f in the figures.

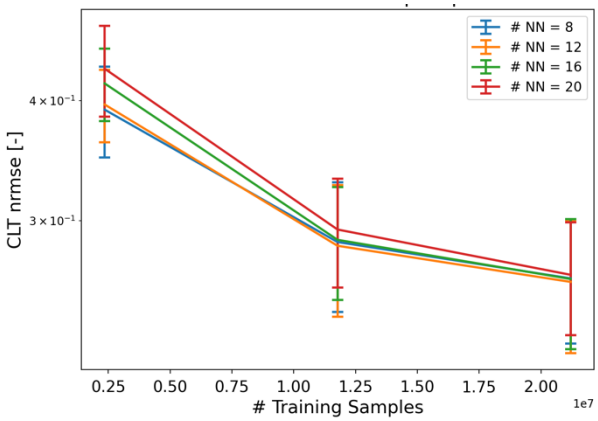

Fig. B-2 The nrmse metric for prediction of the CLT as a function of the amount of training samples for different values of the number of Nearest Neighbors (NN) used.

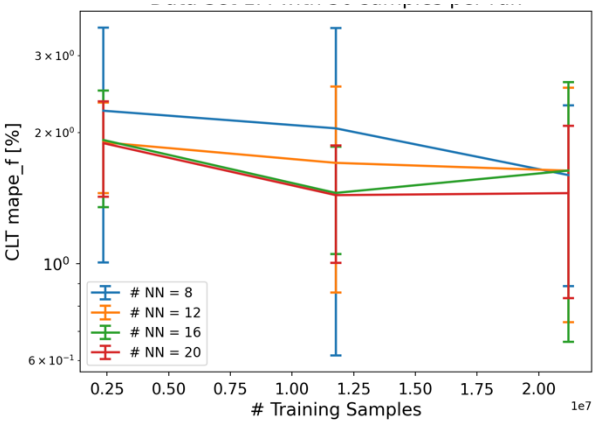

Fig. B-3 The mape_f metric for prediction of the CLT as a function of the amount of training samples for different values of the number of Nearest Neighbors (NN) used. Errors are on the order of 1 – 2 %.

Fig. B-2 and Fig. B-3 show that the incorporation of the CLT at the previous time step along with the time step size as inputs, allows a very accurate prediction of the CLT, with *mape* errors down to about 1 – 2% on the validation data.

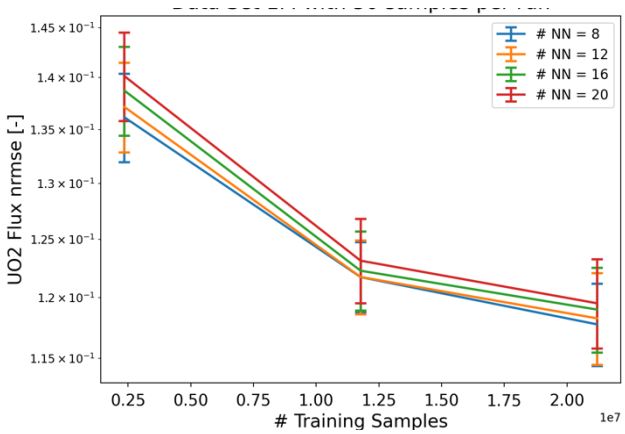

Fig. B-4 The nrmse metric for prediction of the UO_2 flux as a function of the amount of training samples for different values of the number of Nearest Neighbors (NN) used.

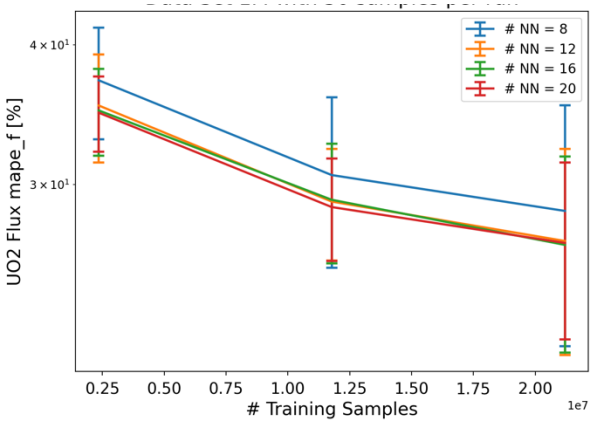

Fig. B-5 The *mape* metric for prediction of the UO_2 flux as a function of the amount of training samples for different values of the number of Nearest Neighbors (NN) used. Given enough data points, the *mape* error is less than 30 %.

Fig. B-4 and Fig. B-5 similarly show nice convergence of the kNNr surrogate approximation error in the UO_2 flux as more training data are provided.

Based on the trends in this preliminary tuning of the kNNr meta parameters, both the CLT and UO_2 flux are best predicted using about 8 – 12 nearest neighbors with as much training data as possible. Note that the number of nearest neighbors used here is much lower than the 80 nearest neighbors used for the kNNr surrogates that did not include CLT information. As such, the addition of the CLT as an input allows for faster table lookups and may also be more robust as there is less danger of grabbing points that are too far away when fewer neighbors are used in the interpolation. Based on these tuning results, a kNNr configuration of 10 nearest neighbors using all available training data (all 23 million samples from the data set that was downsampled to 50 samples per FMD process model run) was selected to predict the testing data. This testing data has not been used in any of the training and tuning of the kNNr surrogate.

Fig. B-6 and Fig. B-7 below compare the kNNr predictions of the CLT and UO_2 flux to the testing data for 50 randomly sampled trajectories of the FMD process model. Note that in this comparison, each data point in the time trajectories was predicted on its own, using the inputs provided by the testing data. In a practical PFLOTRAN repository simulation, the CLT value at the previous time step would not be readily

available as the PFLOTRAN model does not track CLT independently. This CLT value would therefore need to be approximated by the same surrogate operating on the inputs from the prior time step. As such, if Fig. B-6 had been generated with a true time integration approach, where only the initial values of the CLT were specified, errors in the successive surrogate approximations for the CLT would have compounded over time, and might have caused the trajectories to diverge from the MATLAB model predictions over time. The analysis shown here is still useful as it shows where such errors are most likely to originate.

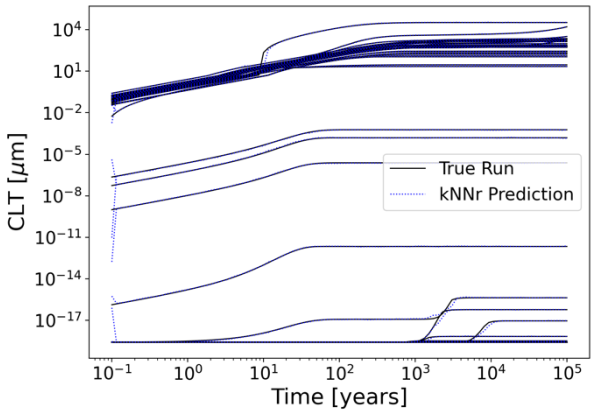

Fig. B-6 Comparison of the True and kNNr prediction of the CLT for 50 randomly selected runs in the testing data.

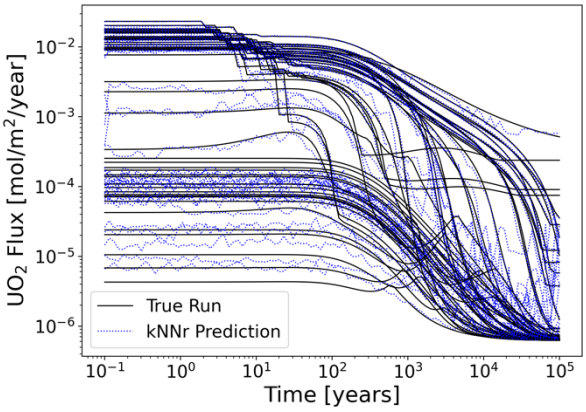

Fig. B-7 Comparison of the True and kNNr prediction of the UO_2 flux for 50 randomly selected runs in the testing data.

Aside from some deviations early in time, the kNNr predictions of the CLT in Fig. B-6 are very close to the true values in the testing data. This graph also illustrates the very wide range in CLT values. It is believed that the errors in the CLT predictions at early time, when the CLT is often very small, are the ones that tend to inflate the *mape* error if no floor value is applied.

The predictions of the UO_2 fluxes in Fig. B-7 show good agreement with the test data, although the agreement is not as good as for the CLT predictions. As observed also in (Debusschere et al., 2022), the kNNr prediction is noisy as it is a local prediction, drawing information only from 10 nearest neighbors to each query point in the training sample space.

Overall, with this kNNr configuration of 10 nearest neighbors and 23 million training samples, the prediction of the UO_2 flux in the testing data shows an $nrmse$ error of 0.11, and a $mape$ error of 29%. Even without extensive tuning of the kNNr metaparameters, this is a significant improvement from the $nrmse$ error of 0.48 and $mape$ error of 44% reported in Tab. B-3 for the case where no CLT information was used.

Ongoing Work

We are continuing to tune the kNNr meta parameters to optimize both the accuracy and speed of the predictions. In this process, we are also investigating the cause of the large (in relative sense) deviations in the CLT predictions that show up at early times. Besides kNNr, we will also train Artificial Neural Networks (ANNs) using the same input set. As ANNs use a functional representation rather than local approximations, the predictions by the ANN surrogates are likely to be smoother than the kNNr predictions when looking at time trajectories. The resulting kNNr and ANN configurations will then be employed to full scale nuclear waste performance assessment simulations.

CONCLUSIONS

Two machine learning surrogate models are under development to rapidly emulate the effects of the Fuel Matrix Degradation (FMD) model in the GDSA Framework. One is a k-Nearest Neighbors regressor (kNNr) method that operates on a lookup table, and the other is an Artificial Neural Network. Both approaches have a high degree of accuracy, provided that enough training data is available with inputs that are informative of the UO_2 flux that results from the fuel degradation.

While earlier work (Debusschere et al., 2022) used only inputs that do not require detailed information about the internal state of the fuel cask, the current work explored the use of the Corrosion Layer Thickness (CLT). While this quantity of interest would need to be predicted along with the UO_2 flux at every time step in a repository simulation, the preliminary results in this work with the kNNr surrogate show that the CLT is very informative of the UO_2 flux. Including CLT as an input therefore results in dramatically better accuracy. Ongoing work is incorporating the CLT as an input in the ANN surrogate, and further refining the sampling schemes and meta-parameter tuning processes before employing this approach in realistic, full scale repository simulations.

The aim of these surrogate models is to enable the GDSA Framework to simulate spent fuel dissolution for each individual breached spent fuel waste package in a probabilistic repository simulation. Having the ability to emulate spent fuel dissolution in probabilistic PA simulations will have the added capability of allowing uncertainties in spent fuel dissolution to be propagated and sensitivities in FMD inputs to be quantified and ranked against other inputs.

REFERENCES

Abadi, M., et al. (2016). “TensorFlow: A System for Large-Scale Machine Learning”, 12th USENIX Conference on Operating Systems Design and Implementation (OSDI’16), Savannah, GA, November 2–4

Ben-David, S. and S. Shalev-Shwartz (2014). Understanding Machine Learning: From Theory to Algorithmsed. Cambridge, United Kingdom, Cambridge University Press.

Debusschere, B.J., D.T. Seidl, T.M. Berg, K.W. Chang, R.C. Leone, L.P. Swiler, P.E. Mariner (2022), “Machine Learning Surrogates of a Fuel Matrix Degradation Process Model for Performance Assessment of a Nuclear Waste Repository”, Nuclear Technology, submitted.

Ghanem, R. and P. Spanos (2002). *Stochastic Finite Elements: A Spectral Approach*. New York, New York: Springer Verlag.

Helton, J. C. and F. J. Davis (2003). "Latin hypercube sampling and the propagation of uncertainty in analyses of complex systems." Reliability Engineering & System Safety 81(1): 23-69.

Jerden, J., G. Hammond, J. M. Copple, T. Cruse and W. Ebert (2015b). Fuel Matrix Degradation Model: Integration with Performance Assessment and Canister Corrosion Model Development. FCRD-UFD-2015- 000550. Washington, DC, US Department of Energy.

Jerden, J., J. M. Copple, K. E. Frey and W. Ebert (2015a). Mixed Potential Model for Used Fuel Dissolution - Fortran Code. O. o. U. N. F. Disposition. FCRD-UFD-2015-000159. Washington, DC, US Department of Energy.

Kennel, M. B. (2004). KDTREE 2: Fortran 95 and C++ software to efficiently search for near neighbors in a multi-dimensional Euclidean space. https://arxiv.org/pdf/physics/0408067.pdf, Institute for Nonlinear Science, University of California.

Mariner, P. E., W. P. Gardner, G. E. Hammond, S. D. Sevougian and E. R. Stein (2015). Application of Generic Disposal System Models. FCRD-UFD-2015-000126, SAND2015- 10037 R. Sandia National Laboratories, Albuquerque, New Mexico.

Pedregosa, F., G. Varoquaux, A. Gramfort, V. Michel, B. Thirion, O. Grisel, M. Blondel, P. Prettenhofer, R. Weiss, V. Dubourg, J. Vanderplas, A. Passos, D. Cournapeau, M. Brucher, M. Perrot and E. Duchesnay (2011). "Scikit-learn: Machine Learning in Python." Journal of Machine Learning Research 12: 2825-2830.

Rasmussen, C. E. and C. K. I. Williams (2006). Gaussian Processes for Machine Learninged., MIT Press.

Santner, T., B. Williams and W. Notz (2003). The Design and Analysis of Computer Experimentsed. New York, New York, Springer.

Simpson, T. W., V. Toropov, V. Balabanov and V. F.A.C. (2008). Design and analysis of computer experiments in multidisciplinary design optimization: A review of how far we have come or not. Proceedings of the 12th AIAA/ISSMO Multidisciplinary Analysis and Optimization Conference, Victoria, British Columbia, Canada. AIAA Paper 2008-5802.

Storlie, C. B., L. P. Swiler, J. C. Helton and C. J. Sallaberry (2009). "Implementation and evaluation of nonparametric regression procedures for sensitivity analysis of computationally demanding models." Reliability Engineering & System Safety 94(11): 1735-1763.

Viana, F.A.C., R.T. Haftka, and V. Steffen (2009). "Multiple surrogates: how cross-validation errors can help us to obtain the best predictor," *Structural and Multidisciplinary Optimization*, 39(4), 439-457

Xiu, D. (2010) *Numerical Methods for Stochastic Computations: A Spectral Method Approach*. Princeton University Press.

(This page is intentionally blank.)

Appendix D. GROUNDWATER CHEMISTRY MODELING FOR THE CRYSTALLINE REFERENCE CASE

APPENDIX D. GROUNDWATER CHEMISTRY MODELING FOR THE CRYSTALLINE REFERENCE CASE

INTRODUCTION

The chemical composition of groundwater is important to consider in repository performance assessment because it affects the corrosion and performance of engineered barriers and waste forms and the mobility of radionuclides. To begin to incorporate groundwater chemistry processes in repository system models, development of a hydrogeochemical reactive transport model for the crystalline reference case was initiated. The studies performed at the Onkalo spent nuclear fuel repository (Posiva 2021) are used to guide development. The Onkalo spent nuclear fuel repository is a repository located on the island of Olkiluoto in Eurajoki, Finland, with disposal tunnels excavated in fractured gneiss and granite bedrock. Because crystalline bedrock is largely impermeable, the main conduit for water movement is through the fractures. Fractures exist naturally and from drilling disturbances.

Four main water endmembers were identified by Posiva (2021): meteoric HCO_3-type water, brackish SO_4-type water, and two saline Cl-type waters. These endmember waters exist at progressively deeper depths and are mixed at certain intervals. The geochemistry of these endmembers and how they mix and interact with the rock determines the production of sulfides. Sulfides are of particular concern to the performance assessment of spent nuclear fuel repositories as sulfides can corrode the copper cannisters that seal and store the spent uranium fuel rods.

Two cases of hydrogeochemical evolution are considered: the steady-state base case and the transient disturbed case. The base case considers diffusion and slow advection through fractures as the main mass transport mechanism for major ions, at near-thermodynamic equilibrium conditions. In the base case, elevated sulfide concentrations are found (HS^- concentrations up to approximately 3 mg/L) at the transition zone between the brackish SO_4-type water and the saline Cl-type water. The disturbed case considers ion transport by advection promoted by drawdown caused by open tunnels and highly conductive fractures intersecting open drillholes. This causes rapid mixing of groundwaters, moving the system to thermodynamic disequilibrium. Microbial communities are then able to take advantage of the

newly-introduced electron donors and acceptors and promote redox reactions, resulting in elevated sulfide concentrations in the disturbed zones.

The main chemical reactions surrounding the reduction of sulfate are described below by depth. Many reactions are common among different groundwater endmembers and are repeated within the relevant endmember sections for completeness.

OLKILUOTO GEOCHEMISTRY BY DEPTH

0-100 m: Meteoric HCO_3 water (0-40 m), mixed meteoric HCO_3 + brackish SO_4 water (40-100 m)

Fracture-lining minerals

The meteoric HCO_3 endmember water is characterized by a high concentration of dissolved carbonate. This endmember is considered in equilibrium with goethite,

$$FeOOH + 3H^+ \leftrightharpoons Fe^{3+} + 2H_2O,$$

calcite,

$$CaCO_3 \leftrightharpoons CO_3^{2-} + Ca^{2+},$$

kaolinite,

$$Al_2(Si_2O_5)(OH)_4 + 6H^+ \leftrightharpoons 2Al^{3+} + 2H_4SiO_4,$$

and chalcedony,

$$SiO_2 + 2H_2O \leftrightharpoons H_4SiO_4.$$

In this region and throughout the entire depth, fracture-lining calcite exhibits control on the pH and buffers it to slightly alkaline conditions ($7 < pH < 8$). Meteoric water that flows through acidic soil is neutralized by the weathering of silicate clays at shallow depths (Lahdenpera et al., 2005), which is reflected in elevated dissolved silica values in shallow HCO_3^- groundwaters.

The minerals in equilibrium with the mixed meteoric + brackish region are largely the same as the pure meteoric water interval, but without goethite, and precipitating mackinawite:

$$FeS + H^+ \leftrightharpoons Fe^{2+} + HS^-$$

Carbon

Dissolved organic carbon, denoted as CH_2O, is introduced to the system through infiltration of meteoric water. The flux of meteoric water flushes organic matter from the soil through the first ~10 m. The carbon content in the shallow groundwater is ~20 to 90 mg/L. Ferrous iron (Fe^{2+}) is likely a result of the reduction of iron oxyhydroxides by anaerobic microbial organic carbon oxidation:

$$CH_2O + 4FeOOH + 7H^+ \rightarrow 4Fe^{2+} + HCO_3 + 6H_2O.$$

Sulfide production

Baseline sulfide concentrations in this shallow interval are low, with concentrations in the range of approximately 0.01 to 0.1 mg/L. Possible mechanisms of sulfide production are through dissolved organic matter (CH_2O) reacting with SO_4^{2-} to produce sulfide:

$$SO_4^{2-} + 2CH_2O + H^+ \rightarrow HS^- + 2CO_2 + 2H_2O.$$

Alternatively, methane (CH_4) can act as an electron donor for microbial reduction of sulfate:

$$CH_4 + SO_4^{2-} \rightarrow HS^- + H_2O.$$

While H_2 is a common electron donor for the microbial reduction of sulfate, repeated intrusion of meteoric and marine water along with continuous microbial consumption of H_2 likely causes low H_2 concentrations in fractures and the bedrock matrix.

Sulfide attenuation

Ferrous iron (Fe^{2+}) reacts with HS^- to precipitate mackinawite, and over a longer time period, pyrite. Meteoric water (<40 m) contains a low concentration of sulfides, which allows for higher accumulations of Fe^{2+} (up to 8 mg/L). The highest concentration of Fe^{2+} is found in this shallow (<40 m) interval. Ferrous iron concentration is governed by the weathering and dissolution of iron silicates and the reduction of iron oxyhydroxides by anaerobic microbial organic carbon oxidation:

$$CH_2O + 4FeOOH + 7H^+ \rightarrow 4Fe^{2+} + HCO_3 + 6H_2O.$$

This reaction occurs under slightly acidic conditions (5 < pH < 7). As HS^- is highly reactive with Fe^{2+}, the presence of a high concentration of Fe^{2+} indicates low sulfide production in this depth interval.

Brackish SO_4-type water (100-260 m), mixed brackish SO_4 + saline Cl-type waters (260-400 m)

Fracture-lining minerals

The fracture-lining minerals in this interval are the same as in the mixed meteoric + brackish interval (40-100 m). The reactions in this interval (100-400 m) include the precipitation of mackinawite,

$$FeS + H^+ \leftrightharpoons Fe^{2+} + HS^-,$$

and the dissolution of calcite,

$$CaCO_3 \leftrightharpoons CO_3^{2-} + Ca^{2+},$$

kaolinite,

$$Al_2(Si_2O_5)(OH)_4 + 6H^+ \leftrightharpoons 2Al^{3+} + 2H_4SiO_4,$$

and chalcedony,

$$SiO_2 + 2H_2O \leftrightharpoons H_4SiO_4.$$

Carbon

Dissolved organic carbon concentration in this interval is low, < 10 mg/L. Infiltration of DOC from meteoric water does not penetrate to this depth, and acetate concentrations are similarly low. Methane concentrations at 300 m are ~ 100 mL/L, increasing with depth to over 1200 mL/L at 1100 m. The source of this methane is likely to be microbial, due to the lack of longer-chain hydrocarbons (ethane, propane, etc.) and a highly negative $\delta^{13}C$ signature.

Sulfide production

Elevated sulfide concentrations are found in this region, with concentrations as high as 17 mg/L around 300 m depth, within the brackish-saline mixing region. The introduction of SO_4-rich water to the Cl-type water presents the opportunity for microbial reduction of sulfate. Because the DOC is low, S(VI) becomes a major electron acceptor, resulting in elevated sulfide concentrations:

$$SO_4^{2-} + 4H_2 + H^+ \rightarrow HS^- + 4H_2O.$$

Hydrogen is the electron donor used by sulfate-reducing bacteria, which is introduced from two sources: diffusion out of the crystalline rock matrix. H_2 concentrations in the crystalline rock matrix are higher than in the fractures. While the exact mechanism by which abiotic generation of H_2 occurs is unknown, there are many ways that H_2 can be generated, including graphitization, radiolysis of water, reaction of ^{40}Ca with water, serpentization, cataclasis, and reactions between dissolved magmatic gases (Gregory et al., 2019). The H_2 concentration profile with depth spans several orders of magnitude (Fig. D-1), suggesting that the concentration gradient is a result of slow diffusion of H_2 upwards from water-rock interactions in diabase dykes (Trinchero et al., 2014).

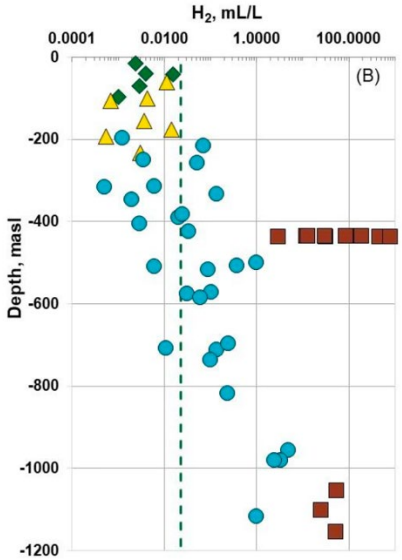

Fig. D-1 Aqueous H_2 concentrations within the fractured rock matrix. Adopted from Posiva (2021), Fig. 3.1-8.

Sulfide attenuation

This depth interval hosts a low concentration of ferrous iron (< 0.5 mg/L). Ferric iron silicates have a low solubility at a neutral pH under anoxic conditions. Iron-reducing bacteria use iron minerals and silicates

as an electron acceptor and conserve energy from the reduction of Fe(III) in chlorite to dissolved Fe^{2+}. Chamosite is an iron-rich chlorite:

$$Fe_5Al_2(AlSi_3)O_{10}(OH)_8 + 16H^+ \rightarrow 5Fe^{2+} + 2Al^{3+} + 3H_4(SiO_4) + 6H_2O.$$

Ferrous iron (Fe^{2+}) reacts with HS^-, precipitating iron sulfides (FeS):

$$Fe^{2+} + HS^- \rightarrow FeS + H^+.$$

The dissolved sulfides can reduce the solid Fe(III) silicate phase:

$$2HS^- + 2Fe^{3+} \rightarrow Fe^{2+} + S^0 + FeS + 2H^+$$

This FeS can either stay in solution as a colloid or attach to a mineral surface (Fe(II)(s) or (Fe(III)(s)). Pyrite is formed through an aging sequence, typically FeS(am) →Mackinawite →Pyrite (Schoonen & Barnes, 1991). The conversion of FeS(am) to mackinawite is a fast process, occurring on the timescale of minutes to weeks. Mackinawite solubility largely controls iron and sulfide concentrations in the short term. Pyrite grows much more slowly from solution. Pyrite is formed from FeS via the polysulfide pathway:

$$FeS + S^0 \rightarrow FeS_2,$$

or the hydrogen sulfide pathway:

$$FeS + H_2S \rightarrow FeS_2 + H_2.$$

Pyrite is supersaturated (saturation index ~ 3 to 9) throughout the entire domain, suggesting that pyrite formation is kinetically limited. Over a longer timescale, pyrite, rather than mackinawite, controls the solubility of sulfide and iron.

Saline 1 Cl-type water (350-400 m), mixed Saline 1 + Saline 2 Cl-type water (400-850 m), Saline 2 Cl-type water (850+ m)

Fracture-lining minerals

The minerals present here are the same as the minerals in the prior depth interval. The minerals in equilibrium with this interval (100-400 m) include mackinawite,

$$FeS + H^+ \leftrightharpoons Fe^{2+} + HS^-,$$

calcite,

$$CaCO_3 \leftrightharpoons CO_3^{2-} + Ca^{2+},$$

kaolinite,

$$Al_2(Si_2O_5)(OH)_4 + 6H^+ \leftrightharpoons 2Al^{3+} + 2H_4SiO_4,$$

and chalcedony,

$$SiO_2 + 2H_2O \leftrightharpoons H_4SiO_4.$$

Carbon

Anomalously high concentrations of acetate at depths greater than 400 m have been found and are likely the result of microbial activity. The dissolved organic carbon concentration in these regions is ~ 200

mg/L, mostly comprised of acetate (CH_3COO^-). One common feature of the regions containing the high acetate concentrations are regions with low transmissivity ($5 \cdot 10^{-11}$ to $5 \cdot 10^{-9}$ m^2/s). Acetate production occurs by microbial activity. Autotrophic acetogens use H_2 and CO_2 to form acetate:

$$4H_2 + 2CO_2 \rightarrow CH_3COO^- + H^+ + 2H_2O.$$

Sulfate-reducing bacteria activity is high in the high acetate-containing regions, resulting in sulfide concentrations as high as 15 mg/L:

$$SO_4^{2-} + CH_3COO^- \rightarrow HS^- + 2HCO_3^-$$

Sulfide production

Electron acceptors such as SO_4^{2-} and Fe^{2+} are at low concentrations, so H_2 and CH_4 are able to accumulate in Cl-type groundwater. Abiotic H_2 generation can occur through a number of different pathways, as described in the section on brackish SO_4 sulfide production. However, the scarce quantity of electron acceptors in this region limit the production of sulfide.

Sulfide attenuation

Sulfide attenuation occurs via the same processes as in the brackish SO_4^{2-}-saline Cl water mixture region (Section 1.1.2.4).

POSIVA PFLOTRAN MODELING

Posiva used PFLOTRAN to model major ion reactive transport and sulfide fluxes in the subsurface at Onkalo (Posiva 2021). PFLOTRAN is a massively parallel subsurface flow and reactive transport simulator. The parallel capability of the code makes it suitable for modeling systems such as the Onkalo spent nuclear fuel repository, as it can reduce the simulation runtime of systems with millions of degrees of freedom by increasing the number of processors used (Hammond et al., 2014). PFLOTRAN sequentially couples flow and reactive transport, which is suitable for modeling systems with evolving pressure and flux conditions over long periods of time.

The Posiva study modeled a 7700 x 5760 x 1980 m subsurface region surrounding the Onkalo spent nuclear fuel repository. The simulations were split into four time periods corresponding to the different repository conditions. First, a simulation was run for the 499.99 years prior to repository construction (1500-1999.99 AD) to provide the quasi-stationary flow and pressure conditions. A 0.01 yr simulation was then performed to define the geochemical equilibrium conditions prior to repository construction. Following the initial flow and geochemistry simulations, an operational phase simulation was run for 121 yr (2000-2121 AD), during which various repository panels open and close. The final simulation is a 47,000 yr post-closure period, after which global warming-induced sea level changes alter the flux conditions applied to the upper boundary.

Several variant cases were additionally performed. The first considered Ripidolite-14A instead of Chamosite as a source of Fe^{2+}. The second variant case increased the maximum H_2 concentration reached in the fracture by four times. The third variant case increased the water extraction rates from 50 L/min to 100 L/min. The final variant case added an additional sulfate source from within the rock matrix within the first 300 m of depth.

PHREEQC REACTIVE TRANSPORT MODELING

To model and study the chemical processes and controlling phases of the Posiva study, PHREEQC was used in the current work to speciate the endmember waters described by Posiva (2021). PHREEQC was chosen for this initial scoping work because of its extensive toolbox and user interface. The Thermochimie v.9 database (Giffault, 2014) was used, following POSIVA (2021). Once the initial scoping work is complete, a PFLOTRAN reactive transport model will be developed.

The four endmember waters are described in the geologic context in the following subsections. They include a meteoric HCO_3^- water, a brackish SO_4^{2-} water, and two saline Cl-type waters. In this study, the endmember waters were equilibrated with the fracture-lining minerals, then mixed proportionally as described in (Posiva, 2021).

Endmember Speciation

The chemical compositions of the endmember reference waters are presented in Tab. D-1. Those chemical compositions are equilibrated with the fracture-lining minerals present at the depths where the water resides, described earlier.

Tab. D-1 Endmember water compositions presented in (Posiva, 2021)

	Meteoric	Brackish	Saline 1	Saline 2
pH	7.26	7.50	7.40	7.80
Cl (mg/L)	6.75	4600	6400	43000
SO_4 (mg/L)	44.95	523	1	1
S^{2-} (mg/L)	0.0	0.04	0.18	0.0
HCO_3 (mg/L)	323	67.1	15.3	5.0
PO_4 (mg/L)	0.15	0.1	0	0.04
DIC[1] (mg/L)	66	10.1	3.0	1.0
DOC[2] (mg/L)	11	2.8	3.3	31.4
Al (µg/L)	0.0	38	12.5	3.0
Ba (µg/L)	0.0	150	180	0.0
B (mg/L)	0.0	1.1	1.3	0.9
Br (mg/L)	0.15	18	44	348
Ca (mg/L)	74.5	750	1300	15700
F (mg/L)	0.7	0.69	1	1.6
Fe^{2+} (mg/L)	2.25	0.5	0.13	2
Mg (mg/L)	14.9	160	62	110
Mn (mg/L)	0.0	0.79	0.32	2.2
K (mg/L)	6.68	16	11	22
Rb (µg/L)	0.0	12	13	120
SiO_2 (mg/L)	19.3	7.7	10	5.3
Na (mg/L)	18	1900	2650	9750
Sr (mg/L)	0.15	6.6	14	161.04

[1] DIC = dissolved inorganic carbon
[2] DOC = dissolved organic carbon

The Meteoric water endmember is used below as a demonstration of how chemistry is entered in PHREEQC:

```
SOLUTION 1 Meteoric HCO3 water
   pH 7.26
   Temperature 20
   units mg/L
   Cl 6.75
   S(6) 44.95 as SO4
   S(-2) 0.0
   C(4) 323 as HCO3
   P 0.15 as PO4
   Al 0.0 ug/L
   Ba 0.0 ug/L
   B 0.0
   Br 0.15
   Ca 74.5
   F 0.7
   Fe(2) 2.25
   Mg 14.9
   Mn 0.0
   K 6.68
   Rb 0.0 ug/L
   Si 19.3 as SiO2
   Na 18
   Sr 0.15
END
```

The output displays a description of the solution, along with species concentrations:

```
----------------------------Description of solution----------------------------

                                    pH  =   7.260
                                    pe  =   4.000
      Specific Conductance (µS/cm,  20°C)  = 480
                         Density (g/cm³)  =   0.99860
                              Volume (L)  =   1.00192
                     Activity of water  =   1.000
                 Ionic strength (mol/kgw)  =   8.406e-03
                       Mass of water (kg)  =   1.000e+00
                 Total alkalinity (eq/kg)  =   4.754e-03
                       Total CO2 (mol/kg)  =   5.296e-03
                         Temperature (°C)  =  20.00
                  Electrical balance (eq)  =   6.342e-05
 Percent error, 100*(Cat-|An|)/(Cat+|An|)  =   0.56
                               Iterations  =  10
                                  Total H  = 1.110184e+02
                                  Total O  = 5.552471e+01

----------------------------Distribution of species----------------------------

                                          Log       Log       Log     mole V
   Species     Molality    Activity   Molality  Activity    Gamma    cm³/mol

   OH-        1.372e-07   1.245e-07    -6.863    -6.905    -0.042     -4.27
   H+         5.977e-08   5.495e-08    -7.223    -7.260    -0.037      0.00
   H2O        5.551e+01   9.998e-01     1.744    -0.000     0.000     18.05
```

Br	1.878e-06					
Br-	1.878e-06	1.703e-06	-5.726	-5.769	-0.043	24.36
C(4)	5.296e-03					
HCO3-	4.628e-03	4.222e-03	-2.335	-2.375	-0.040	24.35
CO2	5.579e-04	5.590e-04	-3.253	-3.253	0.001	34.19
CaHCO3+	6.498e-05	5.936e-05	-4.187	-4.227	-0.039	9.51
MgHCO3+	2.107e-05	1.915e-05	-4.676	-4.718	-0.041	5.37
FeHCO3+	9.226e-06	8.391e-06	-5.035	-5.076	-0.041	(0)
CaCO3	5.941e-06	5.953e-06	-5.226	-5.225	0.001	-14.62
CO3-2	4.672e-06	3.235e-06	-5.331	-5.490	-0.160	-5.52
NaHCO3	1.734e-06	1.737e-06	-5.761	-5.760	0.001	1.80
FeCO3	1.540e-06	1.543e-06	-5.813	-5.812	0.001	(0)
MgCO3	1.128e-06	1.130e-06	-5.948	-5.947	0.001	-17.08
SrHCO3+	6.578e-08	6.001e-08	-7.182	-7.222	-0.040	(0)
NaCO3-	3.643e-08	3.314e-08	-7.438	-7.480	-0.041	-1.45
(CO2)2	4.830e-09	4.840e-09	-8.316	-8.315	0.001	68.37
SrCO3	1.961e-09	1.965e-09	-8.708	-8.707	0.001	-14.15
Ca	1.860e-03					
Ca+2	1.734e-03	1.200e-03	-2.761	-2.921	-0.160	-18.02
CaHCO3+	6.498e-05	5.936e-05	-4.187	-4.227	-0.039	9.51
CaSO4	5.498e-05	5.509e-05	-4.260	-4.259	0.001	7.30
CaCO3	5.941e-06	5.953e-06	-5.226	-5.225	0.001	-14.62
CaHPO4	2.712e-07	2.717e-07	-6.567	-6.566	0.001	(0)
CaH2PO4+	1.262e-08	1.152e-08	-7.899	-7.939	-0.040	(0)
CaPO4-	1.165e-08	1.063e-08	-7.934	-7.973	-0.040	(0)
CaOH+	3.983e-09	3.622e-09	-8.400	-8.441	-0.041	(0)
CaHSO4+	2.043e-11	1.858e-11	-10.690	-10.731	-0.041	(0)
Cl	1.905e-04					
Cl-	1.905e-04	1.731e-04	-3.720	-3.762	-0.042	17.96
FeCl+	5.221e-09	4.748e-09	-8.282	-8.323	-0.041	(0)
F	3.686e-05					
F-	3.599e-05	3.267e-05	-4.444	-4.486	-0.042	-1.33
MgF+	8.551e-07	7.784e-07	-6.068	-6.109	-0.041	-10.52
NaF	1.334e-08	1.336e-08	-7.875	-7.874	0.001	7.06
FeF+	7.140e-09	6.494e-09	-8.146	-8.187	-0.041	(0)
HF	2.458e-09	2.463e-09	-8.609	-8.608	0.001	12.26
HF2-	3.256e-13	2.961e-13	-12.487	-12.529	-0.041	21.86
SiF6-2	1.249e-29	8.618e-30	-28.903	-29.065	-0.161	42.44
Fe(2)	4.031e-05					
Fe+2	2.854e-05	1.988e-05	-4.545	-4.702	-0.157	-22.29
FeHCO3+	9.226e-06	8.391e-06	-5.035	-5.076	-0.041	(0)
FeCO3	1.540e-06	1.543e-06	-5.813	-5.812	0.001	(0)
FeSO4	8.623e-07	8.640e-07	-6.064	-6.063	0.001	24.60
FeOH+	8.581e-08	7.821e-08	-7.066	-7.107	-0.040	(0)
FeHPO4	3.588e-08	3.595e-08	-7.445	-7.444	0.001	(0)
FeF+	7.140e-09	6.494e-09	-8.146	-8.187	-0.041	(0)
FeCl+	5.221e-09	4.748e-09	-8.282	-8.323	-0.041	(0)
FeH2PO4+	4.518e-09	4.122e-09	-8.345	-8.385	-0.040	(0)
Fe(OH)2	7.767e-12	7.782e-12	-11.110	-11.109	0.001	(0)
FeHSO4+	3.384e-13	3.078e-13	-12.471	-12.512	-0.041	(0)
Fe(OH)3-	5.491e-15	5.004e-15	-14.260	-14.301	-0.040	(0)
H(0)	4.489e-26					
H2	2.245e-26	2.249e-26	-25.649	-25.648	0.001	28.61
K	1.709e-04					
K+	1.706e-04	1.550e-04	-3.768	-3.810	-0.042	8.89
KSO4-	2.930e-07	2.673e-07	-6.533	-6.573	-0.040	34.02
KHPO4-	1.505e-10	1.373e-10	-9.823	-9.862	-0.040	38.55

Mg	6.132e-04					
Mg+2	5.682e-04	3.954e-04	-3.245	-3.403	-0.157	-21.46
MgSO4	2.177e-05	2.181e-05	-4.662	-4.661	0.001	5.63
MgHCO3+	2.107e-05	1.915e-05	-4.676	-4.718	-0.041	5.37
MgCO3	1.128e-06	1.130e-06	-5.948	-5.947	0.001	-17.08
MgF+	8.551e-07	7.784e-07	-6.068	-6.109	-0.041	-10.52
MgHPO4	1.209e-07	1.211e-07	-6.918	-6.917	0.001	(0)
MgOH+	1.804e-08	1.650e-08	-7.744	-7.782	-0.039	(0)
MgH2PO4+	5.298e-09	4.833e-09	-8.276	-8.316	-0.040	(0)
MgPO4-	5.180e-09	4.726e-09	-8.286	-8.326	-0.040	(0)
Na	7.834e-04					
Na+	7.806e-04	7.109e-04	-3.108	-3.148	-0.041	-1.67
NaHCO3	1.734e-06	1.737e-06	-5.761	-5.760	0.001	1.80
NaSO4-	1.014e-06	9.254e-07	-5.994	-6.034	-0.040	14.37
NaCO3-	3.643e-08	3.314e-08	-7.438	-7.480	-0.041	-1.45
NaF	1.334e-08	1.336e-08	-7.875	-7.874	0.001	7.06
NaHPO4-	6.903e-10	6.297e-10	-9.161	-9.201	-0.040	34.16
NaOH	8.837e-21	8.854e-21	-20.054	-20.053	0.001	(0)
O(0)	0.000e+00					
O2	0.000e+00	0.000e+00	-42.726	-42.725	0.001	29.98
P	1.580e-06					
HPO4-2	6.586e-07	4.543e-07	-6.181	-6.343	-0.161	7.07
H2PO4-	4.535e-07	4.137e-07	-6.343	-6.383	-0.040	33.38
CaHPO4	2.712e-07	2.717e-07	-6.567	-6.566	0.001	(0)
MgHPO4	1.209e-07	1.211e-07	-6.918	-6.917	0.001	(0)
FeHPO4	3.588e-08	3.595e-08	-7.445	-7.444	0.001	(0)
CaH2PO4+	1.262e-08	1.152e-08	-7.899	-7.939	-0.040	(0)
CaPO4-	1.165e-08	1.063e-08	-7.934	-7.973	-0.040	(0)
MgH2PO4+	5.298e-09	4.833e-09	-8.276	-8.316	-0.040	(0)
MgPO4-	5.180e-09	4.726e-09	-8.286	-8.326	-0.040	(0)
FeH2PO4+	4.518e-09	4.122e-09	-8.345	-8.385	-0.040	(0)
NaHPO4-	6.903e-10	6.297e-10	-9.161	-9.201	-0.040	34.16
KHPO4-	1.505e-10	1.373e-10	-9.823	-9.862	-0.040	38.55
PO4-3	7.939e-12	3.367e-12	-11.100	-11.473	-0.373	-22.33
H3PO4	3.145e-12	3.151e-12	-11.502	-11.502	0.001	47.12
S(6)	4.682e-04					
SO4-2	3.892e-04	2.683e-04	-3.410	-3.571	-0.162	14.01
CaSO4	5.498e-05	5.509e-05	-4.260	-4.259	0.001	7.30
MgSO4	2.177e-05	2.181e-05	-4.662	-4.661	0.001	5.63
NaSO4-	1.014e-06	9.254e-07	-5.994	-6.034	-0.040	14.37
FeSO4	8.623e-07	8.640e-07	-6.064	-6.063	0.001	24.60
KSO4-	2.930e-07	2.673e-07	-6.533	-6.573	-0.040	34.02
SrSO4	5.422e-08	5.433e-08	-7.266	-7.265	0.001	24.04
HSO4-	1.416e-09	1.288e-09	-8.849	-8.890	-0.041	39.96
CaHSO4+	2.043e-11	1.858e-11	-10.690	-10.731	-0.041	(0)
FeHSO4+	3.384e-13	3.078e-13	-12.471	-12.512	-0.041	(0)
Si	3.214e-04					
H4SiO4	3.206e-04	3.212e-04	-3.494	-3.493	0.001	52.53
H3SiO4-	7.921e-07	7.201e-07	-6.101	-6.143	-0.041	27.89
H2SiO4-2	9.204e-13	6.373e-13	-12.036	-12.196	-0.160	(0)
SiF6-2	1.249e-29	8.618e-30	-28.903	-29.065	-0.161	42.44
Sr	1.713e-06					
Sr+2	1.591e-06	1.103e-06	-5.798	-5.958	-0.159	-17.50
SrHCO3+	6.578e-08	6.001e-08	-7.182	-7.222	-0.040	(0)
SrSO4	5.422e-08	5.433e-08	-7.266	-7.265	0.001	24.04
SrCO3	1.961e-09	1.965e-09	-8.708	-8.707	0.001	-14.15
SrOH+	1.129e-12	1.029e-12	-11.947	-11.988	-0.040	(0)

Next, SOLUTION 1 is equilibrated with the fracture-lining minerals. The first value following the phase (mineral) name is the saturation index, and the second value is the quantity in moles.

```
USE SOLUTION 1
EQUILIBRIUM_PHASES 1
   GOETHITE 0.0 1E-4
   CALCITE 0.0 1E-4
   KAOLINITE 0.0 1E-4
   CHALCEDONY 0.0 1E-4
SAVE solution 1
END
```

The output displays the mineral dissolution and precipitation to reach the equilibrium state.

```
-------------------------------Phase assemblage-------------------------------
                                                    Moles in assemblage
Phase          SI      log IAP log K(T, P) Initial      Final       Delta

Calcite       0.00    -8.45     -8.45    1.000e-04   8.423e-05  -1.577e-05
Chalcedony    0.00    -3.61     -3.61    1.000e-04   1.761e-04   7.613e-05
Goethite     -0.00    -0.82     -0.82    1.000e-04   1.369e-04   3.686e-05
Kaolinite     0.00     7.88      7.88    1.000e-04   1.000e-04  -2.201e-09
```

Mixing

Mixing fractions are defined by using two endmember solutions. The mixtures are assigned a number following the MIX keyword, and the solutions (1 and 2, below) are assigned the chosen mixing ratio. In this example, Solution 1 is 90% of the mixture and Solution 2 is 10% of the mixture. The mixed solution is then saved and assigned a value different from the initial solutions to prevent the accidental overwriting of the endmember solutions.

```
MIX 100
   1 0.90
   2 0.10
SAVE SOLUTION 100
END
```

The mixed solutions are then equilibrated with the fracture minerals present at the given depth.

The conservative elements show good agreement with the PHREEQC calculations reported by Posiva (2021) (Fig. D-2).

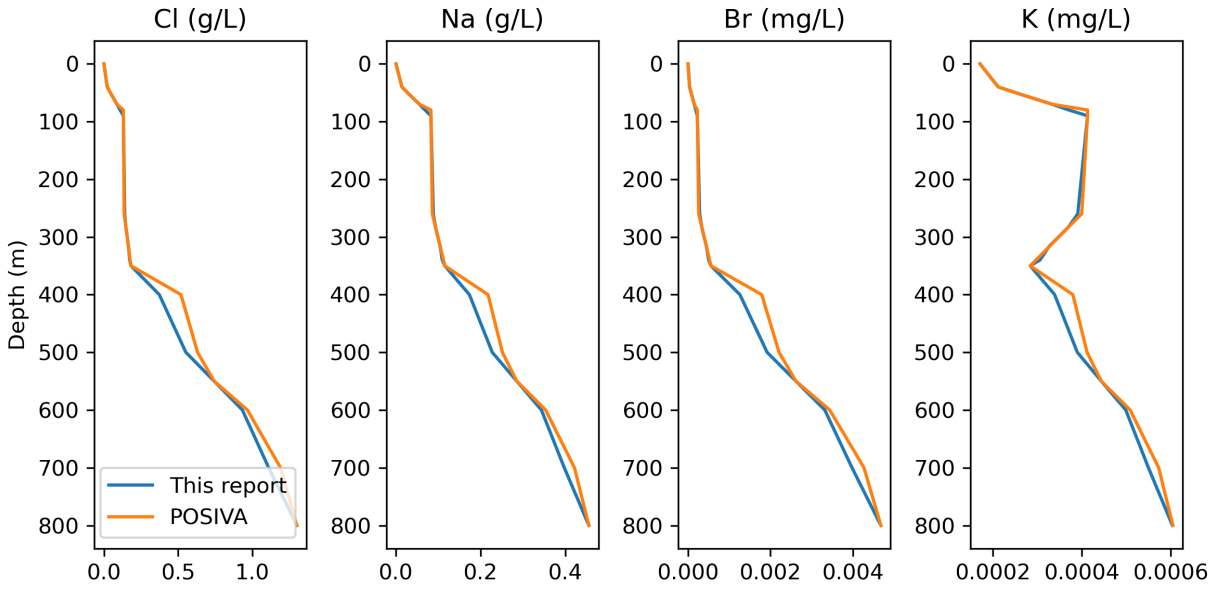

Fig. D-2 Conservative elements following endmember mixing and equilibration with fracture-lining minerals.

The reactive species show similar trends, but slightly different outputs at some depths compared to the reference case given by Posiva (2021) (Fig. D-3). These results are preliminary and may not fully represent Posiva's modeling work.

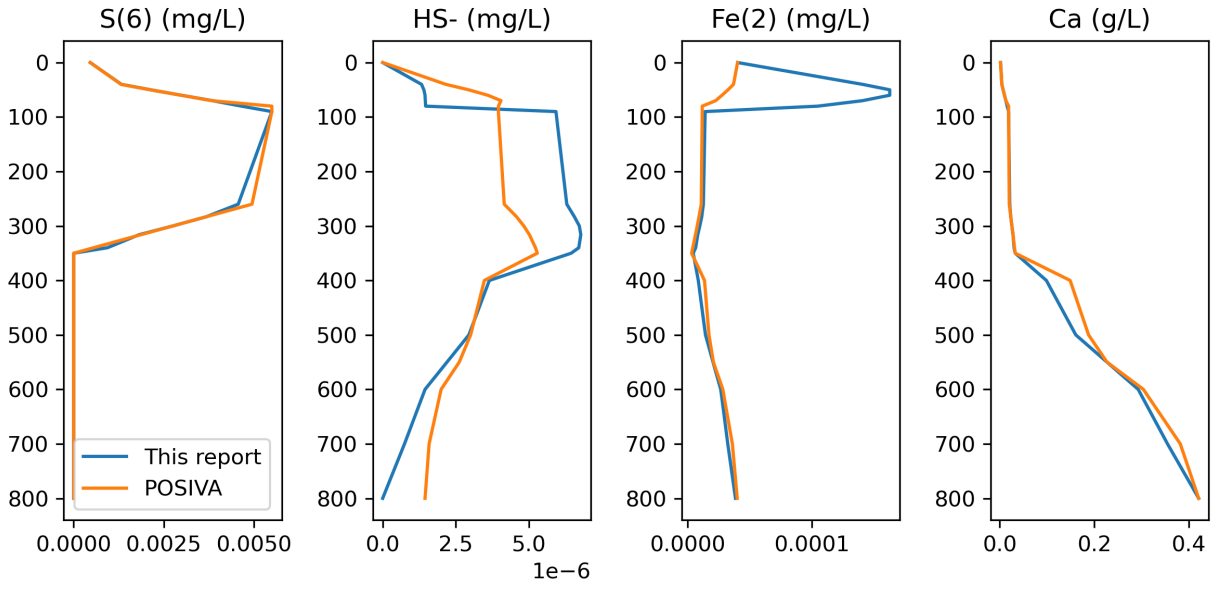

Fig. D-3 Reactive species with depth relevant to sulfide production and attenuation.

Transport

One-dimensional transport of meteoric water infiltration into the fractured crystalline rock is a method by which mixing of groundwaters can occur. This behavior will be studied using the dual porosity advection functionality in PHREEQC, following the formulation of Lipson et al. (2007). The endmember waters and their mixing ratios are initialized with depth and are equilibrated with the fracture-lining minerals. The adjacent matrix cells are initialized with a higher concentration of aqueous hydrogen, which can diffuse into the fracture. A schematic of the fracture-matrix discretization is displayed in Fig. D-4.

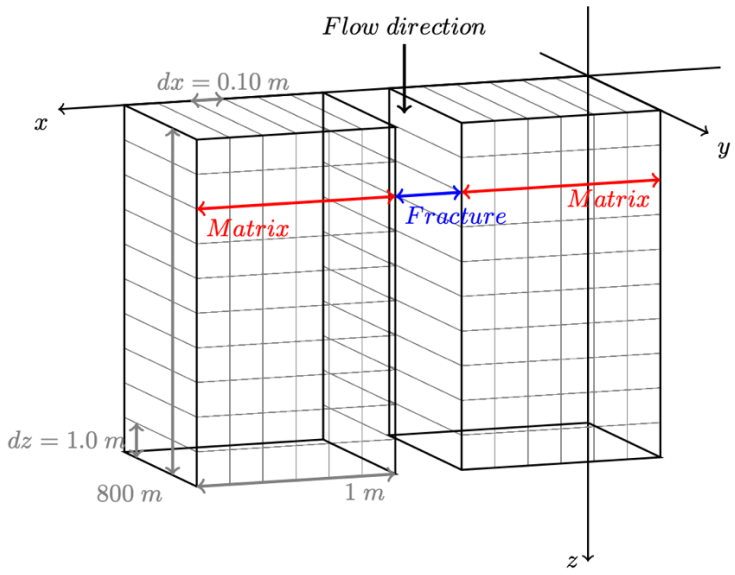

Fig. D-4 Schematic of the proposed fracture-matrix system. The fracture cells are initialized with the major ions and equilibrium mineral phases. The matrix cells are initialized with aqueous hydrogen at concentrations above those in the fracture to allow.

NEXT STEPS

The results from the PHREECQ mixing model will help guide the eventual inclusion of geochemical modeling in the crystalline reference case. Electrolytes such as Na and Cl will be added first, followed by other major ions and mineral phases.

The results of the PHREEQC 1D advective transport will be used to benchmark a 1D advective transport simulation using the multiple continuum functionality in PFLOTRAN. PFLOTRAN handles primary (fracture) and secondary (crystalline rock matrix) continua with the Dual Continuum Disconnected Matrix (DCDM). DCDM permits advection through the primary continuum and diffusion in the secondary continuum. Aqueous hydrogen diffusion from the crystalline rock matrix is a theoretical method of sulfide production and can be modeled in PFLOTRAN using the multiple continuum model.

REFERENCES

Giffaut, E., Grivé, M., Blanc, P., Vieillard, P., Colàs, E., Gailhanou, H., ... & Duro, L. (2014). Andra thermodynamic database for performance assessment: ThermoChimie. Applied Geochemistry, 49, 225-236.

Gregory, S. P., Barnett, M. J., Field, L. P., & Milodowski, A. E. (2019). Subsurface microbial hydrogen cycling: Natural occurrence and implications for industry. Microorganisms, 7(2), 53.

Hammond, G. E., Lichtner, P. C., & Mills, R. (2014). Evaluating the performance of parallel subsurface simulators: An illustrative example with PFLOTRAN. Water Resources Research, 50(1), 208–228.

Lahdenpera, A.-M., Palmén, J., & Hella, P. (2005). Summary of overburden studies at Olkiluoto with an emphasis on geosphere-biosphere interface.

Lipson, D. S., McCray, J. E., & Thyne, G. D. (2007). Using PHREEQC to Simulate Solute Transport in Fractured Bedrock. Groundwater, 45(4), 468–472. https://doi.org/10.1111/j.1745-6584.2007.00318.x

Posiva. (2021). Sulfide Fluxes and Concentrations in the Spent Nuclear Fuel Repository at Olkiluoto—2021 Update (Working Report 2021-07). Posiva Oy.

Schoonen, M., & Barnes, H. (1991). Reactions forming pyrite and marcasite from solution: II. Via FeS precursors below 100 C. Geochimica et Cosmochimica Acta, 55(6), 1505–1514.

Trinchero, P., Delos, A., Molinero, J., Dentz, M., & Pitkänen, P. (2014). Understanding and modelling dissolved gas transport in the bedrock of three Fennoscandian sites. Journal of Hydrology, 512, 506–517.